NOTICE

The quality of this microfiche is heavily dependent upon the quality of the original thesis submitted for microfilming. Every effort has been made to ensure the highest quality of reproduction possible.

If pages are missing, contact the university which granted the degree.

Some pages may have indistinct print especially if the original pages were typed with a poor typewriter ribbon or if the university sent us a poor photocopy.

Previously copyrighted materials (journal articles, published tests, etc.) are not filmed.

Reproduction in full or in part of this film is governed by the Canadian Copyright Act, R.S.C. 1970, c. C-30. Please read the authorization forms which accompany this thesis.

THIS DISSERTATION
HAS BEEN MICROFILMED
EXACTLY AS RECEIVED

AVIS

La qualité de cette microfiche dépend grandement de la qualité de la thèse soumise au microfilmage. Nous avons tout fait pour assurer une qualité supérieure de reproduction.

S'il manque des pages, veuillez communiquer avec l'université qui a conféré le grade.

La qualité d'impression de certaines pages peut laisser à désirer, surtout si les pages originales ont été dactylographiées à l'aide d'un ruban usé ou si l'université nous a fait parvenir une photocopie de mauvaise qualité.

Les documents qui font déjà l'objet d'un droit d'auteur (articles de revue, examens publiés, etc.) ne sont pas microfilmés.

La reproduction, même partielle, de ce microfilm est soumise à la Loi canadienne sur le droit d'auteur, SRC 1970, c. C-30. Veuillez prendre connaissance des formules d'autorisation qui accompagnent cette thèse.

LA THÈSE A ÉTÉ
MICROFILMÉE TELLE QUE
NOUS L'AVONS REÇUE

UNIVERSITÉ D'OTTAWA
UNIVERSITY OF OTTAWA

Experimental Studies of Coarse-Grained Sedimentation

A Thesis
presented to the
School of Graduate Studies
in partial fulfillment of the
requirements for the
Ph.D. degree in Geology

by

Emlyn H. Koster

To my parents in England for making a

beginning possible,

and to Maryse for her love and support.

TABLE OF CONTENTS

		Page
	Abstract	i
	Figures	iv
	Tables	vii
	Plates	viii
	Notation of variables and constants	ix
	Acknowledgements	xiii
1.0	INTRODUCTION	1
1.1	The descriptive framework of fluvial conglomerates	6
1.2	Aspects of the framework amenable to a laboratory study	12
1.21	Clast fabric - a literature review	15
1.211	Imbrication	16
1.212	Orientation	21
2.0	EXPERIMENTAL WORK	27
2.1	Purpose and objectives	27
2.2	Flume apparatus	28
2.3	Design	31
2.4	Flow variables	32
2.5	Material	37
2.51	Clasts as ellipsoids	38
3.0	MOTION OF CLASTS ISOLATE ON A SANDBED BELOW THEIR TRANSPORT THRESHOLD	43
3.1	Measurement of motion	46
3.2	Statistics of response data	48
3.21	Current crescents and the 'imbrication process'	53
3.3	Response to the flow regime of the sandbed	55
3.4	Response to clast properties	63
3.41	Imbrication	63
3.411	Dependence on simple geometric properties	63
3.412	Projection area as a function of nominal diameter	68
3.413	Proposed stability criterion	78
3.42	Orientation	86
3.421	Reorientation from current-parallel alignment	86
3.422	Imperfections of current-normal alignment	92

3.43	A-axis inclination	93
3.44	Motion parallel to the x flow axis	100
3.45	Motion parallel to the y flow axis	107
3.46	Motion parallel to the z flow axis	109
3.47	Magnitude of displacement	112
3.5	Development of the imbrication process	116
4.0	CLAST TRANSPORT	128
4.1	Experimental method	130
4.2	Types of clast motion	132
4.3	Process-response analysis	134
4.31	Influence of clast size	136
4.32	Influence of clast form	139
4.4	Discussion	151
5.0	TRANSVERSE RIBS	154
5.1	Field characteristics	157
5.2	Analysis of process	161
5.21	Hydraulic jump	161
5.22	Antidunes	162
5.3	Discussion	169
5.4	Reconstruction of the paleoflow regime	172
5.5	Clast transport and competence	179
5.6	Comment	183
6.0	SUMMARY AND CONCLUSIONS	185
7.0	REFERENCES	192
8.0	APPENDICES	202
8.1	Projection area of ellipsoidal clasts	202
8.11	Development of equations for calculation of the area projected by symmetric triaxial ellipsoids	202
8.111	Long axis aligned normal to flow: the effect of imbrication	202
8.112	No imbrication: the effect of variable orientation	204
8.113	Variable imbrication: variable orientation	205
8.12	Development of equations for calculation of the required angle of imbrication for a given area by a triaxial ellipsoid	205
8.121	Long axis aligned normal to flow	205
8.122	Long axis aligned parallel to flow	207
8.2	APL computer programmes written for statistical analyses of the flume data	208
8.3	Triaxial dimensions of the clasts used in the experiments	221

ABSTRACT

A 18.3m long, 0.76m wide, tiltable flume was used to investigate selected phenomena observed during fieldwork on modern coarse-grained fluvioglacial outwash in south-western Yukon. These phenomena are clast fabric, below-threshold motion of clasts isolate on a sandbed, transport of single clasts on an artificially roughened bed and the significance of transverse ribs in paleoflow studies. Clasts used in the experiments varied in weight from 50 to 2,500 grams, and in sphericity, the degree of oblateness-prolateness, roundness and asymmetry. Each was numbered to assist the monitoring of individual clast response.

The first set of experiments investigated the attainment of stable imbrication by clasts isolate on a sandbed under steady-state, sub-critical flow conditions, with mean velocity varying between 25 and 90cm.sec^{-1} and depth between 9 and 12cm. Six response variables were measured for each clast, i.e. the three vector components of translation from the initial position, and the three angular quantities of imbrication, orientation and inclination of the a-axis. Except for imbrication and a-axis inclination, each response varies in magnitude according to the topographic relief of the sandbed, and all are dependent to some extent on the size and shape properties of the clasts. Slight deviations from

perfect current-normal alignment are attributable to all these variables, while a-axis inclination is dependent only on the degree of clast asymmetry. Empirical equations are presented which predict the average magnitude of translational motion into current-crescent scours. Imbrication is the fundamental response and develops as the logarithm of time. Optimum stability of imbrication is given by a power relation between projection area and nominal diameter, and is attained at the regime transition, where the flow approaches a steady and two-dimensional character. The imbrication analysis necessitated calculation of projection areas using ellipsoidal clasts; formulae were developed to compute the plane area projected by a symmetric ellipsoid at any configuration with respect to flow direction.

In the second set of experiments, the transport velocities of selected clasts were investigated in shallow, high-velocity flows over an artificially roughened bed. Process-response analysis of transport velocities indicated that the effects of size and form are variable with increasing flow. Pooling the results eliminates the influence of flow velocity, and clast transport velocities are seen to be a complex function of particle size and shape in relation to

flow depth. The results suggest that in a given flow with unimpeded clast motion, the intermediate size grade of the available bedload is preferentially transported, but that small oblate and large prolate forms respectively tend to saltate and roll. For a bedload with wide morphological variation, it appears that size may have a subordinate role to that of shape.

The explanation of transverse ribs by a stepping hydraulic jump condition is challenged on the grounds that super-critical flow is rare in braided outwash. It is alternatively proposed that rib sequences are formed and maintained by a growing train of antidune waves. This latter model is substantiated by observations in a reconnaissance flume run, and by successful prediction of flow parameters on the basis of available field data of rib spacing, width and maximum particle size.

FIGURES

1 Diagrammatic profile of the G.S.C. flume

2 Settling velocity for a bulk sample of the sand used in the first set of experiments

3 Histogram showing the ellipsoidal tendency of clasts

4 Clast configuration in the experiments of isolate gravel fabric

5 Schematic representation of the process-response model

6 Histograms of the translational responses

7 Histograms of the rotational responses

8 Explanation of a Dice-Diagram

9 Dice-Diagrams showing the translational reponse of the the clast population in each run

10 Dice-Diagrams showing the rotational response of the clast population in each run

11 Hydraulic roughness of lower- and upper-flow regime bedforms

12 α-response as a function of maximum projection sphericity

13 Variable influence of clast properties on the α-response with varying Froude number

14 Projection area as a power function of nominal diameter for each run's data

15 Variation in the parameters of the power relation, $A_p = f(d_n)$

16 Observed α-values compared to those calculated according to the optimum relation of A_p versus d_n

17 Diagrammatic illustration of the concept of 'equilibrium area'

18 Sphericity-Form diagram

19 Explanation of α-variation by means of sphericity-form diagrams

20 Rose diagrams of the orientation data from runs with initial current-parallel orientation

21 Variable influence of clast properties on the β-response with varying Froude number

22 Definition of the 'composite asymmetry index'

23 Variable influence of the asymmetry index on the Y-reponse with varying Froude number

24 Y-reponse as an exponential function of the asymmetry index

25 Variable influence of clast properties on the X-reponse with varying Froude number

26 X-reponse as a linear function of b-c plane roundness

27 Observed X-values compared to those calculated according to a multivariate predictive equation

28 Observed Y-values compared to those calculated according to a multivariate predictive equation

29 Inter-dependence of the X- and Z-responses

30 Partial inter-dependence of the Y- and Z-responses

31 Dice-Diagrams showing the magnitude of clast displacement in each run

32 Histogram of mean values of clast displacement

33 Clast elevation as a semi-logarithmic function of time elapsed in each run

34 Variability in the rate of the imbrication process

35 Delineation of hydraulically 'rough' and 'smooth' boundaries

36 Typical velocity profile of the flows in the transport velocity experiments

37 Transport velocity as a curvilinear function of nominal diameter for each run's data

38 Transport velocity as a curvilinear function of nominal diameter for all the data combined

39 Transport velocity as a linear function of oblate-prolate index at a given clast size for each run's data

40 Variation in the parameters of the transport velocity versus oblate-prolate index relations

41 Transport velocity as a linear function of oblate-prolate index at a given $d_n/\overline{Y}$ ratio for all the data combined

42 Inter-relationships of transverse ribs parameters for the data from Spring Creek

43 Computed depositional velocities in relation to the findings of previous studies.

TABLES

1-6 Literature review of gravel fabric

7 Hydraulic data for the experimental runs

8 Size and morphological characteristics of the gravel population used in the experiments of isolate gravel fabric

9 Classification of symmetric ellipsoids and the accuracy of linear size measures

10 Types of clast response

11 Statistical analysis of the α-response

12 Clasts closely conforming to an ellipsoidal geometry

13 Observed parameters for the power function $A_p=f(d_n)$

14 A comparison of observed vlaues of α with those according to the optimum relation

15 Orientation analyses of the data from runs with initial current-parallel orientation

16 Orientation analyses of the data from runs with initial current-normal orientation

17 Statistical analysis of the X-response

18 Statistical analysis of the Y-response

19 Observed values of the coefficient in the relation, $h=f(\Delta t)$

20 Size and morphological characteristics of the gravel used in the experiments of transport velocity

21 Illustration of the two-stage analytical procedure used in the analysis of transport velocity data

22 Sets of regression equations for the relation $U_2=f(\overline{OP})$ for each experimental run

23 Set of regression equations for the relation $U_2=f(\overline{OP})$ for all the data combined

24 Data of transverse rib sequences in Spring Creek

25 Calculated parameters of paleoflow

PLATES

1 The alluvial fan of Spring Creek, south-west Yukon

2-5 Transverse rib sequences on the fan surface

Notation of variables and constants

Units:

mm	millimetre(s)
cm	centimetre(s)
m	metre(s)
l	litre(s)
sec	second(s)
g	gram(s)
kg	kilogram(s)
^{o}	degree(s)
dyn	dyne(s)
dl	dimensionless

Parameters:

a	long axis dimension of clast (cm)
A	area (cm^2)
A_p	area projected by clast in flow y-z plane (cm^2)
AI	asymmetry index of clast(dl)
b	intermediate axis dimension of clast (cm)
b_{max}	average b-axis dimension of ten largest clasts (cm)
c	short axis dimension of clast (cm)
C_D	drag coefficient (dl)
d	unspecified measure of clast size (cm)
d_n	nominal diameter of clast (cm)
D	angular deviation (^{o}) of Θ from current-nominal orientation
f	subscript denoting final clast position
F_g	gravitation force ($dyn.cm^{-2}$)

Fr	Froude number (dl)
g	gravitational acceleration ($cm.sec^{-2}$)
h	elevation of clast relative to bed level (cm)
H	height above datum of static or dynamic water levels in pitot tube apparatus (cm)
H_w	amplitude of water-surface undulations in in-phase waves (cm)
i	subscript denoting initial clast position
$\vec{if}$	magnitude of clast displacement (cm)
l	a length dimension (mm, cm, m)
L	vector magnitude (Z)
min	subscript denoting minimum value
max	subscript denoting maximum value
n	sample size
$\overline{OP}$	oblate-prolate index of clast (dl)
P	roundness of clast b-c plane (dl)
Pr	probability
Q	flow discharge ($l.sec^{-1}$)
r	correlation coefficient
R	hydraulic radius (cm, m)
Re	Reynolds number (dl)
Re_p	particle Reynolds number (dl)
$\overline{S}$	mean spacing of transverse ribs (cm)

S	slope of energy grade line (dl)
S_b	slope of bed surface (dl)
S_w	slope of water surface (dl)
t	time (sec, min)
U	a velocity dimension ($cm.sec^{-1}$)
$\overline{U}$	mean flow velocity ($cm.sec^{-1}$)
U_s	terminal settling velocity ($cm.sec^{-1}$)
U_{surf}	surface flow velocity ($cm.sec^{-1}$)
U_1	threshold velocity ($cm.sec^{-1}$)
U_2	transport velocity ($cm.sec^{-1}$)
U_3	depositional velocity ($cm.sec^{-1}$)
V	measured volume of clast (cm^3)
V_e	volume of symmetric ellipsoid having same axial dimensions as clast (cm^3)
$\overline{W}$	mean width of transverse ribs (cm)
x	flow axis parallel to flow
X	distance of clast motion parallel to x (cm)
y	flow axis vertical and perpendicular to x
Y	distance of clast motion parallel to y (cm)
$\overline{Y}$	mean flow depth (cm)
z	flow axis horizontal and perpendicular to x
Z	distance of clast motion parallel to z (cm)
ρ_s	density of clast ($g.cm^{-3}$)
ρ_f	density of fluid ($g.cm^{-3}$)
γ_s	specific gravity of clast (dl)

γ_f	specific gravity of fluid (dl)
α	angle of imbrication of clast a-b plane (^{o})
β	orientation of clast a-axis ($^\Theta$)
γ	inclination of clast a-axis (^{o})
ψ_p	maximum projection sphericity (dl)
σ	standard deviation of a distribution
τ	shear stress ($dyn.cm^{-2}$)
τ_o	critical shear stress ($dyn.cm^{-2}$)
λ	wavelength of in-phase waves (cm)
Θ	vector mean (^{o})
υ	kinematic viscosity ($cm^2.sec^{-1}$)

ACKNOWLEDGEMENTS

I would like to gratefully acknowledge:-
the Ontario Ministry of Colleges and Universities for a Fellowship (1973-74), and the National Research Council of Canada for a Scholarship (1974-76);
the Arctic Institute of North America at Kluane Lake, Yukon, for logistic support;
Blair Ross and Tom Kent for field assistance;
Dr. Barrie McDonald, formerly of the Geological Survey of Canada, for making the flume available to me;
Dave Morel, formerly of the Geological Survey of Canada, for technical assistance in the flume laboratory;
Dr. Brian Rust, the thesis supervisor, for assisting with my Canadian immigration, for encouragement with all aspects of the research, and for much invaluable editing of the text; and numerous fellow graduate students for their time in fruitful discussions, especially Jean-Marie Sempels and Paul Rochon with regard to computing and mathematical theory.

1.0 INTRODUCTION

The initial aim of the research programme was to study the sedimentology, hydrology and Pleistocene geology of Spring Creek alluvial fan on the north-east flank of the St. Elias Mountains, south-west Yukon (Plate 1). Field work in 1972 was designed to complement investigations by Williams and Rust (1969), and Rust (1972a, 1972b, 1975) of the neighbouring braided outwash deposits of the Donjek River. Owing to a sudden back injury in May 1973, it was not possible to complete the field programme, and a re-direction of the research was necessary. Fortunately, an opportunity arose to do some experimental flume work. The results of these laboratory investigations constitute the subject of this thesis: in certain sections, my observations on the Spring Creek fan are used as supporting field data and for the purposes of discussion.

There have been few experimental studies using natural gravel*-sized sediment. This kind of investigation requires large flumes; most existing facilities were

*The term 'gravel' is used according to the definition of Rust (1975, p.238), i.e. without any upper size limit, sediment in which particles coarser than 2mm predominate.

designed for sand-sized sediment in which the recirculation systems cannot admit particles coarser than granules. The gravel fraction must therefore be caught by a trapping device at the downstream end, and introduced artificially at the upstream end. These limitations essentially mean that experimentation with coarse-grained sediment only provides a simulation of a short channel reach in which equilibrium conditions prevail. Investigations of below-threshold behaviour of large clasts, with or without intermixed sand, encounter considerably fewer operational problems.

The earliest experimental studies of significance involving gravel-sized sediment were those of Rubey (1933) who analysed settling behaviour, and of Krumbein (1941) and Kuenen (1956) who investigated the nature of fluvial abrasion. In addition to these studies, coarse-particle sedimentology relies heavily on the works of Krumbein (1942), Johansson (1963, 1965), Fahnestock and Haushild (1962) and Kelling and Williams (1967). Although the subject of bedload transport has three aspects (i.e. initiation, transport and deposition), threshold velocity has been the aspect most extensively studied. For a particular gravel-sized clast, threshold velocity can be satisfactorily predicted by Helley's (1969) equation, taking into account its triaxial dimensions, shape, density and configuration on the bed. These were some of the parameters acknowledged by McDonald and Lewis (1973) to be the source of variation in computed threshold

velocities when engineering formulae were applied. Numerous river engineers, such as DuBoys (1879), Meyer-Peter and Müller (1948) and Einstein (1950) have evolved formulae to predict competence and capacity: many of these equations have been field-tested (Church, 1972) or critically analysed by flume experiments (Garg, Agrawal and Singh, 1971), and shown to yield rather inaccurate estimates of actual transport. The so-called 'Shields criterion' (Shields, 1936) has been widely employed, but has been recently challenged by Yang (1973).

Many workers (e.g. Potter and Pettijohn, 1963; Johansson, 1965; Rust, 1972a; Davies and Walker, 1974) who have closely studied field aspects of coarse-grained alluvium have stressed the need for more experimental work. Walker (1975, p.133) attempted to construct facies models for coarse-grained deposits, but found a deductive approach necessary because "there is very little directly applicable theoretical or experimental work on which we can build." Gravel-sized sediment has not shared in the rapid expansion of experimental sedimentology that has occurred since 1960. It remains rather unclear, therefore, as to which aspects of conglomerates hold genetic significance. This deficiency in our understanding, together with the apparent scarcity of sedimentary structures, has limited the scope of paleo-hydraulic interpretation and hampered the development of comprehensive facies models for coarse-grained sedimentation.

Plate 1: The alluvial fan of Spring Creek; it is located on the north-east flank of the Icefield Ranges in Yukon. Taken at 1630hrs, 11 June 1972, this photograph looks upstream toward the fanhead where the total discharge was gauged at $6.3 m^3.sec^{-1}$. Flow is braided around large longitudinal bars, and channels are characteristically wide and shallow with high clast size to depth ratios. The largest boulders in the foreground have maximum diameters of 46cm. The fan slope averages 0.019 and the valley side, some 2.5km. from the observer, has maximum relative relief of 1600m. The catchment of Spring Creek is largely ice-covered.

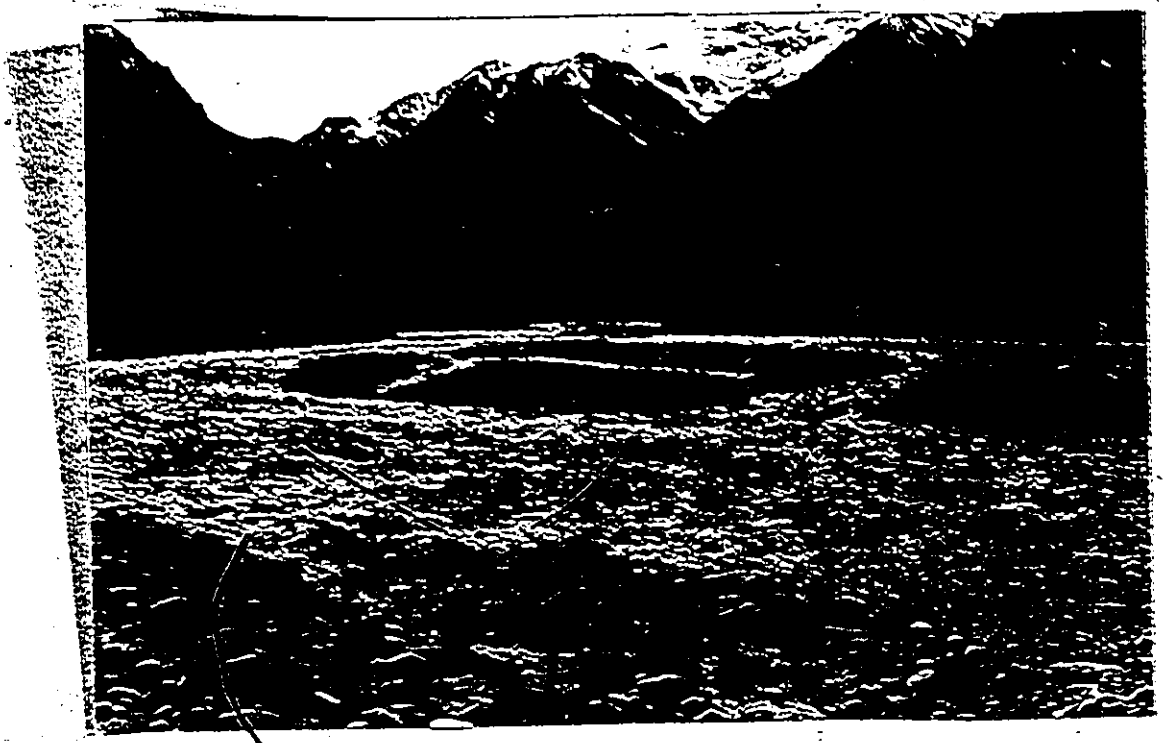

PLATE 1

COLOUR

The steady-state response of an experimental system to variation in sediment size, energy slope, discharge and depth can be easily determined, but information on the rates of response is difficult to obtain without remote sensing apparatus. Even in a flume, the water is seldom clear enough for direct observation of sedimentary structures in formation, either from the surface or through the side-wall glass panels. However, there are great advantages in being able to relate the observed character of the bed to a known flow condition. In high gradient, high velocity streams the field worker is obliged to speculate as the flow conditions which produced the structures observed in abandoned channels; in larger, more sluggish rivers remote sensing from a boat is often practicable and the problem is less acute.

The flume is especially useful for studies of coarse-grained sediments because fluvial conglomerates have few features that obviously indicate the conditions of deposition. This greatly contrasts with sand-sized sediments, for which there exists a clear and well-understood sequence of bedforms with increasing flow strength and sediment size. Moreover, in contrast to flume investigations using sand-sized sediment, where a vast number of previous studies have evolved an almost standard approach, laboratory work using gravel requires innovative techniques for experimental design as well as for data collection and analysis.

A problem, shared by flume studies involving sand bedloads, is that of 'equilibrium'. A flume investigation is considerably simpler, and the interpretations more direct, when two-phase flows are viewed in a steady-state, or equilibrium, condition. Simons and Richardson (1962) state that the criteria for recognising system equilibrium are parallelism between the slopes of the water- and bed-surfaces which manifests itself by a stable flow-bed interaction. Attainment of system equilibrium requires that constant discharge and depth be maintained for a period, the duration of which (at least for sandbeds) is directly proportional to the scale of bedforms (Allen, 1973). In the absence of remote sensing apparatus to monitor developments of the bed subjected to unsteady flow, experiments must necessarily be conducted under equilibrium conditions. This has drawbacks since natural flows rarely have the chance to attain a steady-state owing to hydrologic variation of a diurnal, seasonal, storm or catastrophic character: thus highly sophisticated laboratory analyses of sedimentary structures which have assumed equilibrium to exist must only be extended to natural channels with considerable caution (Miall, 1974, p. 1175). Since reactions to changes in a fluvial system are rarely completed, a state of 'quasi-equilibrium' normally prevails (Langbein and Leopold, 1964, p. 783). However, it can be argued that it is only through a

thorough understanding of the equilibrium condition that disequilibrium can be recognised, and the effects of unsteady flow and lag be ascertained.

In conclusion, therefore, it must be said that providing the limitations in scope of a flume study are realised at the outset, the state of knowledge in clastic sedimentology can only expand, and improve in precision, when aided by careful laboratory experiments.

1.1 The Descriptive Framework of Fluvial Conglomerates

Walker (1975) proposed four sedimentological features of coarse-grained deposits which contribute to their descriptive framework. These are sorting and size distribution, fabric, stratification and grading. Each of these features are briefly reviewed below with regard to their importance as tools in paleo-environmental discrimination.

i) Sorting and size distribution:-

Although coarse-grained deposits vary from clast-supported (with or without a closed framework) to matrix-supported, little environmental significance appears to have been attributed to sorting. Braided environments, owing to the spatial and temporal variability in hydraulic conditions, are generally characterised by a wide variety of sedimentary facies (Williams and Rust, 1969; Rust, 1972b).

Sorting of size modes, however, does allow certain conclusions regarding the transport process and competence levels of the paleoflow. Walker (1975, Figure 7-3) determined empirically a curvilinear function relating size of gravel rolled on the bed to the size of sand than can be transported by suspension in the same flow. For clast-supported, closed-framework conglomerates, this allows one to distinguish between simultaneous and later infiltration of matrix material. Dyer (1970) considers that, on the basis of theoretical grain packing, a figure of about 25% sand in a sandy-gravel separates these two modes of deposition.

Using the diagrams of Novak (1973) and Baker and Ritter (1975), one can also approximate the competence of the paleoflow given accurate data on clast sizes.

ii) Fabric:-

Fluvial gravel fabric typically comprises two elements - upstream dipping imbrication, and preferred orientation of the a-axis normal or parallel to the flow direction. Well-developed fabrics are an indication that individual clasts have moved freely in the transporting medium and have assumed a depositional configuration that results from forces acting on it. In contrast, random fabrics imply inability of the clasts to respond individually to stresses imposed by the flow.

As will be shown later, there is growing evidence that current-normal a-axis fabrics is the 'norm', but that catastrophic river flows and subaqueous density flows with predominantly suspended transport are characterised by current-parallel fabrics. For this and other reasons, coarse-particle fabric would appear to be a good tool not only for discriminating sedimentary environments, but also for estimating aspects of the paleoflow regime.

iii) Stratification:-

It is not clear whether types of stratification possess any reliable environmental significance. Bedding may be outlined by changes in clast size, sorting, lithologic composition or fabric. In coarse-grained, heterogenous sediments which characterise proximal reaches of braided outwash systems, the internal structure of longitudinal bars is dominated by poorly-defined, sub-horizontal bedding or massive bouldery-gravel, with only rare cross-stratification (Rust, 1975). Units of sedimentation are difficult to recognise because aggradation is frequently interrupted by surficial reworking in such an environment. According to Clifton (1973), fluvial gravels are characterised by low levels of textural and structural organisation.

iv) Grading:-

Both Doeglas (1962) and Walker (1975) consider grading to be rarely developed in a braided stream environment: whether 'distribution grading' or 'coarse-tail grading' predominates does not appear to have been established. While a waning flow event could result in the deposition of a graded bed, its potential for preservation in the stratigraphic record seems low in view of reworking. If present however, its development is symptomatic of discrete flow events in which competence levels systematically changed, and as such provides insight into the nature of bedload transport. In resedimented conglomerates, grading is more abundant and the various types have environmental significance (Walker, 1975).

In addition to the above, recent literature indicates that bedforms, clast morphology and the relationship between bed thickness and coarsest percentile of the contained sediment may also constitute useful tools in the analysis of paleo-environments.

v) Bedforms:-

The possibility of being able to recognise large-scale bedforms at outcrop seems slight. Eynon and Walker (1974) however, claim the existence of a single, large braid bar in a sand-gravel pit of Pleistocene outwash deposits. Their work

was greatly assisted by excellent exposures, with faces having been cut fortuitously perpendicular and parallel to the apparent paleoflow direction. This situation would be rarely encountered in more ancient successions. The application of remote sensing techniques to the field study of large-scale gravel bedforms in relatively deep channels (Galay, 1967; Fahnestock, 1973) appears to be a rewarding method of investigation.

Distinct, within-channel bedforms comparable to the ripple, dune, plane bed and in-phase wave phases of sand beds are both less conspicuous and seemingly more rarely developed in coarse-grained alluvium. Those small-scale bedforms which have been described include transverse ribs (McDonald and Banerjee, 1971), stone cells (Gustavson, 1974) and Ostler lenses (Martini and Ostler, 1973).

Transverse ribs - narrow, linear, current-normal accumulations of coarse clasts - have been shown experimentally to form beneath an upstream-migrating hydraulic jump (McDonald, 1976), but Gustavson (1974) follows Boothroyd (1972) in believing that they are the product of antidune flow. Stone cells, being somewhat similar to transverse ribs in both morphology and facies occurrence, are considered by Gustavson to be the result of three-dimensional antidunes.

Ostler lenses - isolate mounds of winnowed open-framework gravel - have been attributed to lower-flow regime conditions in channel riffles.

Careful examination of gravel bluffs within an active outwash tract by Gustavson (1974) failed to reveal preserved equivalents of these bedforms, nor were they found in cut-banks bordering Spring Creek. Their potential for preservation and/or ease of recognition therefore appears to be low.

vi) Clast morphology:-

Both Sames (1966) and Dobkins and Folk (1970) showed that for isotropic lithotypes, there are subtle but distinct differences in the shape and form of fluvially abraded clasts as opposed to those formed in the littoral environment. However, internal properties like bedding, jointing and foliation are more important sources of inequidimensional form. Irrespective of these influences, there is evidence (see Section 2·51) for an ellipsoidal tendency in fluvial clasts. Brock (1974) found few indications that coarse-clast morphometry was a satisfactory tool for discriminating sedimentary environments. Bradley, Fahnestock and Rowekamp (1972) concluded that shape-development was lithologically dependent and showed, through abrasion-tank experiments, that proximal-distal changes reflect shape sorting rather than the effects of abrasion.

Proximal-distal changes in clast size, sphericity and roundness have been well documented in outwash systems, but there are few established principles and the effects of sorting versus progressive abrasion have not been unravelled.

vii) Bed thickness and Clast size:-

In an aggradational sequence in which there has been minimal reworking, Bluck (1967) and Steel (1974) found a positive relationship between bed thickness and the maximum clast size contained. Respectively, these features are considered to reflect the competence and sediment discharge of discrete flow events. The position of the regression line and the value of the correlation coefficient may then be used for semi-quantitative conclusions about the paleo-environment. Bluck found that the wedge-shaped strata of fanglomerates best display the relationship between size and thickness, but admitted that this may not be a useful criterion for distinguishing subaqueous from subaerial fans.

1.2 Aspects of the Descriptive Framework amenable to Laboratory Study

In view of the earlier-described limitations of flume work using large clasts, few of the sedimentary features of conglomerates which contribute to their descriptive framework are amenable to laboratory study. Normal-sized flumes, with their limited workable lengths, are only suitable for

studying aspects of flow-bed interaction under non-aggrading, equilibrium conditions. There can be little prospect of ever being able to reproduce aspects of stratification and grading, or indeed anything but the smallest scale of coarse-grained sedimentological features.

The concept of 'scale' in a fluvial system is rationalised by means of a 'sedimentary structure hierarchy' (Allen, 1966; subsequently modified by Miall, 1974). The hierarchy comprises six ranks of structures, in which the highest ranking are the largest scale features (i.e. the entire river system) and the lowest ranking are the smallest, within-channel features (i.e. bedforms). Miall emphasized the fact that directional variance, or paleocurrent variability, is inversely proportional to rank. In terms of the sedimentary structure hierarchy, it is considered that 'rank #6', and to a lesser extent rank #5', structures, (i.e. clast fabric, within-channel bedforms) embrace the possible range of conglomerate features amenable to a flume study. Fabric seems to be a more profitable line of enquiry in view of the low preservation potential and/or difficulty in the recognition of small-scale bedforms.

The commonly accepted viewpoint regarding flow-bed interaction is that not only can the flow 'deform', or mould, the bed but that this induces structural changes in the flow itself (Southard, 1975, p. 8). The dissipation of.

energy on a sand bed is mainly due to 'form roughness', whereas 'grain roughness' predominates in channels transporting pebbles, cobbles or boulders. In the latter situation, an equilibrium flow-bed interaction has yet to be quantitatively defined, although as shown in the ensuing section the literature abounds in qualitative statements which describe well-developed fabric as a stable depositional configuration.

The methodology of field-workers interested in measuring fluvial gravel fabric seems to have been largely conditioned by the morphology of the clasts which comprise the population available for sampling. Thus imbricated flat clasts have been measured for the azimuth and inclination of the a-b plane, and elongate clasts for the orientation or azimuth of the a-axis: more equidimensional clasts, owing to the greater care required to measure their axial directions, have generally been excluded from the sample. One may interpret this sample bias as a feeling that highly prolate clasts, for example, would respond more 'accurately' to the flow condition, and thereby display more perfect relation to the current. The idea that shape influences the degree of equilibrium clast response is an interesting one and deserves more attention.

1.21 Clast fabric - a literature review

More than 10 years have elapsed since the extensive literature review of clast fabric by Johansson (1965). In this period, field studies of coarse-grained sediments have been more frequent and because of their more quantitative approach and their better definition of the paleo-environment, a more thorough understanding of gravel fabric is now possible. The following literature review utilises both the recent studies and the more pertinent investigations previously reviewed by Johansson.

Laming (1966) seems to have been the first field-worker to have recognised the morpho-genetic influence of sorting and size distribution on the fabric pattern. In his study of a fluvial redbed sequence, Laming found that the proximal and distal portions of an alluvial fan environment were characterised by clast-supported and matrix-supported sediments, respectively. Corresponding to this down-fan textural gradation were "two intergrading styles of imbrication" (p. 946): he termed these 'contact imbrication' (in the case of the clast-supported deposits) and 'isolate imbrication' (in the case of the matrix-supported deposits). The genetic implication is that imbrication of the contact variety results from 'shingling' of one clast against another (Laming, 1966; Rust, 1972a) causing imbrication to be instantaneously attained with deposition, whereas isolate clasts become imbricated through the action of current-crescent scour activity (Sengupta, 1966).

Sorting also seems to have a considerable effect both direct and indirect, on a-axis orientation - both its geometric relation to flow direction and its degree of preferred orientation.

In the field, analysis of gravel fabric is impeded by the lack of information on flow variables. It is therefore not surprising that workers have strived to explain its variability merely in terms of size and shape properties of the component clasts.

1.211 Imbrication

Irrespective of a-axis orientation relative to flow direction, upstream-dipping imbrication has always been interpreted as a hydrodynamically stable bed structure. However, the compilation of relevant literature on this apsect of imbrication does not reveal its precise nature in any quantitative manner (Table 1). Johansson's (1965) statement appears to be the most detailed in this respect.

In spite of the claim that various properties of the clasts influence the angle of imbrication (Table 2), the mean angles of imbrication observed by various workers (Table 3) do not span the full possible range of 0 - 90°. Clearly, mean dip angles are largely confined to the 5 - 35° sector. The predominance of low to moderate angles of imbrication has not been the subject of any detailed laboratory

TABLE 1: A review of the literature regarding the nature of stability associated with fabric.

Reference	Nature of the Stability
Jamieson, 1860 (p.349)	Speculated that preferred positions of clasts are those which offer greatest resistance to movement.
Becker, 1893. (p.53-54)	Observed that when clasts are dropped into a stream, there is a tendency for them to rotate until the maximum projection plane faces the flow direction.
Johnston, 1922 (p.388)	"...stones finally assume a position in which they offer least possible resistance to the current..."
Lane and Carlson, 1954 (p.458)	For clast-supported bedloads, they considered that imbrication is increasingly stable with higher velocity.
Johansson, 1965 (p.16)	Considered that the stability associated with imbrication is inversely proportional to the degree of clast flatness as well as to flow velocity and turbulence.
Laming, 1966 (p.945)	"...it appears that stability depends on the balance between particle shape, bed roughness and inclination of the sedimenting surface..."
Sengupta, 1966 (p.367)	For matrix-supported bedloads, he observed that "a final stable position" is achieved by gravity sliding into the current-crescent scour.
Allen, 1971 (p.90)	"...assuming the particle comes to rest on a bed of similar particles, the most stable position for the particle will be that when the forces acting on it are in equilibrium and when the forces of removal are at a minimum..."
Blatt, Middleton and Murray, 1972 (p.108)	"...the flow impinging on an imbricated particle exerts a drag force that presses the particle to the bed and acts against the hydraulic lift..."
Rust, 1975. (p.245)	Considered that the degree of clast contact increases the stability of imbrication.

TABLE 2: A review of the literature regarding controls on the angle of imbrication

Reference	Suggested controls
Cailleux, 1945 (p.385-389)	Proportional to clast concentration on the bed; for 'contact imbrication', inversely proportional to clast size and flatness.
White, 1952	Proportional to clast size.
Unrug, 1957	Proportional to channel slope and clast size.
Johansson, 1963 (p.90-91)	For matrix-supported gravels, he considered the angle of imbrication of oblate clasts to depend upon a) processes connected with current-crescent scour, b) their gravitational weight, c) shear stress and d) "...the friction, which is a function of the mantle area in relation to its mass, the packing and roughness of the substratum and the particle" "... probably the friction as a function of pebble shape and the gravity force are the most important."
Johansson, 1965 (p.16)	"...the particle dip seems to increase with increased water depth, increased particle size, decreased prolateness and increased roundness (causing less form resistance to the flow)..."
Laming, 1966	Proportional to clast size, and inversely proportional to clast concentration on the bed.
Sedimentary Petrology Seminar, 1966 (p.279)	Inversely proportional to clast size - "...an indication that the very large particles of most mixtures are not hydraulically stable when their angle of inclination is high..."
Katzung, 1971	Proportional to channel slope.
Rust, 1975 (p.245)	"...no conclusive relationship between pebble size and inclination..."

TABLE 3: A review of the literature regarding the angle of imbrication(*)

Reference	Principal orientation of clast a-axes	Reported angles
Krumbein, 1939	current-parallel	mean: 36^{o}
Cailleux, 1945	current-normal	range: $15-30^{o}$
Folk and Ward, 1957	variable	range: $20-30^{o}$
Unrug, 1957	current-parallel	range: $10-30^{o}$
Johansson, 1963	current-normal	range: $10-20^{o}$
Laming, 1966	current-parallel	"usually less than 25^{o}" (p.946)
Sedimentary Petrology Seminar, 1966	current-normal	modal class: $20-25^{o}$
Helley, 1969	current-normal	range: $0-30^{o}$
Eynon and Walker, 1974	not stated	for "bar cross side facies" and "shallow braided stream facies", ranges are $22-26^{o}$ and $12-22^{o}$, respectively.
Rust, 1975	current-normal	range of means: $26-33^{o}$

*N.B. The above-listed studies are for the fluvial environment only, and exclude the generalised reports of textbooks.

analysis, although it would seem logical to attribute this feature to some a hydrodynamical aspect of the flow-bed interaction. Moreover, while the field characteristics of imbrication have been fairly well-documented, the controls on its variability are very poorly understood. The contents of Table 2 may be summarised as follows:

i) the angle of imbrication appears to be inversely proportional to the degree of clast flatness (Cailleux, 1945; Johansson, 1965) and

ii) directly proportional to channel gradient (Unrug, 1957; Katzung, 1971);

iii) the observations are not conclusive with regard to the effect of clast size, although there is some support for an inverse relationship in clast-supported gravels (Cailleux, 1945 ; Sedimentary Petrology Seminar, 1965).

iv) there is no consistency regarding the effect of clast concentration on the bed.

The reasons why shape, channel gradient and clast size exert a control on the angle of imbrication are as yet unknown. Johansson (1965, p. 49) stated: "For certain conclusions about the dependence of particle dip in different conditions a thorough factor analysis is needed, including measurements of hydrodynamic parameters, sediment feed, sorting, particle sizes, shape and mass, and pressure distribution under controlled laboratory conditions".

1.212 Orientation

A-axis orientation has attracted speculation as to its relation to different modes of transport and levels of flow competence. Johansson (1965) lists three possible types of orientation patterns with respect to flow direction:

i) transverse,

ii) parallel, or

iii) a combination of i) and ii), but one mode generally predominant.

The field study by Teisseyre (1976) indicates that oblique orientations are developed near channel margins. Johansson recognised that secondary oblique maxima often appear in samples but that they should not be assigned as much genetic significance as the modes orientated normal or parallel to flow.

In attempting to understand the reasons for different a-axis orientation patterns, it would seem instructive to utilise the evidence from all environments where fluid flow is unidirectional: this includes normal and catastrophic open-channel flow as well as subaqueous turbidity flows. A drawback in the interpretation of clast orientation is that few fabric analyses for modern streams have reported details of the flow, although there are many practical reasons why this is not easily achieved. The hydraulic

data for turbidity flows are gained through theoretical analysis, laboratory simulation and speculation.

A review of the literature on preferred a-axis orientation points to two rather different kinds of approach: i) reasons for the principal a-axis mode, whether it be current-normal or current-parallel - this has been attributed to large-scale properties of the flow, (Table 4) and ii) reasons for the spread of deviations about the principal mode, - which has been attributed to variables pertaining to the bed surface (Table 5) and to the clasts themselves (Table 6).

Johansson (1965, p. 15) considered orientation to be a "function of velocity, turbulence and shearing stress of the flowing water, the particle mass, shape and position, the quantity of transported and deposited material and the collision frequency".

Tables 4, 5 and 6 suggest that the isolate or contact nature of the bed is the major control on the patterns of clast orientation. Current-normal orientation, with or without imbrication, appears to be ubiquitous for isolate clasts but is best developed by large prolate clasts. A high collision frequency introduces a random element into the orientation pattern. For contact bedloads, it is clear that both current-normal and current-parallel orientation

TABLE 4: A review of the literature regarding the effect of flow variables on a-axis orientation

Reference	Depositional environment	Suggested effect
Richter, 1936	proglacial stream	Low stage rolling produced current-normal orientation; at high stage, flow capable of saltating large clasts and this evolves current-parallel orientation.
Krumbein, 1939	catastrophic flood in ephemeral stream	Current-parallel orientation, although the degree of preferred orientation decreased downstream, which was attributed to increased sphericity and roundness in the same direction.
Lane and Carlson, 1954	canal test sections	Attribute current-normal orientation to rolling motion in transport.
Johansson, 1965	mountain streams	High velocity and turbulence cause decreased regularity of orientation.
McDonald and Banerjee, 1971; Boothroyd, 1972	proglacial braided outwash	Clasts comprising transverse ribs oriented normal to flow: in view of shallow flow and coarseness of material, clasts presumed to have rolled.
Walker, 1975	sub-aqueous flows	On the basis of an exhaustive review of the literature concerning resedimented conglomerates, considers current-normal orientation to be the characteristic result of clasts rolling on the bed and interprets current-parallel orientation as the result of largely suspended, or dispersed, transport by sub-aqueous debris flows.

TABLE 5: A review of the literature regarding a-axis orientation and the effect of clast concentration

Reference	Clast concentration on the bed	Suggested influence
Hunzicker, quoted by Twenhofel, 1932	isolate	Observed that deposition of pebbles on a sandbed was followed by rotation to a current-normal orientation - this being achieved through current-crescent scour.
Cailleux, 1938	isolate	Observed that rolling and sliding, with a-axes aligned transverse to flow, predominates in the movement of pebbles on a sandbed so that a current-normal orientation pattern evolves.
Johansson, 1963	variable	"...a preference for longitudinal orientation increasing with higher contact frequency..." (p.11)
Johansson, 1965	isolate	"...it might be considered evident that scattered bed-load transporting pebbles and cobbles on a sandy sub-stratum take up a distinct orientation transverse to the current direction" (p. 18). "...tight-settled particles on a hard sub-stratum exhibit a more diffuse orientation pattern, with varying direction maxima and a relatively high frequency of oblique positions..." (p. 18).
Laming, 1966	-	Current-normal orientation is favoured by "...smoother beds and downstream-dipping surfaces..." (p. 945).
Rust, 1972a	-	Higher degrees of preferred orientation normal to flow were found for isolate clasts.
Rust, 1975	contact	"...smaller particles are constrained by the necessity of fitting into the spaces between the larger clasts, and they are oriented by flows that are influenced by the presence of the larger particles..." (p. 244).

TABLE 6: A review of the literature regarding the effects of clast shape and size on a-axis orientation

Reference	Suggested effect
Clast Shape	
Krumbein, 1939	Postulated that increased roundness and/or sphericity causes a more highly preferred orientation in the downstream direction.
Unrug, 1957	"...the control exercised by the shape of pebbles...is observable during reorientation at the moment of deposition...prolate clasts are subjected to the strongest reorientation and retain a stable position even when the longest axis inclines downstream...pebbles with other shapes are less subject to reorientation..." (p. 256).
Johansson, 1965	Clast asymmetry has an adverse effect on preferred orientation.
Sedimentary Petrology Seminar, 1965	Found no apparent control of clast properties on the angular spread about the current-normal mode: "...this lack of effect may result from the fact that during floods, the only time when gravel is transported, the orienting flow is sufficiently penetrative, so that variation of size and flatness has only minor hydraulic importance..." (p. 281).
Laming, 1966	"...particles of bladed form tend to orient parallel to the current, and those in the roller shape class, perpendicular..." (p. 945).
Sengupta, 1966	Considered that prolate clasts are orientated transverse to flow, but that for any other shape...the only stable position is when the long axis is oriented parallel to flow.
Kelling and Williams, 1967	Found that prolate clasts display a more highly preferred orientation that oblate ones.
Clast Size	
Unrug, 1957	128-256mm and 64-128mm size grades displayed tendency for current-parallel and current-normal orientation, respectively: attributed to the fact that size governs depositional order and so large clasts only are able to be deposited in their most stable (i.e. current-parallel) positions.
Johansson, 1965	Concluded that size has an effect if flow is sufficiently competent to saltate or suspend the smaller clasts, in which case current-parallel orientation results: smaller clasts are also more susceptible to collisions and therefore tend to have oblique orientation.
Sedimentary Petrology Seminar, 1965	Found no correlation between clast size and the amount of angular deviation about the current-normal mode.
Rust, 1972a	Increasing clast size found to have a positive effect on the degree of preferred orientation.

can evolve. Dominantly current-parallel orientation appears to the result of suspended transport, whether the sedimentary environment is that of a highly competent river in flood (Krumbein, 1940) or a turbidity current (Walker, 1975). Bedload transport by traction, in which the clasts tend to rotate about their longest dimension, evolves current-normal orientation. To a large extent, the configuration of clasts observed at deposition reflects their configuration during transport: however, owing to different rates of settling and competence (corresponding to the size, shape and density of clasts undergoing transport) this relation is often imperfectly developed. Table 6 does not reveal any consistency as to the role of clast properties, particularly for orientation patterns derived from contact bedloads.

2.0 EXPERIMENTAL WORK

2.1 Purpose and objectives

Many authors (e.g. Potter and Pettijohn, 1963; Johansson, 1965; Rust, 1972; Davies and Walker, 1974) have stressed the need for detailed laboratory investigations of coarse clast fabric. It is apparent from the literature that where interpretations have been attempted, they have been largely based on intuition or on theoretical reasoning, for as Johansson (1965, p. 49) points out, the hydrodynamic conditions are known too incompletely to understand the forces affecting fabric.

Experimental studies were carried out in the large flume of the Geological Survey of Canada in Otttawa. Their purpose was three-fold:-

i) to gain a better understanding of the hydrodynamic variables and clast parameters which govern:

a) observed variability of clast fabric

b) development of certain within-channel bedforms, and

c) entrainment, transport and deposition of large, inequidimensional clasts;

ii) to realise the full potential of clast fabric as a tool in paleoenvir nmental studies, particularly with regard to estimating the direction and magnitude of paleoflow; and

iii) to recognise through the preceding lines of investigation the most hydrodynamically sensitive parameters that should be employed to describe structures composed of coarse-grained poorly-sorted sediment.

Ideally, calculations of paleoflow variables should be accurate. However, because of incomplete exposure and the complex nature of flow-bed interactions, severe limit-

ations are often imposed on such studies. Hence, in an investigation like that of Cant and Walker (1976) where a paleoflow analysis was attempted for Devonian sandstones of braided river origin, variables were estimated and assumptions made. Their results compared favourably with those obtained from similar studies in modern braided alluvium.

2.2 Flume apparatus

The flume of the Geological Survey of Canada has been fully described by McDonald (1972), and so only a brief summary is necessary here.

Designed primarily for research on fluvial processes, the flume is recirculating, tiltable and has many accessory devices to assist the measurement of flow and bed parameters (Fig. 1). The straight, rigid flume channel has the following dimensions: length 18.3m., width 0.76m. and depth 0.6m. However, owing to entrance and exit effects, the channel has an effective 'workable length' of 10m: within this mid-channel portion the flow is undisturbed. The flow-return system (p. 4-7, McDonald, 1972) recirculates the sand-water mix, but coarser sediment must be both introduced at the upstream end and caught at the downstream end above the tail tank. A mobile instrument carriage, mounted on rails above the glass side-panels, is equipped with a mechanical point-gauge (see Fig. 1 and Fig. 10 of McDonald, 1972) which enables flow depth to be measured to the nearest mm. With this device, it is possible to measure any point within the flume channel by means of three mutually perpendicular co-ordinates which parallel the x, y and z axes of the flow reference frame.

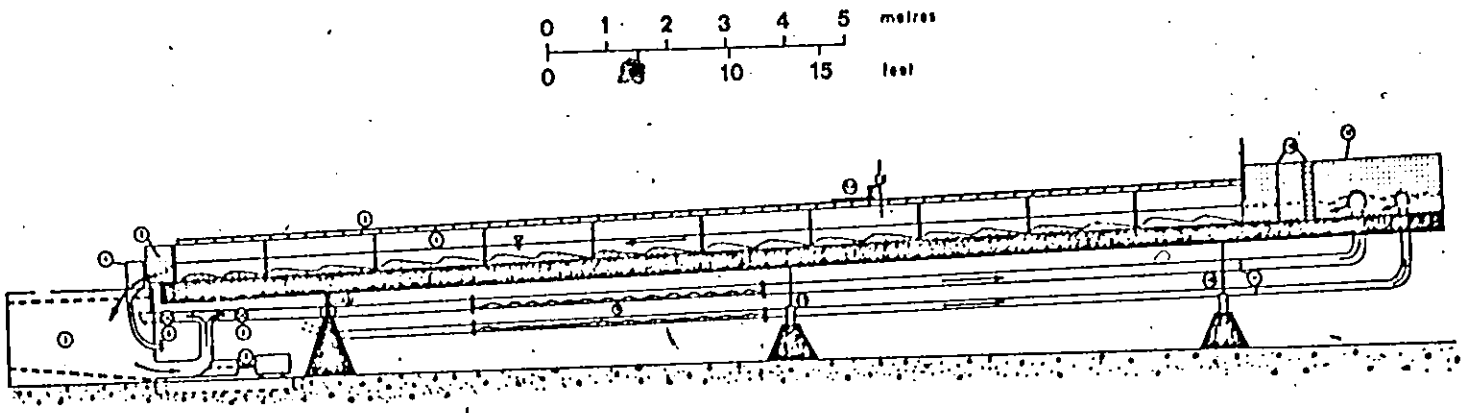

1. main channel
2. rails
3. tailgate assembly
4. total load sampler
5. tail tank
6. flow-control valves
7. pump and motor
   (small pump, not shown, feeds the 25cm return pipe)
8. pivot support
9. transparent sections of return pipe
10. jack supports
11. orifice plates
12. headbox
13. baffles
14. instrument carriage

Figure 1: Generalized longitudinal diagram of flume.
GSC photo 201787.

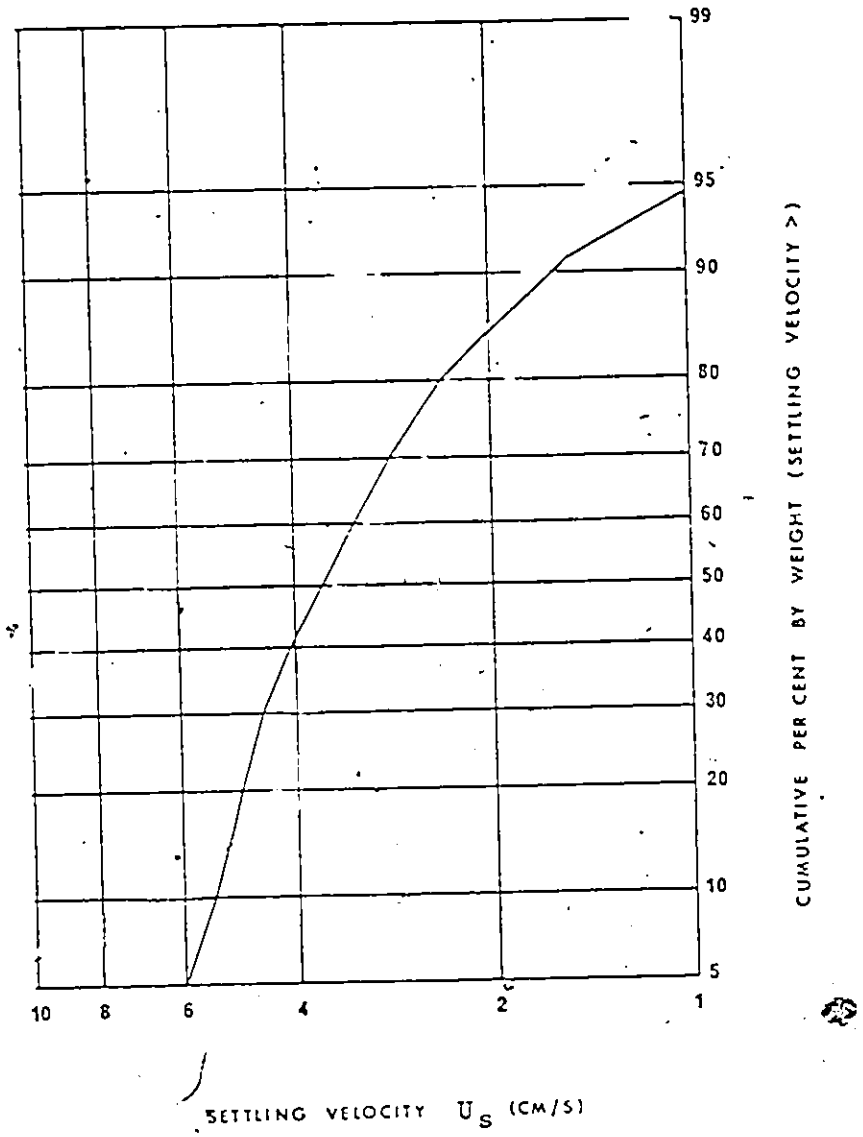

Figure 2 : Distribution of settling velocity for the sand used in the experiments of clast behaviour below their transport threshold.
Modified from Fig. 6A, Forbes (1973).

2.3 Design

The experiments were divided into two groups on the basis of bed character.

The first group (EK3D-1 to -14) investigated the behaviour of isolate clasts on a sandbed at velocities below their threshold for movement. The chief objectives were to examine the nature and development of isolate gravel fabric, to evaluate the role of current-crescent scour activity and to establish criteria for recognising hydrodynamic stability in matrix-supported gravels. The same population of 31 clasts was used in these runs, and their spatial arrangement on the sandbed was kept constant: this served to minimise the number of variables to be considered in the analysis of process and response. Proximity of adjacent clasts varied between 14 and 46cm (larger clasts were spaced further apart, and vice versa): also, clasts were located at least 18cm from the side-walls to avoid the zones of reduced velocity. Bulk samples of the sand have a median settling velocity of 3.65 $cm.sec^{-1}$ with a standard deviation of 0.22$cm.sec^{-1}$ (Figure 2). Before each run equilibrium was established, the sandbed being maintained at a thickness of 10-15cm. Clasts were distributed in their assigned positions with a-b planes horizontal, and a-axes laid parallel (in runs EK3D-2 and -4) or transverse (in runs ED3D-5 to -14) to flow direction. The runs spanned both the lower- and upper-flow regimes, with depth being kept between 9 and 12cm. Following run shutdown, the clasts were carefully exposed in the sandbed using a spatula.

The second group of experiments (EK3D-15 to -18) were designed to elucidate some aspects of contact bedloads, in particular transport velocities, small-scale bedforms and fabric. These runs generally involved the use of a large number of clasts. Flows were sub-critical, but were competent to transport moderately sized cobbles. At mean flow velocities approaching $1 m.sec^{-1}$ it is not possible to maintain a stable sandbed in the flume. It was therefore considered more meaningful to artificially roughen the bed than use the hydraulically smooth aluminum floor. This was achieved by laying down a mat (manufactured by the 3M company) with a granular surface. The mat, having a surface of sand grains (-1 to +1ϕ diameter) adhered in place by thin coating of lacquer, generated considerable 'grain roughness' and effectively retarded the flow near the bed. Clasts were manually introduced in random position at the flume's upstream end, and deposition was induced artificially by a low mesh barrier at the downstream end.

2.4 Flow Variables

During each run, the following flow variables were measured:-

i) slope, S

ii) flow discharge, Q ($l.sec^{-1}$),

iii) flow depth Y (cm.),

iv) surface velocity U_{surf} ($cm.sec^{-1}$),

v) a velocity profile

vi) water temperature (^{o}C).

McDonald (1972) outlined the methods for determining these parameters, but a few additional details are required. Owing to their use in calculating mean flow velocity, Froude Number etc., it is extremely important that flow discharge and depth be measured as accurately as possible. The value of discharge assigned to a run is based on several manometer (p.10, McDonald, 1972) readings taken at intervals. With a sandbed in the flume, precise measurement of depth is difficult owing to the irregular nature of the bed- and water-surfaces. To minimize error, values of depth assigned to each run represent the mean of ten separate determinations at metre intervals along the centre line of the workable length. Dune beds involve the largest possible error, but the rapid, and often erratic migration of upper-flow regime in-phase waves also often prevents precise depth determination. In an attempt to correct for the transient nature of the system during measurement, an additional depth traverse was made approximately one hour after the first: tabulated values of depth for runs in which high-amplitude dunes or breaking antidunes were the stable bed phase therefore represent the mean of twenty measurements. The discrepancy between the results of the two traverses rarely exceeded 5mm. Precise determination of depth requires a remote sensing device, such as the laboratory echo sounder

described by Richardson, Simons and Posakony (1961). Surface velocity was determined by timing the passage of corks through the central 10m. section. A pitot tube, for which point velocity (U) is related to the elevation difference between the static and dynamic water levels (ΔH) by the equation

$$\Delta H = 0.0006U^2,$$

was utilised to obtain velocity profiles. Over sandbeds, the pitot tube was located away from zones of flow separation. Water temperature, measured to the nearest 0.1°C., was not controlled, but only varied between 17 and 20.5°C during the experimental period.

By means of an APL programme called HYDRAULIC (see Appendix), the measured values of flow discharge, depth and slope were employed to compute values for the following additional flow variables:-

i) mean flow velocity, $\bar{U}(cm.sec^{-1}) = \frac{1000(Q)}{76.68(\bar{Y})}$

ii) mean shear velocity, $U_*(cm.sec^{-1}) = (g.\bar{Y}.S)^{\frac{1}{2}}$

iii) Froude Number, Fr (dimensionless) $= \frac{\bar{U}}{(g.\bar{Y})^{\frac{1}{2}}}$

iv) Reynolds Number, Re (dimensionless) $= \frac{\bar{U}.\bar{Y}}{\upsilon}$

Hydraulic data for the experimental runs is given in Table 7.

TABLE 7: Hydraulic data of the experimental runs

Run #	Sand bedform	S(m/m)	Q(l/s)	Y(cm)	U_{surf}(cm/s)	$\bar{U}$(cm/s)	U_*(cm/s)	Fr	Re
Runs with a sand bed									
EK3D-14	ripples	.00070	21	10.9	31.7	24.6	2.7	.238	26,733
-6	ripples	.00114	18	8.2	34.9	28.8	3.0	.322	23,545
-8	dunes with superimposed ripples	.00341	28	9.9	60.6	36.9	5.7	.374	36,422
-11	dunes	.00182	25	8.4	43.3	38.5	3.9	.426	32,243
-13	dunes	.00166	45	11.9	65.5	49.7	4.4	.460	58,966
-10	degenerate dunes	.00310	50	11.7	76.1	55.6	5.9	.519	64,857
-9	plane bed	.00139	61	11.5	85.0	69.1	4.0	.651	79,227
-7	plane bed	.00367	43	8.8	96.2	63.9	5.6	.690	56,064
-4	in-phase waves	.00137	69	12.0	104.9	74.7	4.0	.687	89,372
-2	breaking antidunes	.00200	74	12.0	97.1	80.4	4.8	.740	96,191
-5	breaking antidunes	.00161	69	11.1	94.0	81.4	4.3	.780	90,084
-12	breaking antidunes	.00328	83	12.1	117.4	89.5	6.3	.821	107,971
Runs with an artificially roughened bed									
-15	_____	.01550	44	9.0	227.3	64.3	10.4	.683	57,697
-16	_____	.01510	49	8.6	232.6	74.3	10.2	.809	63,707
-17	_____	.01510	57	8.9	225.7	83.6	10.3	.896	74,181
-18	_____	.01098	72	10.3	198.7	91.4	10.5	.910	93,860

TABLE 8: Size and morphological characteristics of the total sample used in the experimental work.

Sample size = 140

Size (cm):	Range	Mean
a-axis	6.3 - 20.2	10.27
b-axis	3.3 - 13.4	7.28
c-axis	1.1 - 6.7	3.44

Nominal diameter, d_n, is the preferred measure of clast size: it is defined as the diameter of a sphere with equivalent volume to the clast (Wadell, 1934b).

Morphology:

a) Maximum Projection Sphericity, Ψ_p (Sneed and Folk, 1958)

mean	0.55
standard deviation	0.06
range	0.31 - 0.84

b) Oblate-Prolate Index, $\overline{OP}$ (Dobkins and Folk, 1970)

mean	-2.47
standard deviation	7.26
range	-29.24 - 14.87

2.5 Material

Gravel used in the experiments was collected from a local Pleistocene outwash deposit in a pit near Stittsville, Ontario. One hundred and forty clasts were selected for their variable size, shape and lithologic composition; highly angular or broken fragments were excluded. To evaluate the response of individual clasts, each was identified by a number using waterproof ink on a small patch of white Taperaser typists' correction fluid, and lightly sprayed with clear lacquer. These marks resisted the repeated effects of fluvial abrasion, although the successive wetting and drying started to break down some fine-grained lithotypes.

The triaxial dimensions of the clasts (a, b and c) were determined according to the standard technique (Griffiths, 1967) to the nearest mm. The size and morphological characteristics of the sample are outlined in Table 8: statistics were computed by means of APL programme FOLKMUSIC (see Appendix). The sample is characterised by moderate values of sphericity, and a tendency toward oblateness. Roundness was not determined for the

whole sample, but visual appraisal shows that the clasts are mainly sub- to well-rounded. All clasts were weighed, and those used in the isolate experiments were immersed in graduated tanks to determine their volume.

2.51 Clasts as ellipsoids

Large sedimentary clasts have often been likened to ellipsoids. In the formulation of his 'intercept sphericity' measure (Krumbein, 1941b) expressed clast volume by assuming it to be a triaxial ellipsoid with axes a,b and c. He considered that "statistically, they may be represented by such a form" (p. 71). When Sneed and Folk (1958) introduced their 'maximum projection sphericity' measure, they retained Krumbein's assumption. Williams (1965) also followed this idea, while Gibbons (1959) and Helley (1969) utilized the ellipse as the plane geometric shape encountered in sections through clasts.

Flemming (1965) favoured the ellipsoid for comparison with natural forms because it is "a smooth form enclosing the maximum volume for minimum surface area for given axial lengths . . . skew ellipses fit well to the forms of actual particles, and agree remarkably with those which are intuitively seen to be well-rounded but not symmetrical" (p. 382). If the axes intersect at a common point, the

ellipsoid is termed symmetric: in cases of clast asymmetry (Cailleux, 1945), the ellipsoid is said to be skewed. Table 9 describes the various types of symmetric ellipsoid and assesses the accuracy of the various linear size measures. Any set of triaxial dimensions may potentially give rise to an ellipsoidal geometry, the degree of rounding (particularly in the apical regions) determining the degree of similarity, although roundness has long been recognized as geometrically independent of shape (Wadell, 1932).

There appear to be no data on the degree to which clasts approximate ellipsoids. This can be checked by comparing actual measured volume, V, with the volume calculated assuming the body is an ellipsoid, V_e. Given clast weight, computation of V/V_e ratios is exact when the density is known: this was the case for the 31 clasts used in the experiments of isolate imbrication. Ratios for the remainder of the population involve slight error because density was assigned the mean value of 2.75 $g.cm^{-3}$: included in this category are 100 clasts used in the studies of contact bedload, as well as the 10 clasts used by Bradley, Fahnestock and Rowekamp (1972, Table 4). For symmetric ellipsoids, volume is given by the formula

$$V_e = \frac{\pi}{6} abc \ .$$

TABLE 9: The different types of symmetric ellipsoid and their description by linear size measures

a) Types of symmetric ellipsoid

	Zingg's (1935) terminology	type of ellipsoid	axial ratios
1	prolate (or rod-shaped)	rotation ellipsoid	a>>b but b=c
2	oblate (or disc-shaped)	rotation ellipsoid	a=b but b>>c
3	bladed	triaxial ellipsoid	a>b>c
4	equant	tending to a sphere	a=b=c

b) Degree of accuracy of simple linear size measures

	long axis	intermediate axis	arithmetic mean size	nominal diameter
1	Severe overestimate	Underestimate	Acceptable	Accurate
2	Overestimate	Overestimate	Acceptable	Accurate
3	Overestimate	Acceptable	Accurate	Accurate
4	Acceptable	Accurate	Accurate	Accurate

The histogram of the continuous variable V/V_e (Fig. 3) is clearly normally distributed, and is centred close to unit ratio, indicating that this gravel population does closely conform to an ellipsoidal solid geometry. Eighty-nine per cent of the individual values are within the range 0.85 - 1.25.

If this geometric similarity is of general application, then nominal diameter may be directly calculated from the axial lengths as follows:

The volume-radius relation for a sphere, ie.

$$V = \frac{4}{3}\pi r^3$$

can be arranged in terms of diameter, such that

$$d = \frac{6.V}{\pi}^{1/3}$$

For non-spherical clasts, d becomes the nominal diameter, d_n. Substitution into this formula of a re-arranged version of the above equation for volume of an ellipsoid yields

$$d_n \text{ (ellipsoid)} = (abc)^{1/3}.$$

This is a useful equation because it avoids determination of clast volume by immersion: where a good ellipsoidal tendency is present in a clast population, its use is recommended. Nominal diameter is a superior measure of clast size because of its greater sensitivity to hydrodynamic behaviour and because it is a precise measure of clast volume (Table 9).

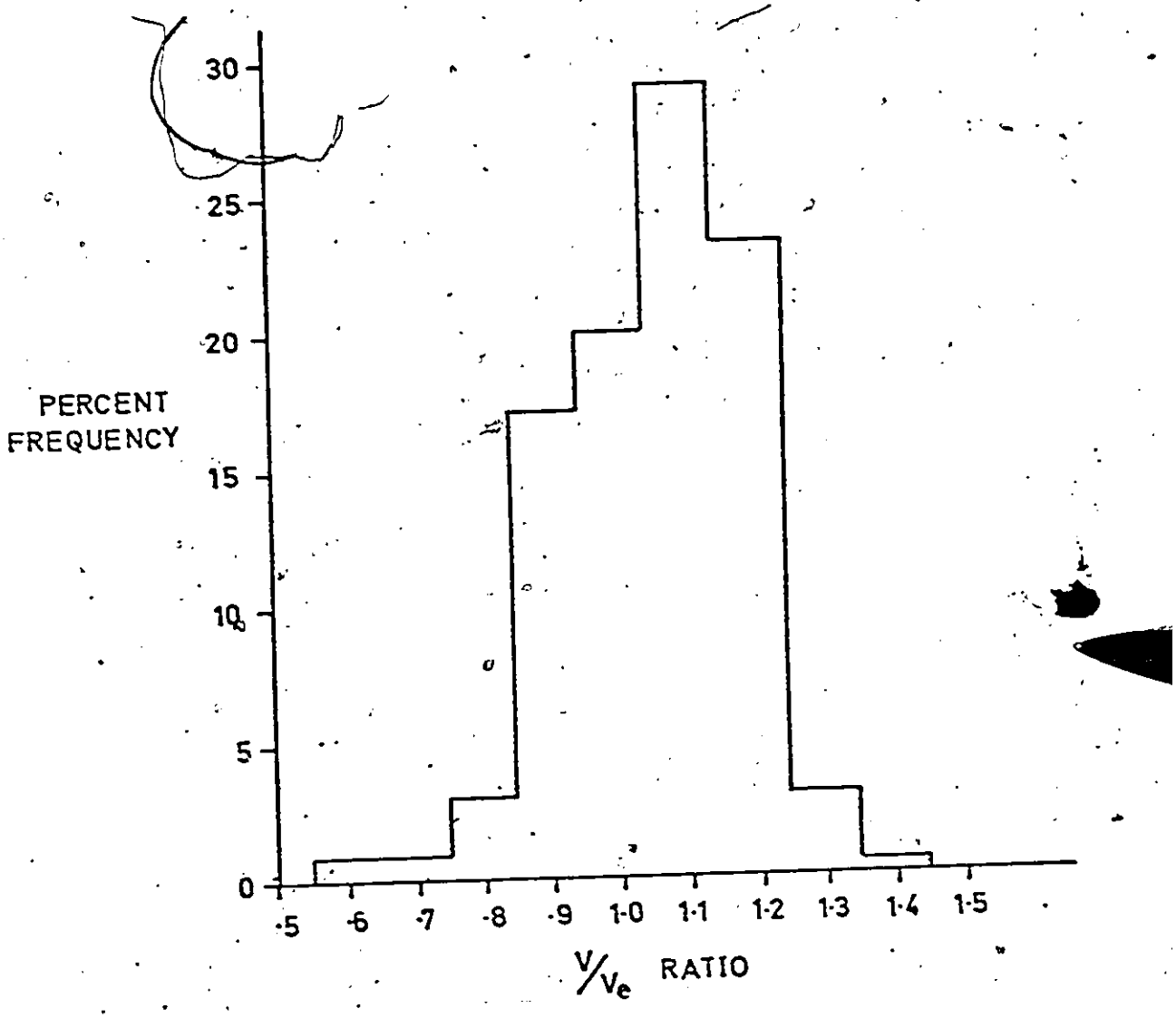

Figure 3: Histogram of the variable V/V_e, i.e. the ratio of actual measured volume to the volume assuming an ellipsoidal geometry. Mean and standard deviation are 0.9539 and 0.1211, respectively.

3.0 MOTION OF CLASTS ISOLATE ON A SANDBED BELOW THEIR TRANSPORT THRESHOLD

Clast motion comprises both rotation and translation, both of which can be expressed in terms of response components relative to axial dimensions. A significant rotation occurred in all experiments with lesser amounts of translational motion. Both categories of clast movement are responses to their unstreamlined disposition at the start of each run, as manifested by the development of current-crescent scour around each clast. Scouring is complete when clasts attain a hydrodynamically stable configuration.

Clast motion was expressed in relation to the coordinates defined in figure 4A. The particles were initially laid out with a-axes current-normal and with a-b planes horizontal. Typical clast motion is illustrated in figure 4B.

The geometric centre of the a-b plane is a convenient reference point from which to measure translation motion as a vector with three components corresponding to the axes of the flow reference frame. At below-threshold conditions, this vector involves motion in the -x, -y and ±z directions (Table 10A). Rotational motion is a scalar quantity, including inclination and orientation of the a-axis, as well as imbrication of the a-b plane (Table 10B).

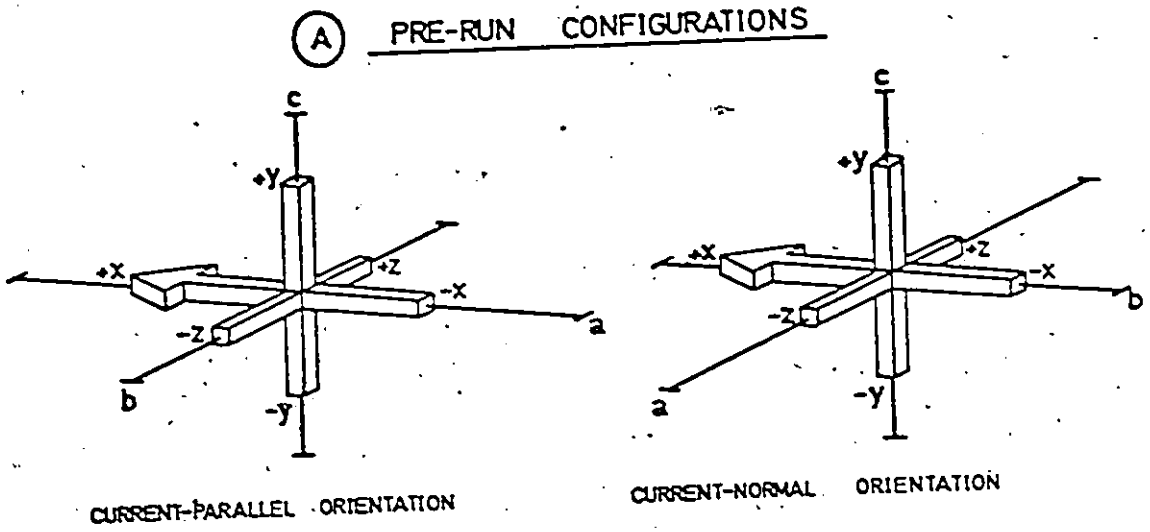

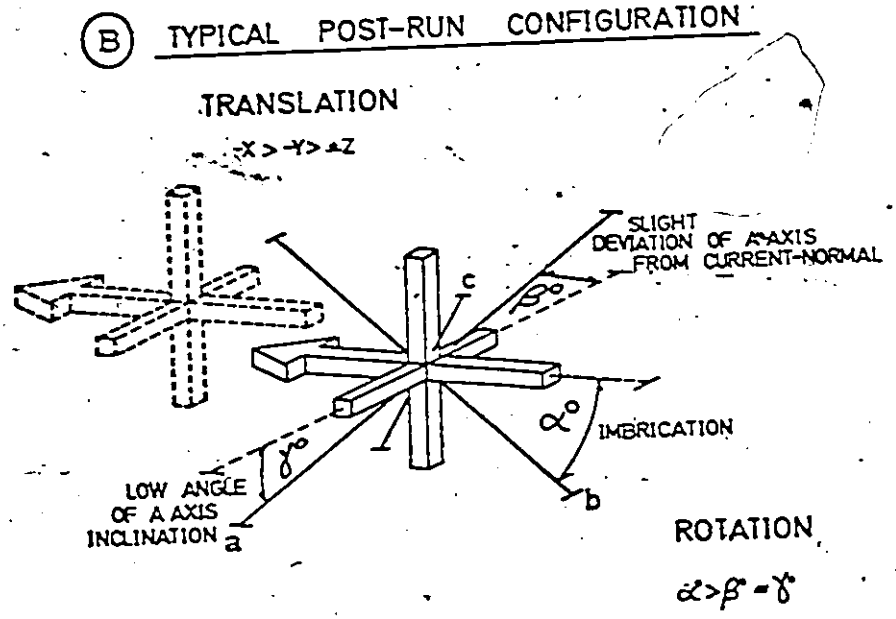

Figure 4: The pre-run and typical post-run configurations for isolate clasts on a sandbed.

TABLE 10: Types of Clast Response

VARIABLE NOTATION	DESCRIPTION OF VARIABLE
A) Vector Quantities (cm):	Translational Motion
X - response	Parallel to flow direction
Y - response	Vertical and perpendicular to flow direction
Z - response	Horizontal and perpendicular to flow direction
B) Scalar Quantities (°):	Rotational Motion
α - response	imbrication of the maximum projection plane
β - response	orientation of the a-axis
γ - response	inclination of the a-axis

3.1 Measurement of Motion

The x, y and z coordinates of translational motion were measured accurately to the nearest mm. using the point gauge. During the design phase of the experiments the initial x_i and z_i coordinates of each clast were selected and subsequently maintained for all runs: this was deemed desirable from the standpoint of keeping the proximity of adjacent clasts on the sandbed constant. The y_i coordinates, because of bed level changes, had to be determined before the start of each run. The three components of translational motion are denoted X, Y and Z respectively. This technique is preferable to the one employed by Fahnestock and Haushild (1962), who marked clasts with a cross and visually determined their combined rotational and translational motion upstream into current-crescent scours.

Rotational motion was determined in situ using a clinometer for inclinations and a semi-circular protractor for orientations. The protractor was mounted at a convenient height on the mobile point gauge, and pierced through its origin by a rotatable rod extending downward to bed level. Two rigid, vertically aligned bars, each 15 cm. long, were attached horizontally at each end of the rod, the upper one being placed flush with the surface of the protractor. The device was manoeuvred over the exposed clast in the

sandbed, visually aligned with the clast's a-axis, and the orientation was recorded by the upper bar on the protractor. Current-normal orientation was recorded as 90°, with upstream (-x flow axis) and downstream (+x flow axis) at 0° and 180°, respectively. Orientations within the sector 46-134° may be regarded as current-normal, and those in the two outside sectors (i.e. 0-45° and 135-180°) as being current-parallel. The measurement of rotational variables may have involved a small degree of error because of the difficulty in precisely locating planes and axes in irregular solid objects. It is considered that the magnitudes of the β- and γ-responses are accurate to $\pm 2°$ and $\pm 4°$, respectively, and with the α-response at an intermediate level of precision.

A-axis orientation data were analysed by the method of Curray (1956) which yields a semi-circular vector mean ($\theta°$), a vector magnitude (LZ) and the probability (P) that the observed degree of preferred orientation is non-random. This is the best method for treatment of whole samples, but does not permit analysis of individual clasts. The latter is achieved by adopting a similar method to that of the Sedimentary Petrology Seminar (1965), in which each measurement of clast orientation is treated as an angular deviation from the current direction. This technique has the additional advantage that all three components of translational motion possess a 90° range, which is convenient for comparative purposes.

3.2 Statistics of response data

A 'process-response' model (Krumbein, 1968) has been applied to the data of clast motion. To completely explain each of the six responses listed in Table 10, and all of the process-response relationships expressed by figure 5 is an ambitious objective owing to:-

i) the complexity of fluvial processes, in particular the nature of two-phase systems in which some forces derive from the fluid phase alone, while others derive from the contained solid phase (which in the present experiments includes both the isolate large clast population as well as the sandbed);

ii) the difficulty in quantifying certain of the process variables;

iii) flow variables that cannot be held constant for all experiments; and

iv) the infinite morphological variation of natural clasts which cannot be expressed by any single size measure (Briggs and Middleton, 1965).

Statistical analyses of process-response relationships were assisted by APL programmes BIVARIATEANALYSIS, LOGREG, EXPONENTIALREGRESSION and FULLLOGREGRESSION (see Appendix for details).

The sets of response data number 279 (9 runs each with 31 clasts) except for the α-response for which there were 257 observations.

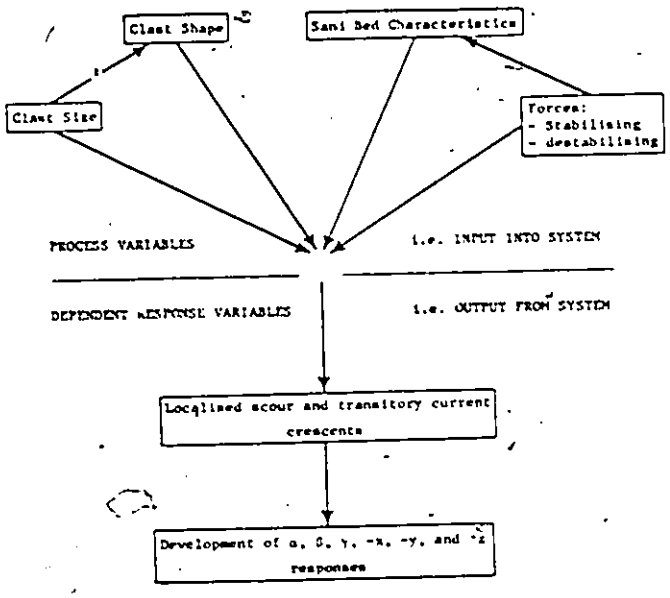

Figure 5 : A schematic representation of the process-response model used in the analysis of data from the experiments of isolate gravel fabric.
From Fig. 1, Koster (1974).

The histograms of translational responses (Fig. 6) show that upstream motion is the most significant, with an average of nearly 5cm. Truncation of the histogram for vertical motion at Y=0 indicates that this response is less significant. Lateral motion is almost insignificant as indicated by the extreme truncation against Z=0: if motion towards the right and left banks is distinguished, the histogram becomes centred about Z=0.

Of the three rotational responses (Fig. 7), imbrication is clearly the major variable and displays a near-normal distribution of angles: its histogram has a mode in the 25-30° class with a mean at 30.7°, indicating a slight negative skewness. The predominance of low-moderate angles of imbrication, as well as the other properties of the distribution, are in accordance with the findings of other studies (Table 3). A-axes of clasts are sub-horizontal and current-normally orientated. The histograms for these responses are therefore sharply truncated at zero angle, with 45-50% of observations lying in the 0-5° classes.

To summarise, it appears that of the six responses, only X, Y and α are hydrodynamically significant. The $\pm Z$, β and γ responses are of lesser magnitude because the initial configuration is stable. Thus over a wide range of flow conditions, in which both the lower- and upper-flow regimes were represented, large isolate clasts are stable when imbricated and orientated transverse to flow. Current-crescent scour enables translational motion, in turn allowing the attainment of imbrication.

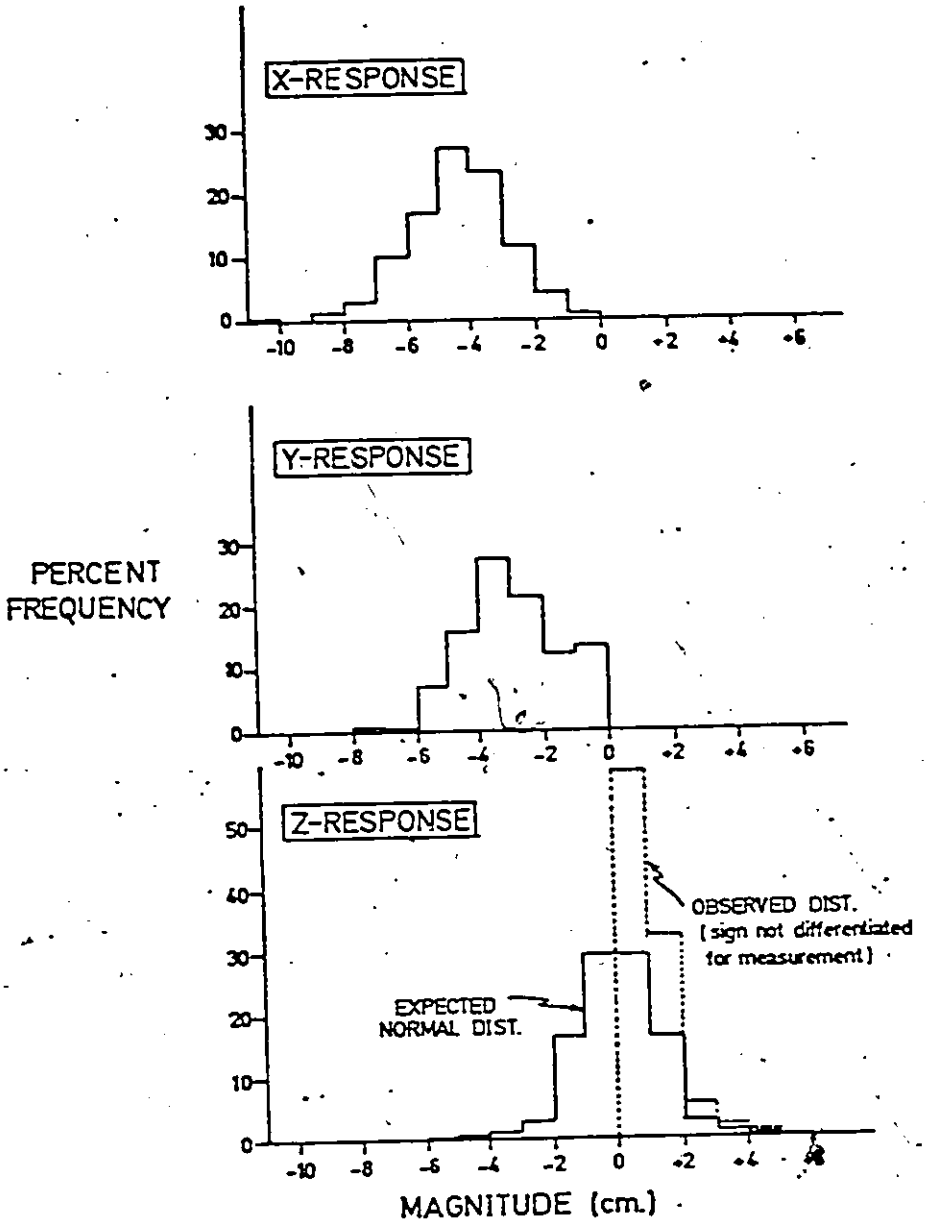

Figure 6: Histograms for the translational responses.
Each is based on 279 values.
Statistics for each distribution are as follows:

	Mean	Standard Deviation
X	-4.70cm	1.23cm
Y	-3.44cm	0.87cm
Z	1.06cm	0.79cm

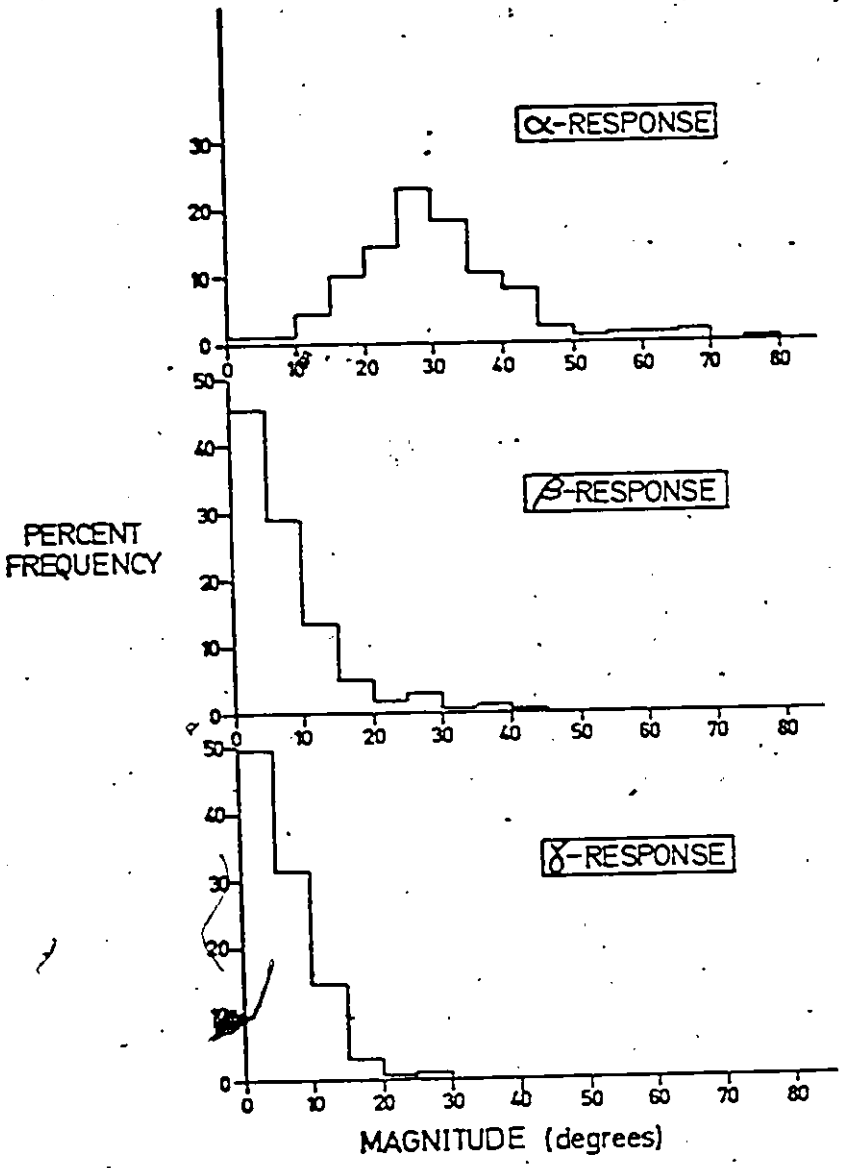

Figure 7: Histograms of the rotational responses. Statistics for each distribution are as follows:

	Mean	Standard Deviation
α	30.7^{o}	9.3^{o}
β	7.9^{o}	5.4^{o}
γ	5.8^{o}	4.7^{o}

3.21 Current crescents and the 'imbrication process'

Structures on sand beds resulting from localised scour around stranded objects have been variously referred to as 'current crescents' (Peabody, 1947), 'obstacle marks' (Dzulynski and Sanders, 1962) and 'scour marks' (Richardson, 1968). The term current crescent is morpho-genetically correct, and is adopted here.

Fluid resistance associated with flow separation, which occurs at points of abrupt surface curvature around the submerged body, is termed 'form drag' (Rouse, 1950). At high Reynolds number additional energy loss occurs through 'surface drag' because high velocity flow is pressed close to the body surface. Localised scour is active in response to the unstreamlined nature of the stationary object: a body is said to be streamlined if there is no boundary layer separation (Shapiro, 1961). Flow around obstacles is accelerating because of the lateral compression of the streamlines. An "adverse pressure gradient causes the fluid to curl into a horse-shoe shaped vortex, with horns extending downstream along the sides of the obstacle....the vortex filaments are stretched, the fluid particles rotate and advance helically..." with the "...diving components inducing scour" (p.151, Karcz, 1973).

Most of the research on this type of scour has been conducted by by bridge engineers. However this is not directly applicable to current crescent scour around isolate

clasts on a sandbed for three reasons. Firstly, clasts are potentially mobile through the imbrication process, whereas bridge piers are fixed. Secondly, piers intercept the entire flow, whereas gravel clasts are generally fully immersed. Thirdly, piers have uniform geometry, whereas sedimentary clasts are typically irregular in their morphology.

For current crescent scour around clasts on a sandbed, Karcz (p.1008, 1968) stated:

> "Hydrodynamic and hydraulic evidences indicate that the magnitude and nature of the secondary circulation around obstacles are determined by the various properties of the approaching flow (e.g. velocity, discharge, depth, density stratification), of the sediment (e.g. composition of the streambed material, grain size, grain shape, composition and amount of the bedload) and of the obstacles (e.g. orientation, shape, dimensions). Another factor to be considered is the duration of scouring."

The significance of current crescents in the development of isolate imbrication was first recognised by Sengupta (1966). Provided the sandbed is sufficiently thick to permit unimpeded motion, a stable configuration will eventually be attained by the clast. During this process, form drag becomes of diminishing importance and current crescent scour becomes progressively less vigorous (see Section 3.5). The onset of flow conditions capable of transporting the clasts marks the upper limit for current crescent scour. At this point, the capacity for bed degradation predominates over localised scour causing clasts to become re-exposed. For any given clast therefore, there are only a limited range of flow conditions within which current crescent scour is active.

3.3 Response to the flow regime of the sandbed

Laboratory studies of coarse-clast behaviour have generally used either a representative flow velocity (e.g. Kelling and Williams, 1967) or Froude Number (e.g. Krumbein, 1942). Hydraulic engineers have tended to use tractive force (Novak, 1973), but there is some evidence (Wolman and Brush, 1961) which suggests that this measure is somewhat misleading. For particles larger than 5mm, entrainment is principally determined by velocity, rather than by the depth-slope product. A similar deduction could be made from the typical at-a-station hydraulic geometry of braided channels carrying coarse alluvium (e.g. Spring Creek), where a wide range in competency is accompanied by little change in the depth-slope product.

Hence for the large clast sizes employed in the present flume study, a parameter related to velocity appears to be a preferable measure of flow strength. Froude Number was selected because together with Reynolds Number it determines the dynamic similarity between flume channels and natural channels (Southard, 1975).

The effect of Froude Number on clast response is best illustrated by means of Dice-Diagrams (Dice and Leraas, cited by Sokal, 1965) which depict all pertinent statistical information about the distribution (Fig. 8). APL programme SCAT (see Appendix) was written to

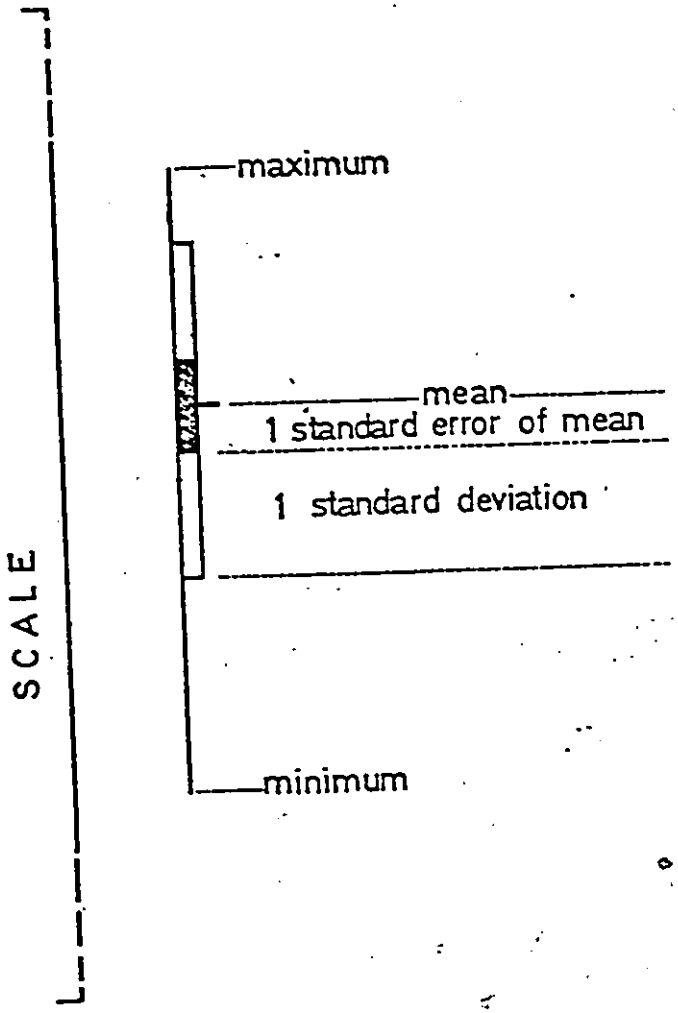

Figure 8: Properties of a Dice-Diagram (after Dice and Leraas, cited by Sokal, 1965).

furnish all the necessary values. Dice-Diagrams for the two sets of responses are shown in figures 9 and 10. The standard error of the mean gives a visual impression of the significant differences that exist between groups of mean values.

All three translational responses display a similar pattern of variation with increasing Froude Number. Of the three rotational responses, the δ-response is the only one to show a similar pattern. The α-response attains a maximum value at $Fr \approx 0.7$; the reason for the relatively high mean value encountered at $Fr \approx 0.24$ is unknown. The γ-response is essentially constant over the range of flows studied.

Variation in the mean value of each clast response, with the exception of the α- and γ-responses is remarkably consistent. Ignoring the sign of the response, which is merely a function of axial definition, mean values increase from zero to $Fr \approx 0.5$, decrease to $Fr \approx 0.7$, then increase again. This effect must be due to some over-riding influence of the two-phase system, because the same clasts were used in all runs. It appears unlikely that a feature of the fluid phase alone is responsible since the flow parameters were either steadily increased (e.g. velocity), or were held constant (e.g. depth). Water density, viscosity and temperature are considered ineffective.

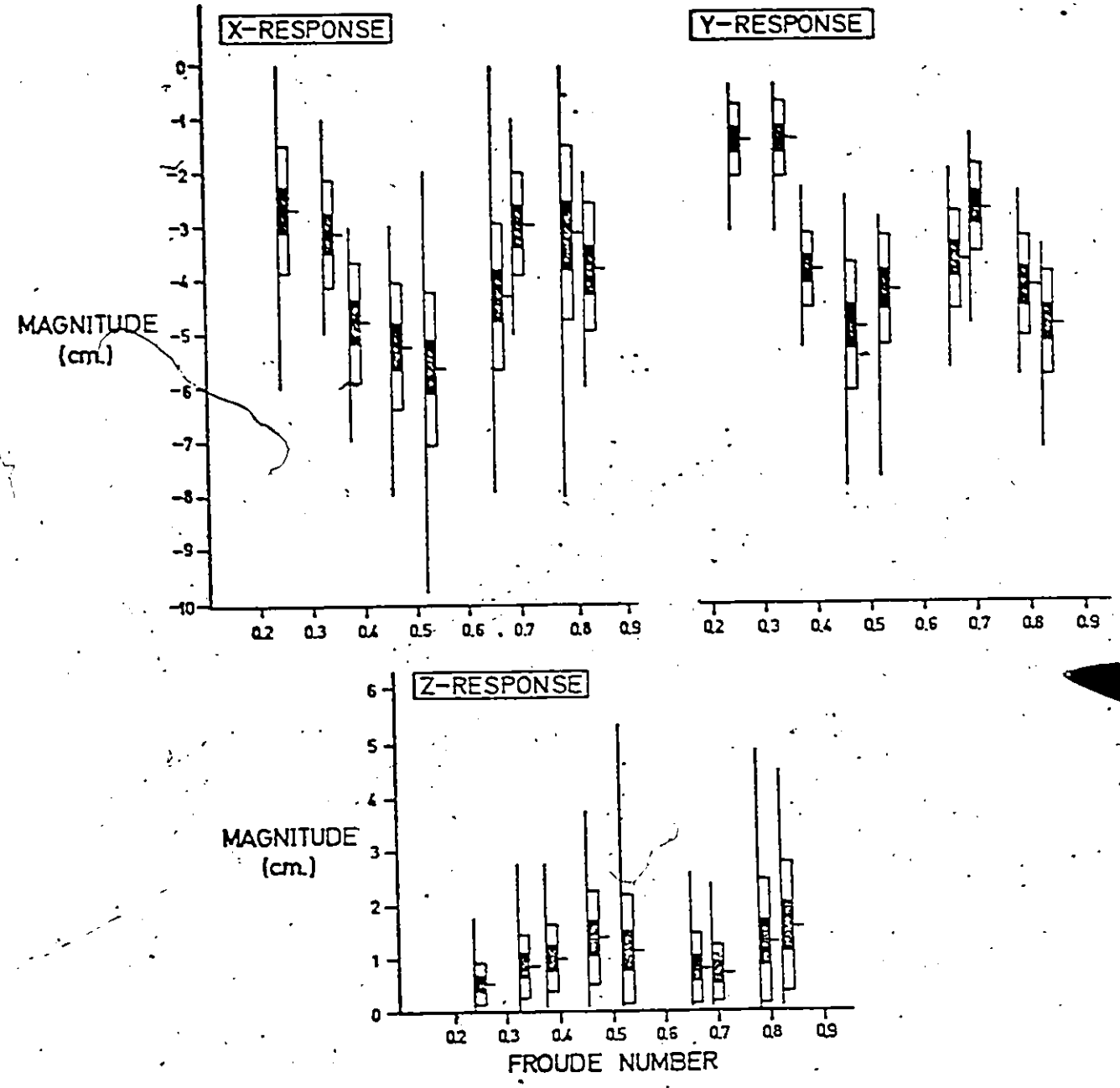

Figure 9: Dice-Diagrams for the translational responses showing the statistics of motion at each run.

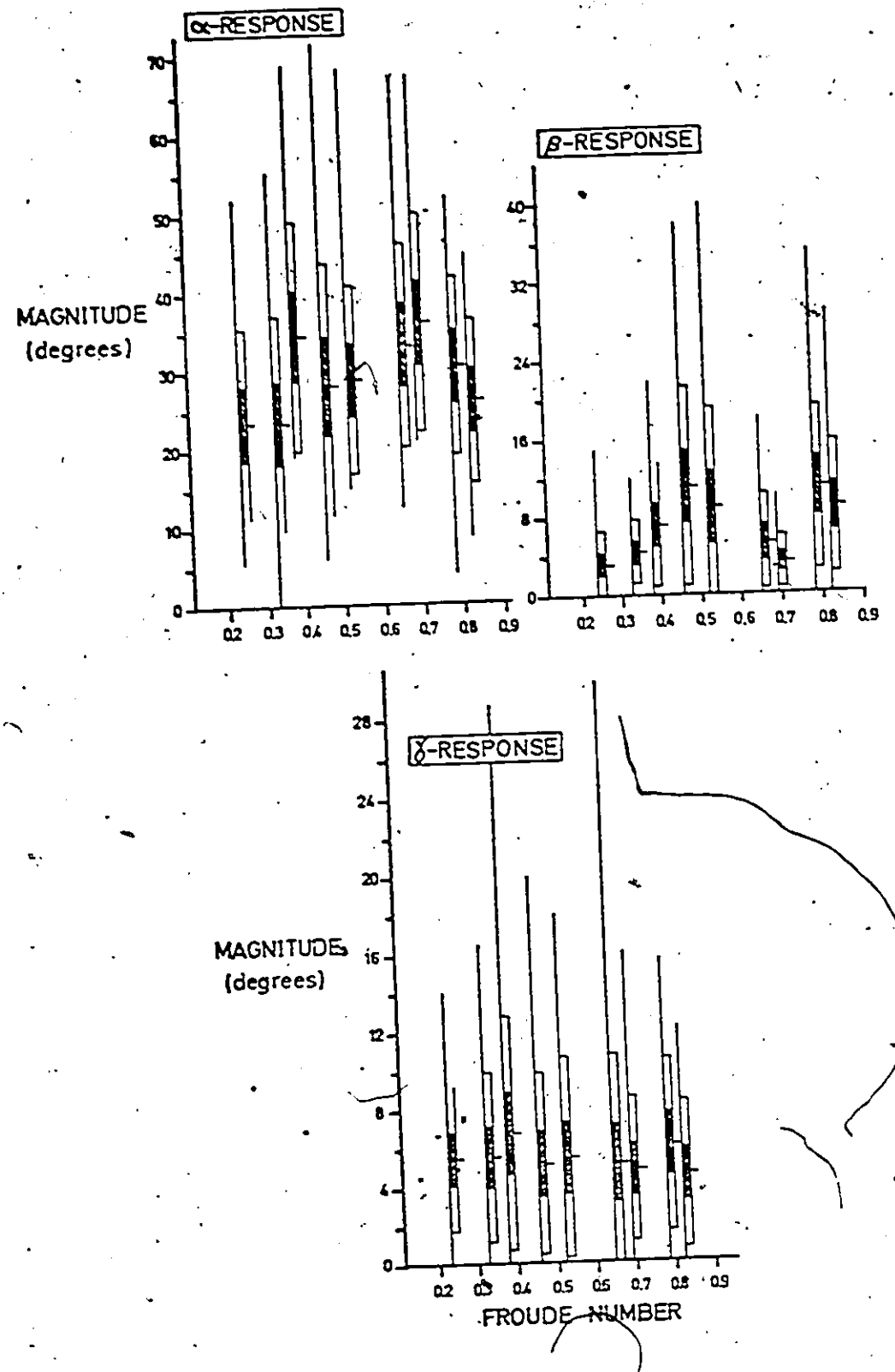

Figure 10: Dice-Diagrams for the rotational responses showing the statistics of motion at each run.

The sandbed and the scattered large clasts constitute the 'contained solid phase'. However since the coarse bed-load component was invariant, the sandbed itself must be responsible for the observed systematic pattern of variation in four of the six responses. The median settling velocity of the sand used in the flume experiments is 3.65cm.sec^{-1} (Forbes, 1973), which corresponds to a grain diameter of approximately 0.35mm (Gibbs, Matthews and Link, 1971). The variation of form roughness encountered in the present experiments should therefore be intermediate between the two examined by Simons and Richardson (1962) (Fig. 11). diagram was compiled from numerous laboratory experiments, and a prominent feature is the large range of roughness values for a bedform at a given sediment size. A simplified version of their diagram is given by Harms and Fahnestock (1965, Plate 1).

There is a close similarity between the patterns of variability of mean values of clast responses (Figs. 9 and 10) and of form roughness expressed by the Manning coefficient (Fig. 11). Clast response increases as a result of higher amplitude and/or greater wavelength of

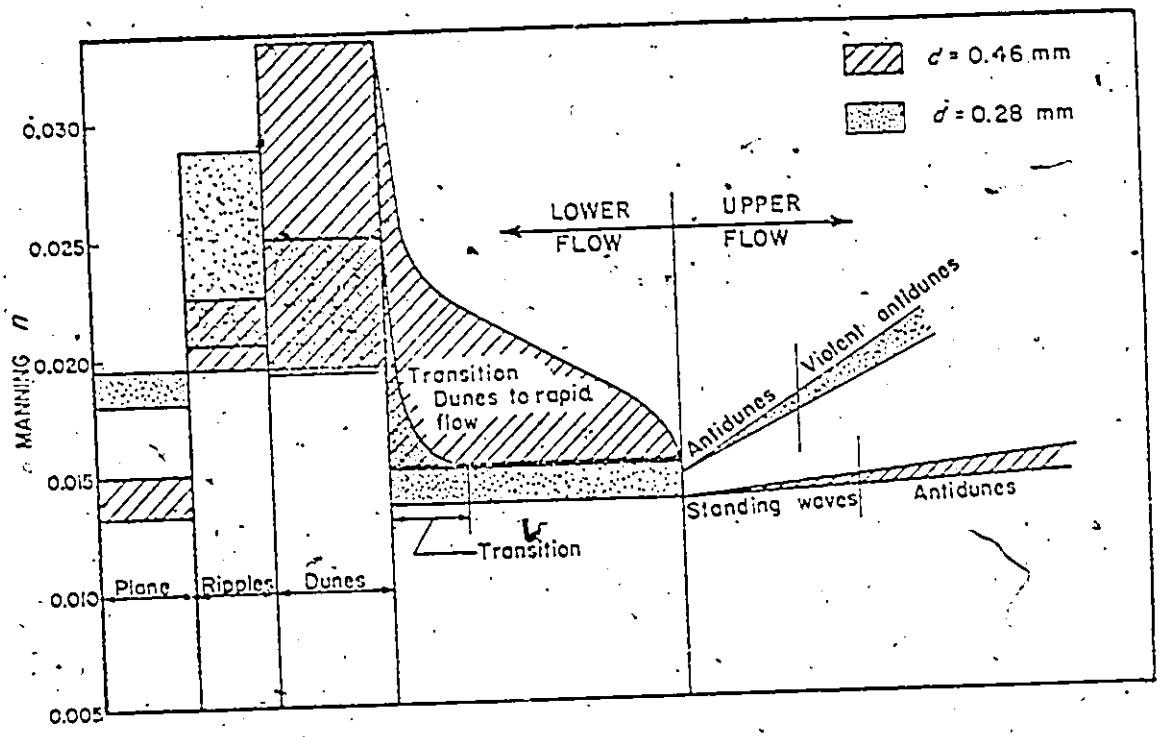

Figure 11: Variation in the roughness of two sandbeds over the range of bedfroms which characterise the lower and upper flow regimes.
Modified from Figure 2 of Simons and Richardson (1962)

sand bedforms, and vice versa. If a flat bed remained stable under conditions of rising velocity, isolate clasts would move a diminishing distance upstream as the transport threshold was approached. However, this trend is greatly modified by the variation of form roughness which accompanies the series of lower- and upper-flow regime bedforms. Kelling and Williams (1967) in their flume study of clast reorientation in the lower-flow regime (Fr<0.35) attributed the S-shaped kink in their graphs of angular deviation against Froude Number to the change in bedform from ripples to dunes. As bedforms migrate past the effectively stationary clasts, bed elevation fluctuates from 1 to 7cm, depending on the type of bedform. High amplitude is obviously conducive to greater translational motion. An additional consequence of pronounced three-dimensional topography is wide variation in the direction and magnitude of 'skin-friction lines', ie. streamlines at the flow-bed interface (Allen, 1970): this is the likely cause of peturbations from the otherwise stable current-normal orientation.

Visual comparison of figures 9 and 11 clearly reveals the close dependence of all three translational responses on the degree of bed roughness. However, the β-response (Fig. 10) is the only rotational response to display the same relation. It will be recalled that the γ-reponse (Fig. 10),

lacks variation in mean values. The α-response is unique in that imbrication is at its maximum angle at the transition of the flow regimes (Fr=0.7), indicating that a hydraulically plane bed with a two-dimensional flow field is conducive to the attainment of maximum angles. Any appreciable form roughness causes imbrication at lower angles.

3.4 Response to clast properties

3.41 Imbrication

From the literature review of studies of imbrication, it was apparent that certain geometric features of the clasts influence the angle of imbrication. On this basis, the following process-response analysis first investigates the role of shape and size and then examines the effect of more hydrodynamically sensitive properties.

3.411 Dependence on simple geometric variables

Results of bivariate analyses of the α-response as a function of maximum projection sphericity Ψ_p (Sneed and Folk, 1958), oblate-prolate index $\overline{OP}$ (Dobkins and Folk, 1970) and nominal diameter d_n are shown in Table 11. Shape is a significant process variable, while size has no appreciable effect. Of the two shape parameters, Ψ_p gives the better correlation; the influence of $\overline{OP}$ is less clear, since 25% of

TABLE 11: Bivariate analysis of the α-response

Variables

Dependent response variable:- α, imbrication of clast a-b plane, range 0-90°.

Process variables:- Ψ_p, maximum projection sphericity

$\overline{OP}$, oblate-prolate index

d_n, nominal diameter.

Correlation Matrix

Mean values for each clast used.

	α	Ψ_p	$\overline{OP}$	d_n
α	1.000	0.577*	0.458*	-0.043
Ψ_p		1.000	0.501*	-0.029
$\overline{OP}$			1.000	-0.033
d_n				1.000

N.B. * denotes significance level in excess of 95%.

Regression Equations

$$\alpha = 101.98\,\Psi_p - 19.85$$

$$\alpha = 0.87\overline{OP} + 37.57$$

its variability is accounted for by Ψ_p. These results confirm the observations of Cailleux (1945) and Johansson (1965) that the angle of imbrication is inversely proportional to the degree of clast flatness.

The correlation with sphericity is shown in figure 12. Although the data can be fitted to a linear regression, the spread of points suggests that it may represent the central portion of a curvilinear relation with terminal coordinates ($\Psi_p \rightarrow 0; \alpha \rightarrow 0^\circ$) and ($\Psi_p \rightarrow 1; \alpha \rightarrow 90^\circ$). Both limits are theoretical since a perfect sphere cannot imbricate and the effective minimum value of sphericity is about 0.15.

Any variation in the effect of these clast properties with increasing Froude Number can be recognized by subdividing the clast population into two groups separated by the median values, which are 0.52, zero and 4.95cm for Ψ_p, $\overline{OP}$ and d_n respectively. Average values are then calculated for each group.

In the lower flow regime, the influence of sphericity (Fig. 13A) is nearly constant while in the upper flow regime it has less effect: in between, at the regime transition, sphericity has the greatest influence as shown by the 16° span between the two groups. The same pattern is developed by the oblate-prolate index (Fig. 13B), but to some extent, the similarity is due to the partial inter-dependency of $\overline{OP}$

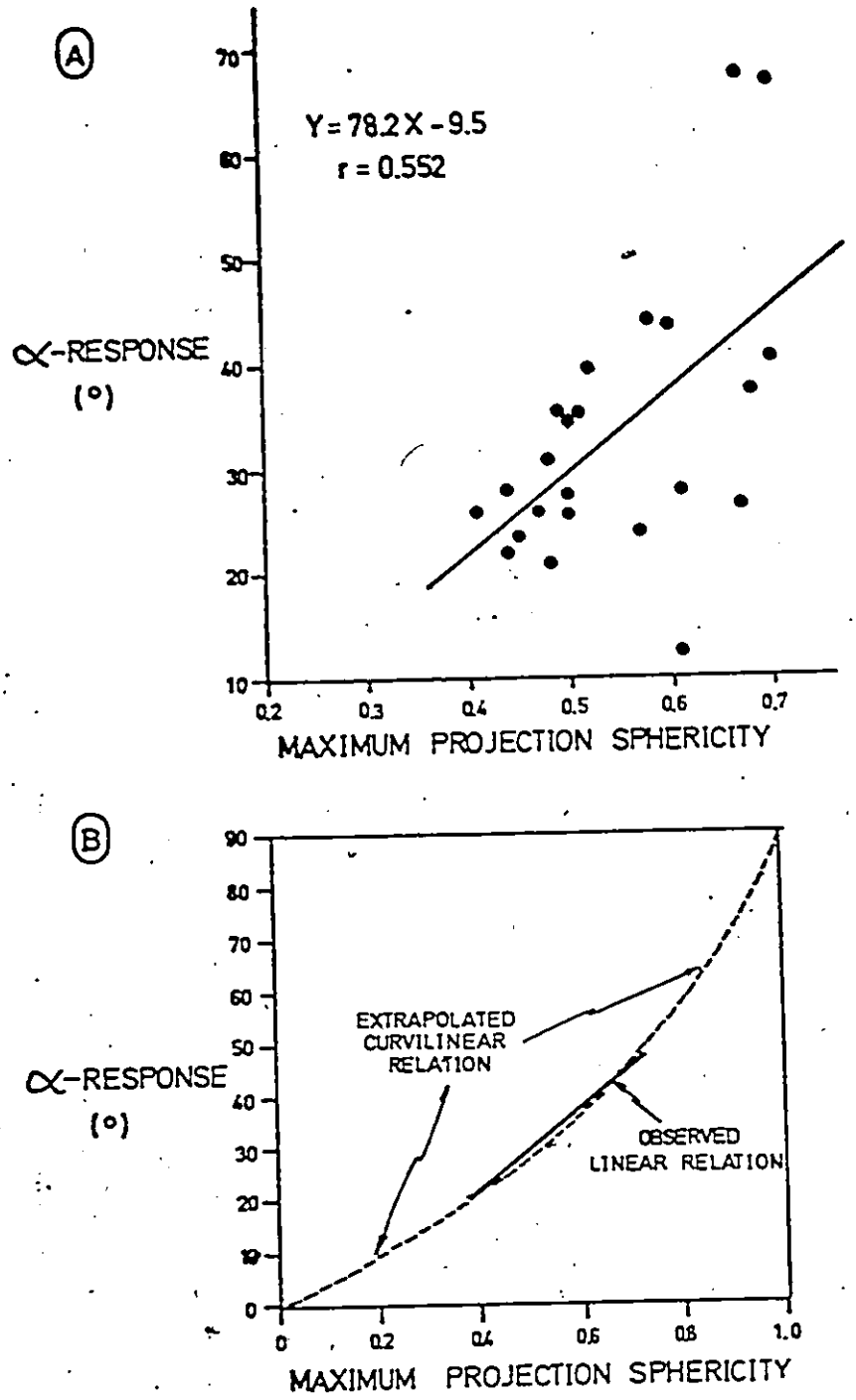

Figure 12: The relationship between angle of imbrication and maximum projection sphericity. In (A), data are from the run EK3D-7 for which the stable sand bed phase was a plane bed; in (B) a speculative total relation is shown.

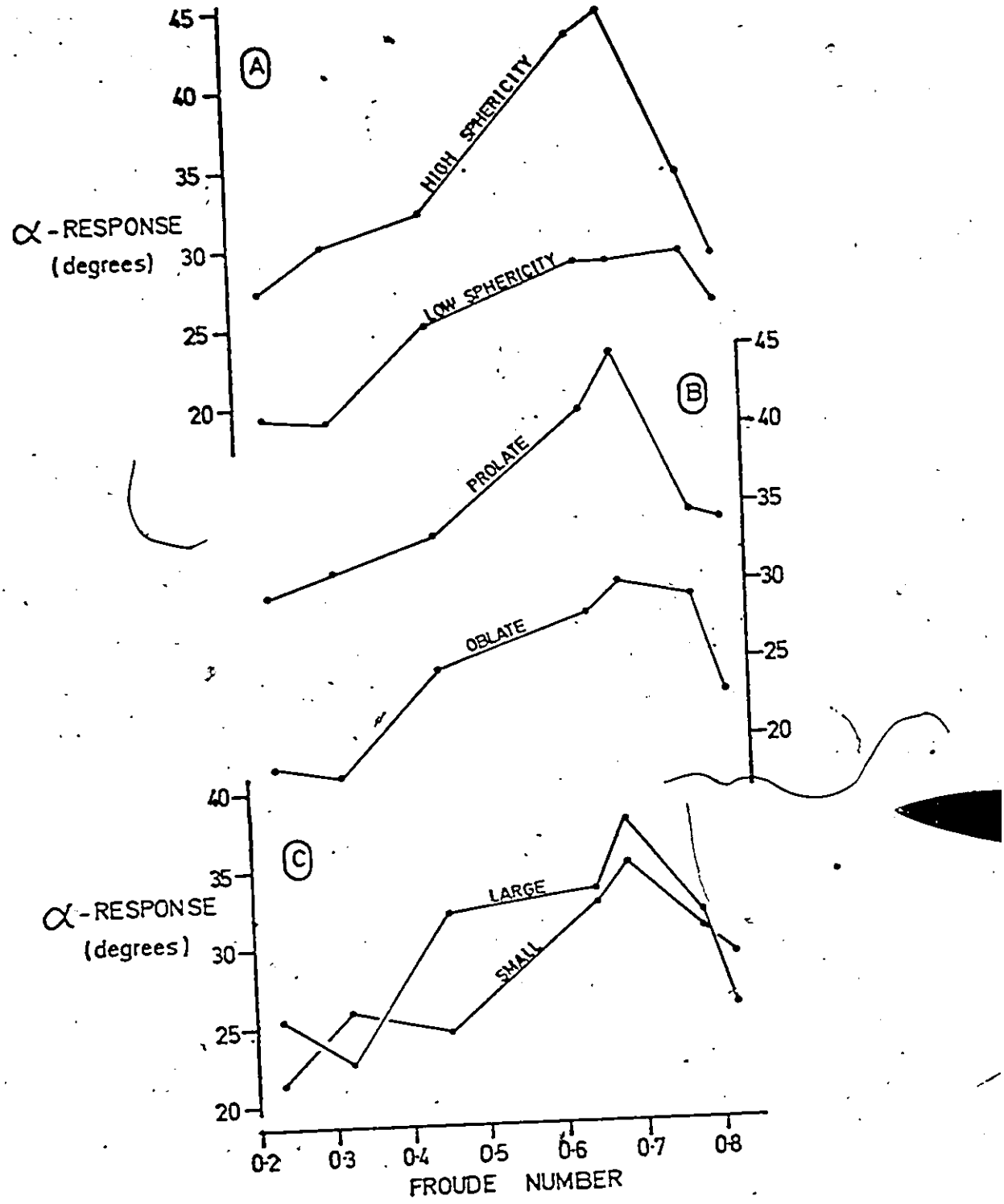

Figure 13: Variable influence of clast properties - A. maximum projection sphericity, B. oblate-prolate index, C. nominal diameter - on the α-response with varying Froude Number.

with Ψ_p. There is no consistent effect with respect to clast size (Fig. 13C), except that within the dune phase, size appears to have a positive influence on the angle of imbrication.

3.412 Projection area as a function of nominal diameter

Even under controlled laboratory conditions, explanation of the α-response in terms of simple geometric clast properties is incomplete. It was therefore decided to investigate the statement of Johansson (1963, p.90-91) that the angle of imbrication is influenced by "...the friction, which is a function of mantle area in relation to its mass". 'Mantle area' is interpreted as the area projected by the clast in the y-z plane, i.e. normal to the flow direction. Projection area, denoted $\bar{A}_p$, is a particularly useful measure because it combines the effects of clast size and shape, as well as those of variable orientation with respect to current direction. Nominal diameter was employed as a measure of clast mass, since it relates directly to volume.

An investigation of this relation requires that projection area be accurately known. A_p could be precisely determined by reproducing the imbricated clast in a light beam and then measuring the silhouetted area on a wall with a planimeter: this method is too laborious for repeated use.

Alternatively, projection area was calculated on the basis that the solid geometry of the clasts closely approximates a symmetric ellipsoid (see Section 2.51).

For the purpose of this study, values of the ratio V/V_e between 0.9 and 1.1 are considered acceptable for accurate determination of projection area. Of the 25 clasts measured for imbrication in each of the 'isolate' experiments, nine were found to closely conform to an ellipsoidal geometry (Table 12). Having established this, formulae were derived to compute the area projected by an ellipsoid at any configuration with respect to the flow.

A symmetric ellipsoid projects a plane shape with elliptical outline. For a given ellipsoidal clast, A_p attains maximum and minimum values when its long-axis is aligned

i) transverse to flow with the principal plane vertical, and

ii) parallel to flow with the principal plane horizontal,

respectively.

Clearly the range between maximum and minimum values diminishes as the degree of clast sphericity increases.

For ellipsoidal clasts orientated normal and parallel to the flow, A_p is calculated by means of equations 2 and 3 respectively:

$$A_p = \frac{\pi . a . b'}{2} \qquad \ldots\ldots\ldots(2)$$

$$A_p = \frac{\pi . a' . b}{2} \qquad \ldots\ldots\ldots(3)$$

TABLE 12: Clasts closely conforming to symmetric ellipsoids

Clast #	Measured volume, V (cc)	Calculated volume assuming ellipsoidal, V_e (cc)	V/V_e
119	45.1	46.0	0.98
99	79.0	71.9	1.09
12	77.1	71.5	1.07
88	121.0	115.5	1.05
20	53.0	52.0	1.02
93	67.0	70.9	0.94
71	267.4	268.2	1.00
65	292.8	262.7	1.10
73	724.2	675.0	1.07

where $$a' = \left(J_* - \frac{K_*^2}{4.L_*}\right)^{-\frac{1}{2}}$$

$$b' = \left(L - \frac{K^2}{4.J}\right)^{-\frac{1}{2}}$$

in which $$J_* = R.\cos^2\beta + S.\sin^2\beta$$

$$K_* = (R - S)\sin 2\beta$$

$$L_* = R.\sin^2\beta + s.\cos^2\beta$$

$$J = S.\cos^2\alpha + T.\sin^2\alpha$$

$$K = (S - T)\sin 2\alpha$$

$$L = S.\sin^2\alpha + T.\cos^2\alpha, \text{ for which}$$

$$R = \left(\frac{2}{a}\right)^2, \quad S = \left(\frac{2}{b}\right)^2 \text{ and } T = \left(\frac{2}{c}\right)^2.$$

Oblique orientation requires the use of a more involved calculation using equation 4:

$$A_p = \frac{\pi.a'.b'}{2} \qquad \ldots\ldots\ldots(4).$$

Full details of the above mathematical theory as well as of APL program FULLIMBRIC, which was written to compute values of A_p (cm^2), are given in the Appendix.

Regression analysis indicates that A_p is a power function of d_n (Table 13). The data obtained from the nine ellipsoidal clasts (Table 12) in each flume run necessarily fall within a linear band defined by the minimum and maximum

TABLE 13: Observed parameters for the power function $A_p = f(d_n)$ at each flume run.

Run	Froude Number	Regression Equation	Correlation coefficient
EK3D-14	0.238	$A_p = 1.45(d_n^{1.69})$	0.977
-6	0.322	$A_p = 1.24(d_n^{1.73})$	0.965
-8	0.374	$A_p = 1.13(d_n^{1.93})$	0.989
-10	0.519	$A_p = 1.06(d_n^{1.92})$	0.979
-9	0.651	$A_p = 0.95(d_n^{2.01})$	0.983
-7	0.698	$A_p = 1.21(d_n^{1.90})$	0.991
-5	0.780	$A_p = 1.16(d_n^{1.89})$	0.985
÷12	0.821	$A_p = 1.35(d_n^{1.75})$	0.987

N.B. All of the above equations are statistically significant at the 99% level.

possible values of A_p for a given d_n. The equations for these two relations, assuming current-normal orientation of a-axes, are

$$A_p(min) = 0.48(d_n^{1.98}) \quad \ldots\ldots\ldots\ldots(5),$$

and $$A_p(max) = 1.37(d_n^{2.05}) \quad \ldots\ldots\ldots\ldots(6),$$

respectively.

In figure 14, observed regression lines are shown in relation to those of equations 5 and 6. Pairs of exponents and coefficients obtained at each experimental run are inversely related by the equation:

$$e = 1.98(c^{-0.37}), \quad r = -0.927.$$

The high value of correlation strongly implies a consistent and close control by the process variables. The exponents and coefficients of the A_p versus d_n relationship attain maximum and minimum values, respectively, in the vicinity of the flow regime transition (Fig. 15). On theoretical grounds, one might expect the highest degree of clast stability to be attained in the two-dimensional flow field of a transition plane bed. Under these conditions, the present data suggest that the optimum relation is given by the simple equation:-

$$A_p = d_n^2 \quad \ldots\ldots\ldots\ldots(7).$$

From Table 13, it is seen that Run EK3D-9 during which the equilibrium sand bed phase was a plane bed, stably imbricated

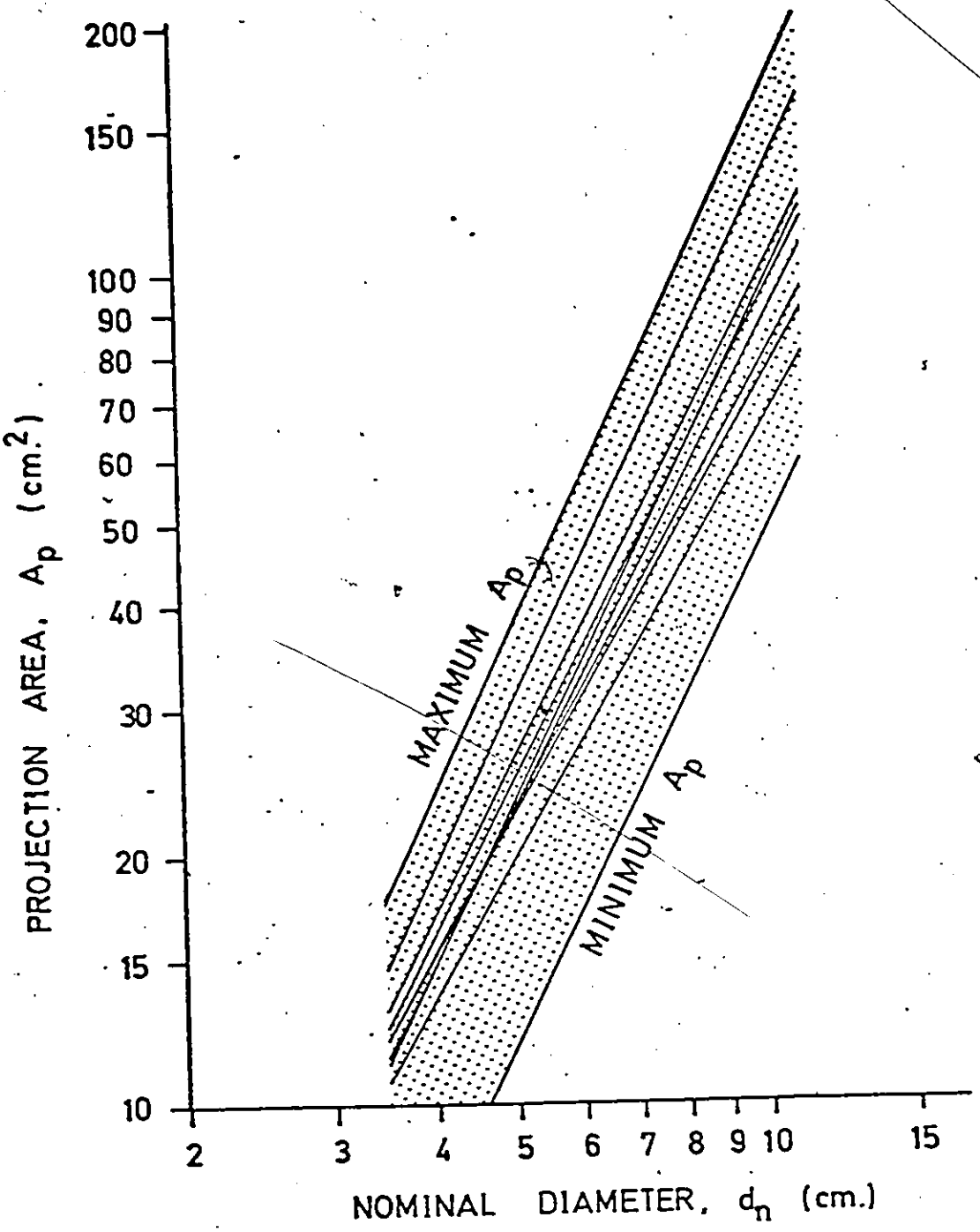

Figure 14: Projection area of ellipsoidal clasts as a power function of their nominal diameter. The shaded zone is bounded by equations 5 and 6, and indicates the possible range of projection areas for the nine ellipsoidal clasts. This zone contains the eight regression lines as listed in Table 13.

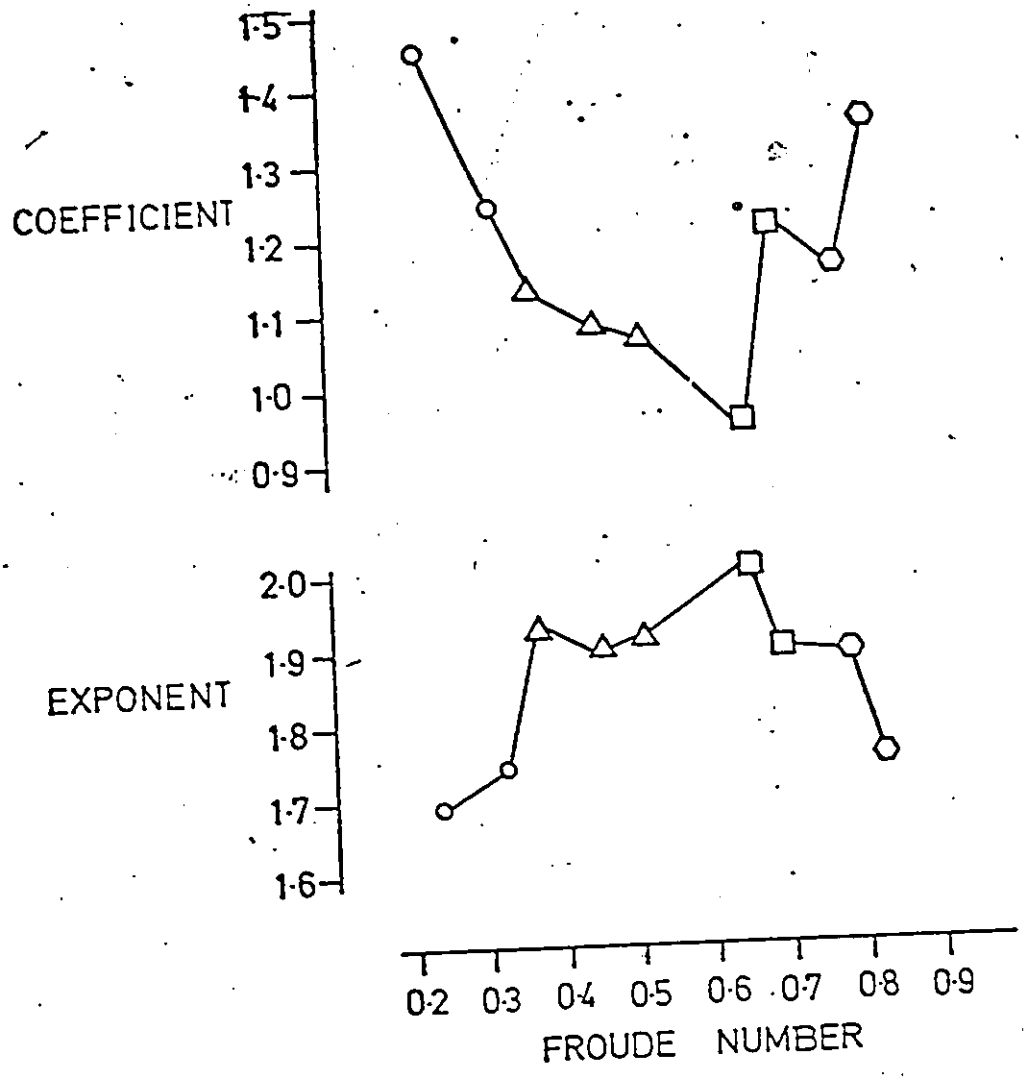

Figure 15: Variation in the parameters of the power function $A_p = f(d_n)$ with increasing Froude Number: plotted data are those listed in Table 13. In the vicinity of the flow regime transition (i.e. Fr $\approx$ 0.65), the coefficient and exponent reach minimum and maximum values, respectively: these correspond to those of the proposed optimum relation. See text for details. Symbols indicate different sand-bed phases as follows: circles – ripples, triangles – dunes, squares – transition of flow regimes, and hexagons – standing waves, antidunes.

clasts generated the equation

$$A_p = 0.95(d_n^{2.01});$$

the parameters of this relation are closely similar to those of equation 7. Statistical similarity between two regression lines can be checked using the method of Imbrie (1956). The test confirms what is visually apparent on figure 15, that flows at the transition of the lower- and upper-flow regimes yield A_p versus d_n relations are both

i) statistically similar to the form of equation 7, and

ii) statistically different from equations 5 and 6.

The validity of the proposition that equation 7 constitutes an optimum relation with dynamical significance can be further tested by comparing α values observed in runs surrounding the flow-regime transition (i.e. EK3D-10, -9, -7 and -5) with those calculated on the basis of theory (Table 14).

For a given clast, the angle of imbrication required to project an area equivalent to the square of its nominal diameter can be found using a mathematic procedure derived from that previously outlined on page 4. For ellipsoidal clasts orientated normal and parallel to flow, α is calculated by means of equations 8 and 9 respectively:

$$\alpha = \arcsin\left(\frac{b'^2.S.T. - S}{T - S}\right)^{\frac{1}{2}} \qquad .....(8)$$

$$\alpha = \arcsin\left(\frac{a'^2.R.T - R}{T - R}\right) \qquad .....(9)$$

TABLE 14: A comparison of observed values of α with those calculated by the optimum relation, $A_p \quad d_n^2$

Clast #	Observed values of α° in Runs EK3D-10	EK3D-9	EK3D-7	EK3D-5	Mean α°	Calculated values of α°
119	25.0	25.5	25.5	25.0	25.2	32.0
99	42.0	67.0	63.0	52.0	55.9	50.0
12	30.5	35.5	36.0	37.0	34.8	34.5
88	30.0	44.0	45.0	25.5	36.2	37.0
20	44.0	39.5	40.0	24.5	37.0	29.5
93	30.0	23.5	28.0	30.0	27.8	26.5
18	27.0	26.0	26.5	30.0	27.4	32.0
65	28.0	28.0	27.0	35.5	29.7	33.0
73	16.0	31.0	30.0	29.0	26.5	33.0
				Average:	33.7°	34.2°

where $a' = \frac{2.d_n^2}{\pi.b}$ and $b' = \frac{2.d_n^2}{\pi.a}$,

with R, S and T as previously defined.

The results of the comparison are shown graphically in figure 16 and indicate that equation 7 is an acceptable predictor of the observed angles of imbrication.

3.413 Proposed stability criterion

The optimum relation between A_p and d_n is thought to have considerable dynamical significance with regard to clast stability at the flow-bed interface. It is proposed that equation 7 constitutes a 'criterion of optimum stability' for large, inequidimensional clasts isolate on a sand bed. Using this criterion allows one to recognize hydrodynamically stable imbrication (Table 1) by the attainment of α-values which satisfy equation 7: Imbrie's (1956) method of statistical discrimination is recommended for checking the conformity of observed A_p versus d_n relations with the stability criterion.

The required A_p value for a given clast may be referred to as the 'equilibrium area'. Clearly, equilibrium area is a more meaningful parameter of clast response than the angle of imbrication. For clasts with equal nominal diameter, the angle of imbrication required for projection of the equilibrium area is shape-dependent (Fig. 17): for a

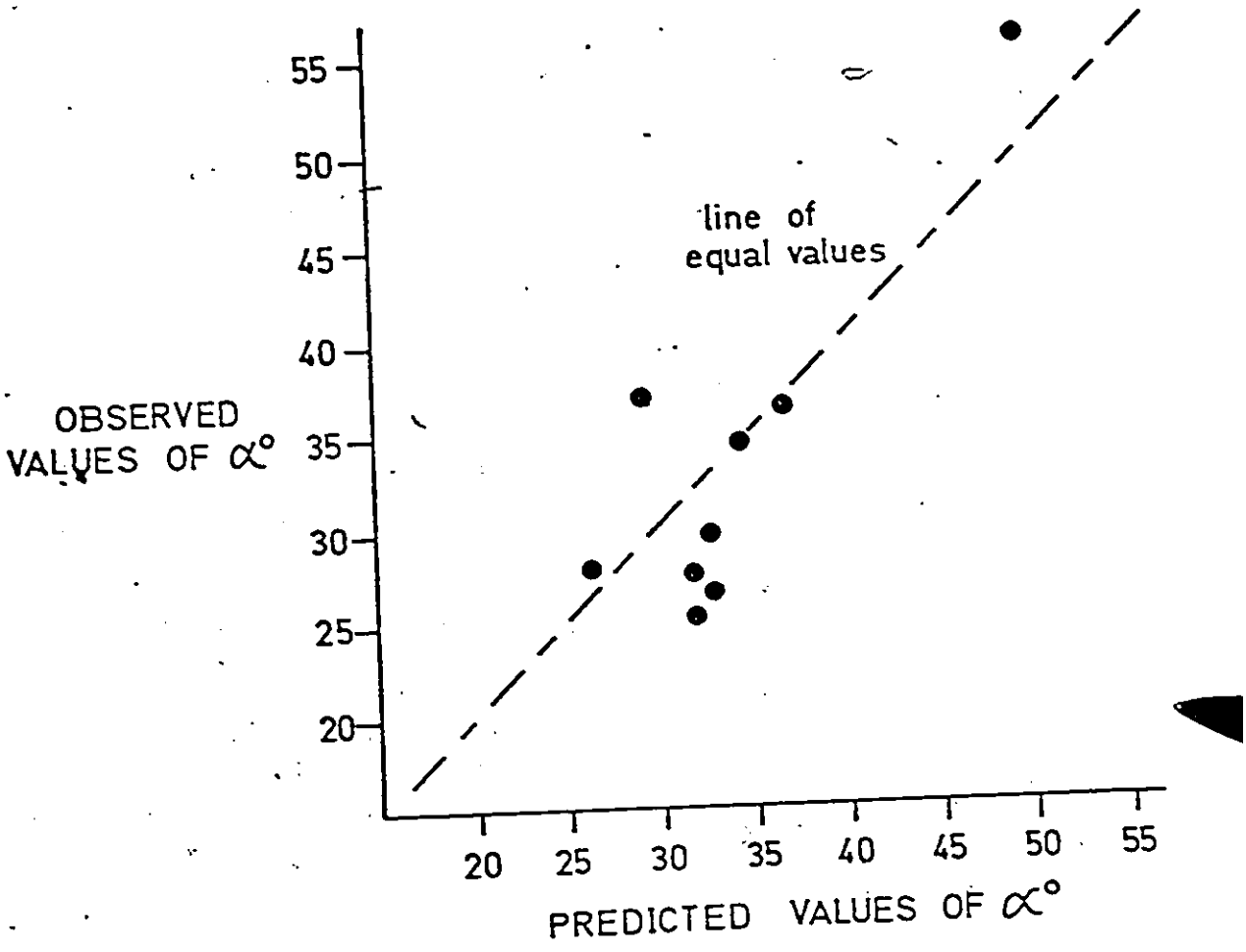

Figure 16: Observed α values for the nine ellipsoidal clasts compared to those calculated according to the proposed optimum relation. Plotted data are according to those listed in Table 14.

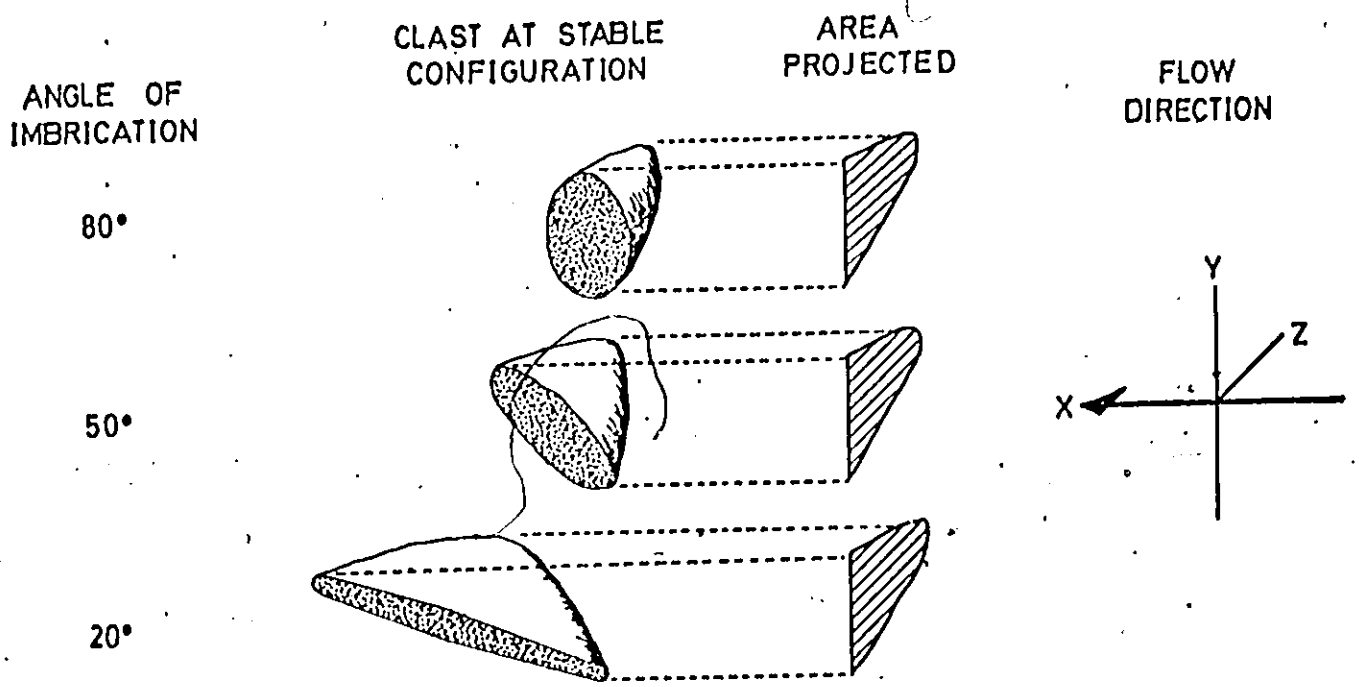

CLASTS HAVE - 1) EQUAL NOMINAL DIAMETERS
2) VARIABLE SPHERICITY
3) CURRENT-NORMAL ORIENTATION

Figure 17: A diagrammatic illustration of the concept of 'equilibrium area'. See text for details.

series of discoidal clasts, it is apparent that required angles are inversely proportional to the degree of clast flatness. This agrees with the present data of α versus Ψ_p shown in figure 12A as well as the speculated total relation shown in figure 12B: in the former diagram, scatter probably derives from the secondary effects of clast size. In addition, the findings of Cailleux (1945) and Johansson (1965) (Table 2) are firmly endorsed.

Use of the stability criterion also offers an explanation for the predominance of low to moderate angles of imbrication (Table 3). In the present analysis, using a small number of ellipsoidal clasts, the average angle necessary for the projection of equilibrium areas is $\overline{34.2}^{\circ}$ (Table 14). It is also worthwhile noting that the 36 α-values listed in Table 14 render a distribution with slight negative skewness and with a modal class of $25-30^{\circ}$ (see p.50).

A more thorough explanation of variability in the imbrication angle is achieved by means of sphericity-form diagrams (Sneed and Folk, 1958) (Fig. 18). By confining within-diagram variation to shape (i.e. by making constraints for clast size and orientation with respect to flow), the triangular diagram can be used to show the required imbrication angle. For symmetric ellipsoids, data points for construction of α-contours can be found using equations 8 and 9. Since the nominal diameter of an ellipsoid is given by the formula

$$d_n = (a.b.c)^{1/3} \qquad \text{.....(10),}$$

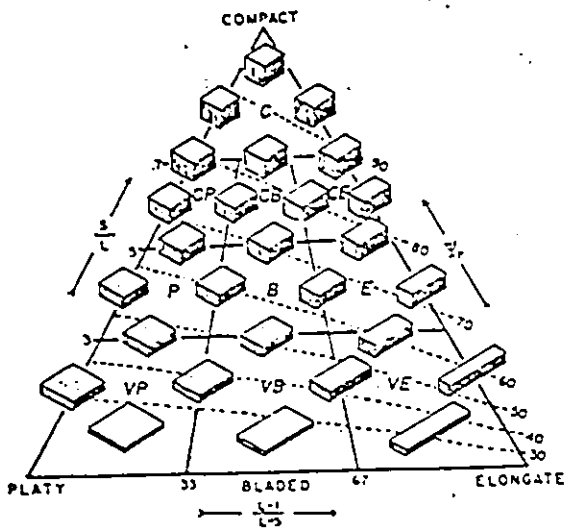

Form triangle. Shapes of particles falling at various points on the triangle are illustrated by a series of blocks with axes of the correct ratio; all blocks have the same volume. Independence of the concepts of sphericity and form may be demonstrated by following an isosphericity contour from the disklike extreme at the left to the rodlike extreme at the right.

Figure 18:. The sphericity-form diagram of Sneed and Folk (1958). Iso-sphericity contours are shown as dashed lines. L, I and S refer to the long, intermediate and short axes of the blocks, respectively.

the calculation of triaxial dimensions all yielding the same volume is made easier by selecting figures such as 100 and 1000 for the product (a.b.c): using equation 10, d_n is equal to 4.64 and 10cm, respectively. These values were selected for the calculation of α-values, both because of their relative ease of computation and because they encompass the range of clast sizes employed in the flume experiments.

Comparison of the contour patterns for these two clast sizes failed to indicate any dependence of the imbrication angle on clast size, and therefore only the contour pattern for d_n = 4.64 cm is illustrated (Fig. 19). The trend of α-contours parallels those of sphericity, especially for current-parallel orientation. In each diagram, a zone of '90° imbrication' beneath the upper apex for spheres is a prominent feature.

Current-parallel orientation produces a slightly larger zone of vertical imbrication, and for bladed-prolate shapes (with $(a-b)/(a-c)>0.4$) higher angles of imbrication are involved. The discrepancy between the two orientation modes increases from zero degrees to over 30° commensurate with the oblate-prolate trend across the diagram. Shape is principally responsible for the observed contour patterns: the inter-relationship between values of α and Ψ_p are in

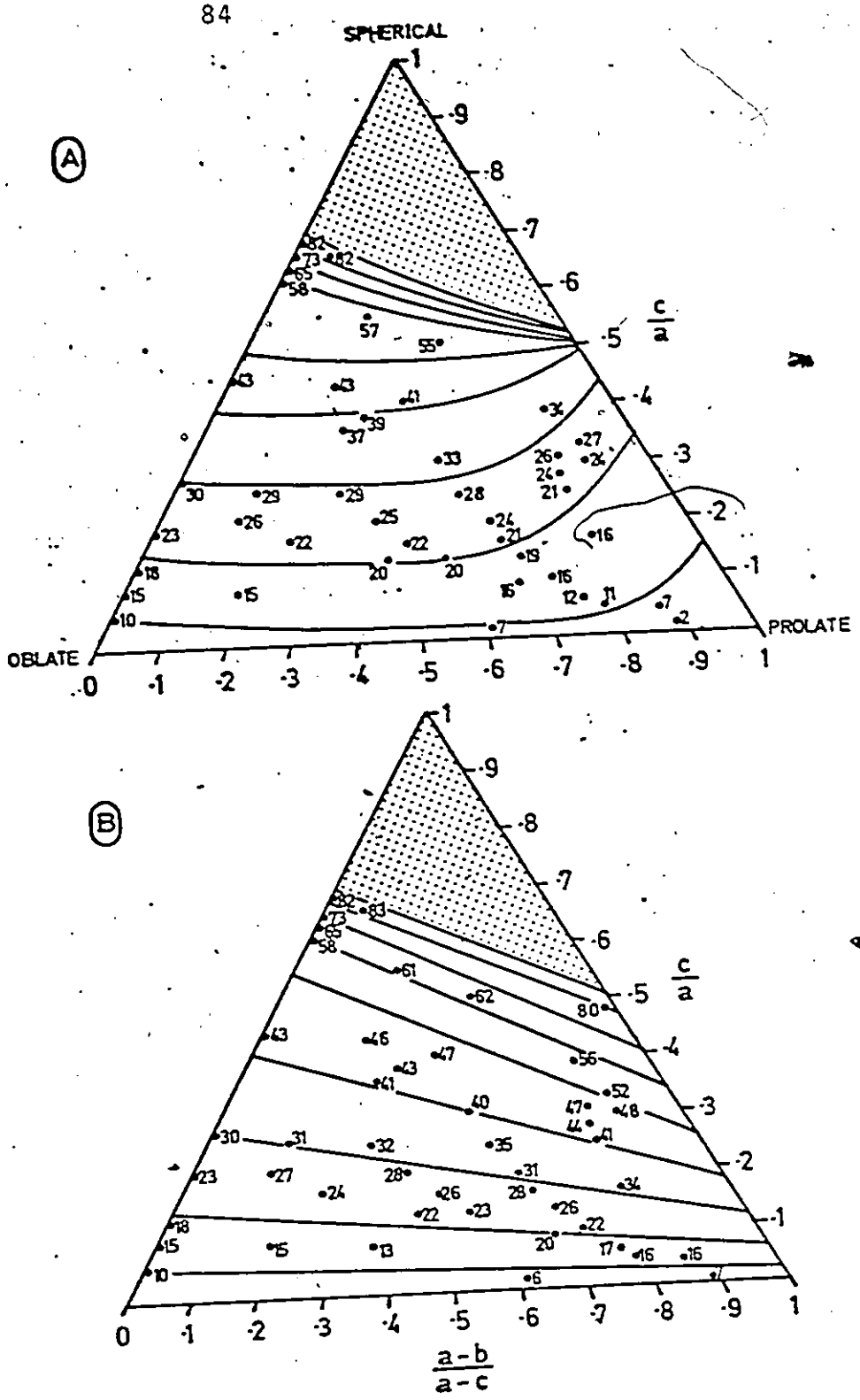

Figure 19: Sphericity-form diagrams showing α-contour patterns for ellipsoidal clasts with d_n = 4.64cm: A. current-normal orientation, B. current-parallel orientation.

agreement with the findings of previous investigations (Table 2), and of this study (Fig. 12). Field workers interested in clast fabric have been correct in confining measurement to the less spherical component of the available clast population.

Although the contoured diagrams embrace the full range of α from zero to 90°, the area occupied by high angles is relatively narrow, so that low-moderate angles predominate: this is also in accordance with all previous work. The literature review found no conclusive effect of clast size on the angle of imbrication for natural clast populations with considerable shape variation; the calculations of theoretical α values revealed a negligible influence of variable size. There is also some evidence (Johansson, 1965, p. 18) to support the present finding that current-parallel orientation of a-axes is associated with somewhat steeper angles of imbrication. In the channel sediments studied by Unrug (1957) there was a tendency for oblate and prolate clasts to be orientated transverse and parallel to flow, respectively. If there is a tendency for steep angles of imbrication to be unstable, Unrug's observation would be anticipated from the present findings.

As a concluding note in support of the proposed stability criterion, Gibling (personal communication, 1975) has found that some Devonian conglomerates from the Canadian Arctic contain beds in which clast populations conform to the

optimum relation of A_p versus d_n. It seems likely that many environments of coarse-grained sedimentation would not be conducive to the attainment of perfect equilibrium: in such cases, it is proposed that the theory outlined in this section would enable recognition of that disequilibrium.

3.42 Orientation

The δ-response of inequidimensional clasts on a sand bed at below threshold conditions is highly dependent on clast properties and on the degree of form roughness of the bed.

The equilibrium response can be tested by purposely creating disequilibrium and viewing the attainment of equilibrium. For example, Kelling and Williams (1967) began their experimental runs with clast a-axes aligned at 45° to the current direction, and observed reorientation to the current-normal position.

3.421 Reorientation from current-parallel alignment

Two preliminary runs (EK3D-2 and -4) were conducted in the upper-flow regime to ensure that current-normal orientation remained the equilibrium response, and also to compare the process variables related to the clasts themselves. The runs were commenced with a-axes parallel to

flow which constitutes a more stringent test of the flow's ability to achieve an equilibrium response. Run EK3D-2 was characterized by the larger standing wave forms and periodically, more violent breaking antidune activity.

Orientation data were analysed using the method of Curray (1956): the results are given in Table 15. To assess the role of clast properties on clast reorientation, the clast population was equally divided on the basis of nominal diameter and oblate-prolate index.

Analysis of the total population indicates that the degree of angular rotation increases with rising flow, with a distinct trend towards a dominantly current-normal orientation. However, analysis of individual size and form categories clearly points to a bimodality of orientation. Owing to this bimodality, vector means of undivided populations reflect the stronger mode and vector magnitudes are lower than when the groups are subdivided. The current-normal and current-parallel modes are principally occupied by small prolate clasts and large oblate clasts, respectively: this trend was particularly developed at the higher-velocity run. The most conspicuous feature is the ease with which prolate forms reorientate towards a current-normal orientation.

TABLE 15: Orientation analyses of the data from runs with initial current-parallel orientation: n-sample size, D-angular deviation from current-normal orientation, L-vector magnitude, and P-probability that the observed degree of preferred orientation resulted from a random distribution

	Run EK3D-4				Run EK3D-2		
	n	D	L	P	D	L	P
Total population		58.9^{o}	7.4%	<0.19	19.6^{o}	9.7%	<0.8
Large category, $d_n > 4.95$cm	15	53.4^{o}	21.9%	<0.6	85.9^{o}	10.2%	<0.19
Small category, $d_n < 4.95$cm	16	11.9^{o}	5.7%	<0.95	14.4^{o}	27.3%	<0.3
Oblate category, $\overline{OP}<0$	14	73.2^{o}	60.2%	<0.01	80.2^{o}	32.2%	<0.3
Prolate category, $\overline{OP}<0$	17	11.3^{o}	26.8%	<0.8	1.7^{o}	38.7%	<0.06

The rose-diagrams in figure 20 more clearly illustrate the relative effect of clast size and form: prolate clasts show significant current-normal orientation, whereas oblate clasts essentially retained their current-parallel orientation. For the clast population used in these experiments, there is no inter-dependency between d_n and $\overline{OP}$ ($r = -0.033$). Accordingly, the tendency of small clasts toward current-normal orientation is unrelated to form. The large clasts essentially retain a current-parallel orientation which may indicate that three hours is insufficient for completed response. However, high degrees of oblateness pose a definite limit on reorientation.

These results generally agree with those of Kelling and Williams (1967) who found an appreciable form effect, but no apparent influence of clast size within the range 1.2-2.3cm arithmetic mean size. Kelling and William's figure 6 shows prolateness to be a more critical shape factor than oblateness in that the former category was related to a greater response towards a current-normal configuration.

Current-normal orientation of elongate clasts has been observed to result from transport by rolling (Johansson, 1963). However, the present experiments in which clasts were initially laid with long axes parallel to flow and underwent a 90° rotation in situ require additional explanation. The cause

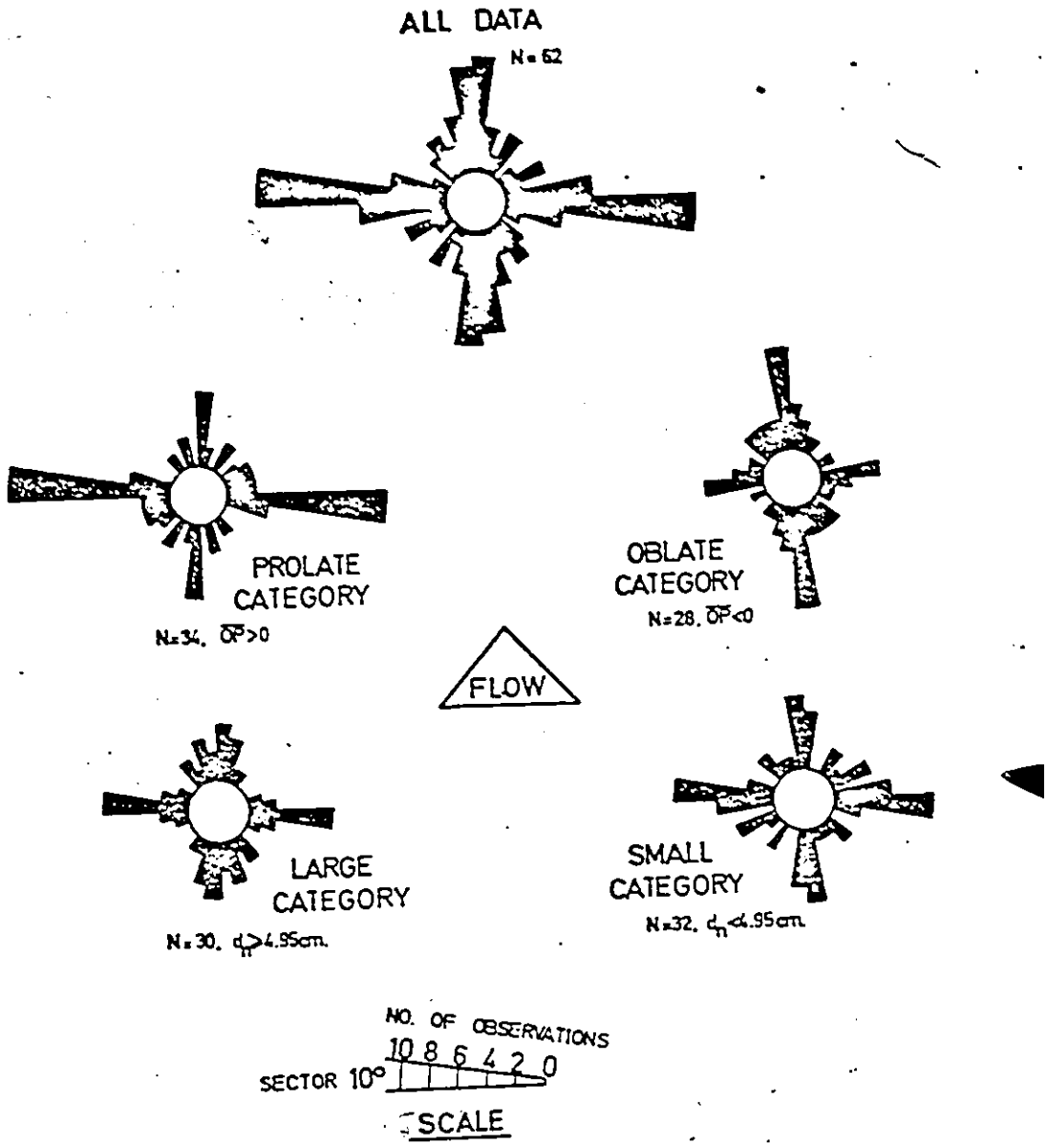

Figure 20: Rose diagrams of the grouped orientation data from runs with initial current-parallel orientation.

of reorientation cannot be determined merely by simple bivariate correlations between process variables and the amount of angular deviation. The observation that degree of reorientation is correlated with a shape property, for example, does not provide any insight into the cause of reorientation - rather it shows that clasts with a certain shape are more readily reorientated. The reorientation only occurs in a sandbed of adequate thickness, and after sufficient time. These two conditions allow the attainment of hydrodynamically stable imbrication. With increasing prolateness, the A_p/d_n (Section 3.412) ratio becomes increasingly different for clasts in current-normal and current-parallel positions, whereas with increasing sphericity the ratio shows less variation related to orientation. For a particular clast size, the projection area required for hydrodynamically stable imbrication is attained at lower angles when the clast is aligned transverse to flow. This is especially the case for prolate clasts; for oblate clasts, having subequal a and b axial lengths, orientation is immaterial. It is therefore proposed that current-normal orientation of clasts on a sandbed is an indirect result of reaching stability. Current-crescent scour around each clast facilitates clast reorientation.

Stability of clasts on a streambed may be broadly analagous to settling behaviour (Blatt, Middleton and Murray, p.65, 1972) where particles achieve stability by maximising resistance.

Elongate pebbles isolated on a sandbed are typically orientated transverse to flow (Laming, 1966; Rust, 1972a; this study), usually with unimodal distribution. In the light of the present findings however, a tendency toward bimodality raises the possibility that the pebbles were initially deposited from suspension and/or saltation in current-parallel alignment but were subsequently reorientated to give a dominant current-normal mode. It is unlikely that sedimentary structures in the host sandbed would assist in distinguishing the initial depositional fabric of the isolate pebble population. Complete 90° reorientation requires that the bed be non-aggrading, and that motion of clasts be unimpeded throughout the time required for realignment.

3.422 Imperfections of current-normal alignment

Having established that over a wide range of flow intensity, current-normal orientation of isolate clasts is a stable steady-state configuration, ten experimental runs spanning the lower- and upper-flow regime were conducted with a-axes laid normal to flow.

The initial fabric is hydrodynamically stable but undergoes slight, systematic variation owing principally to the indirect effects of variable form roughness of the sandbed. The process variables governing these minor realignments were found to be extremely similar to those of the first two runs.

Table 16 and figure 21 indicate the combined effects of flow regime and clast properties. The salient point is that vector magnitude considerably declines (down to 80%) in runs where dunes and antidunes are the host bedform, but remains close to 100% in runs with ripples and the transition plane bed (cf. Fig. 11). Form roughness appears to act as a means by which variability of clast properties are able to achieve an effect on clast alignment.

3.43 A-axis inclination

Section 3.2 indicated that a-axis inclination is not a major response (the histogram of its distribution does not show significant departure from 0°) and is independent of the nature of the host sand bedform (Section 3.3). Current-normal orientation obviously necessitates that a-axes be essentially horizontal.

The γ-response, however, does display a high degree of dependency on the 'composite asymmetry index', denoted AI. The definition of clast asymmetry used in this study is similar to that of Cailleux (1945): the word 'composite' is

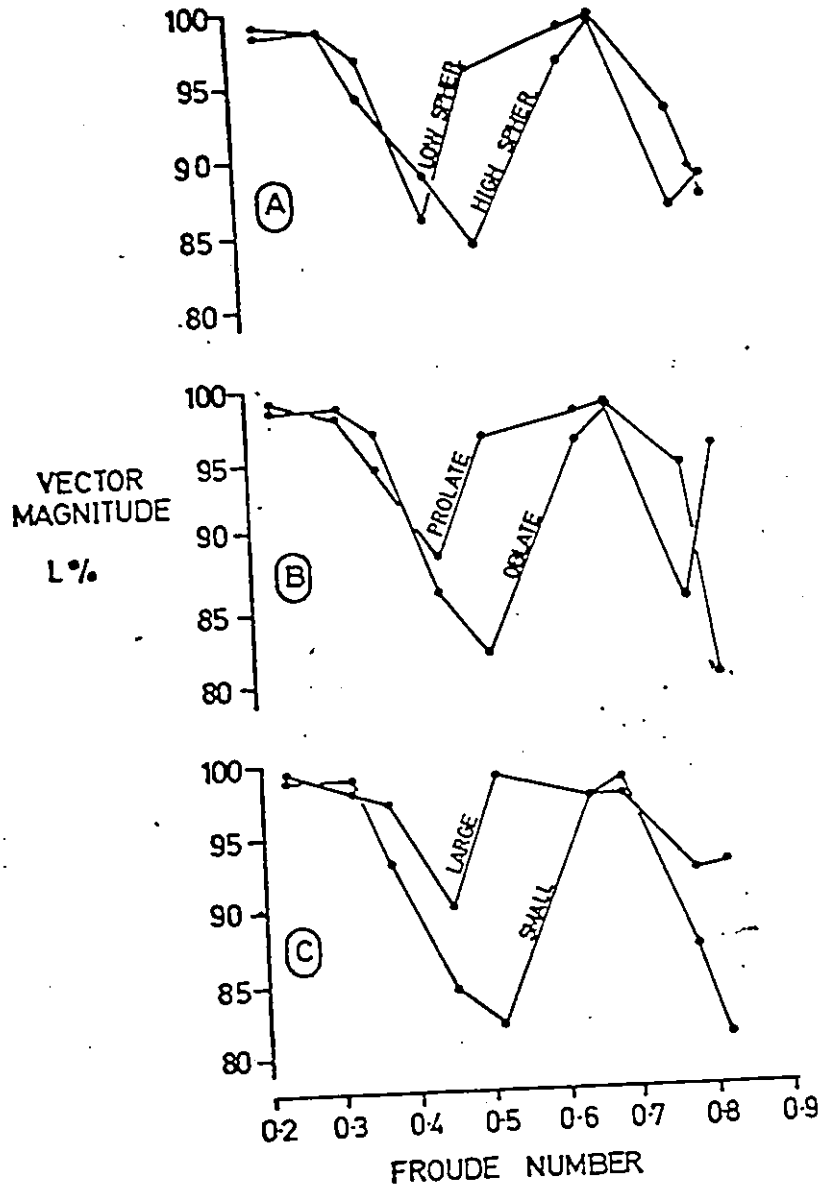

Figure 21: Variable influence of clast properties - A. maximum projection sphericity, B. oblate-prolate index, C. nominal diameter - on the β-response with varying Froude Number.

TABLE 16: Orientation analyses of the data from runs with initial current-normal orientation: all preferred orientations are significant at $<10^{-3}$ level. D and L are as previously defined in Table 16.

Run #	Total population D		Large category D		Small category D		Oblate category D		Prolate category D		Low Spher. category D		High Spher. category D	
	L		L		L		L		L		L		L	
EK3D-14	.7°	98.8%	.4°	99.4%	1.7°	98.8%	.1°	98.5%	1.2°	99.2%	1.2°	98.4%	.3°	99.1%
-6	1.8°	98.4%	.7°	98.0%	2.9°	98.8%	1.2°	98.7%	2.3°	98.1%	.4°	98.7%	3.9°	98.6%
-11	.9°	97.5%	.6°	98.0%	1.2°	97.1%	1.6°	96.4%	.3°	98.5%	0.5°	96.8%	1.3°	97.8%
-13	.6°	87.2%	1.7°	90.1%	.5°	84.7%	1.4°	86.1%	2.2°	88.5%	1.4°	88.9%	.2°	85.8%
-10	1.2°	90.0%	.5°	98.9%	2.9°	82.1%	1.4°	82.0%	.9°	96.7%	2.5°	84.1%	.1°	95.8%
-9	2.4°	97.2%	.4°	97.4%	4.2°	97.4%	3.6°	96.1%	1.4°	98.1%	4.5°	96.5%	.4°	98.3%
-7	.4°	98.9%	1.2°	99.3%	.3°	98.5%	1.1°	98.4%	.1°	98.3%	1.3°	98.7%	.4°	99.1%
-5	2.7°	89.3%	1.0°	92.3%	4.4°	87.0%	3.6°	85.4%	.6°	94.4%	4.9°	86.4%	.7°	92.7%
-12	1.0°	86.7%	.8°	92.7%	1.3°	81.0%	1.6°	95.5%	3.4°	80.0%	2.9°	88.1%	4.8°	86.7%

used here to convey the fact that values of AI are average values of two measurements taken on the a-b and a-c planes. This index expresses the degree to which particle mass is unequally distributed along the a-axis (Fig. 22).

Clast asymmetry causes inclination of the a-axis in the direction of greater mass concentration. When the median value of AI is used to equally subdivide the population for each run, this role is clearly seen (Fig. 23). Asymmetric clasts respond with a-axis inclinations 2-5° steeper than the symmetric group, although this difference may incorporate some degree of error (see p.47). When the Froude number approaches 0.1, current-crescent scour is too sluggish to allow any systematic influence of clast asymmetry: this onset of the threshold for scour is indicated by the closure of the graph lines toward the data points of the low flow runs. The trend of asymmetric clasts towards greater γ-response terminates in the upper-flow regime; the data from the run with Froude number 0.812 lack a difference between the symmetric and asymmetric groups. This is probably because stable imbrication is attained too rapidly to permit any systematic development of a-axis inclination.

The average effect of composite AI on the γ-response (Fig. 24) is expressed by the equation

$$\gamma^{\circ} = 0.19(157.3^{AI})$$

MEASUREMENT:

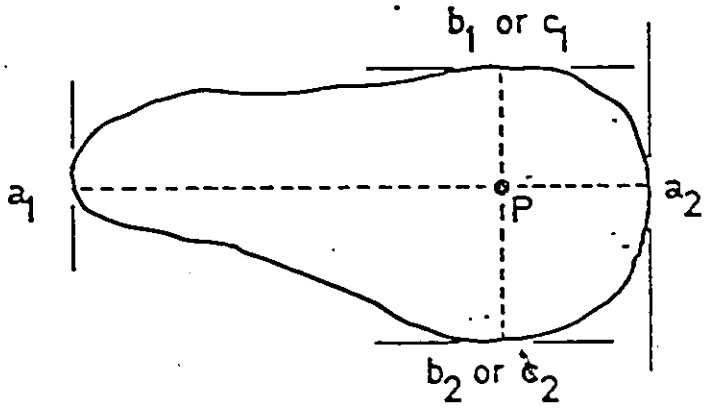

CALCULATION:

$$A.I. = \frac{P - a_1}{a_2 - a_1}$$

$$0.5 \leqslant A.I. \leqslant 1.0$$

AFTER CAILLEUX (1945)

Figure 22: Measurement and calculation of the 'Composite Asymmetry Index'.
a, b and c denote the long, intermediate and short axial lengths, respectively.
Subscripts $_1$ and $_2$ denote extremities of clast axes.
P denotes the point of intersection of a and b, or a and c, axes. For the purposes of calculation, both positions of P are considered to yield an average (hence 'composite') value of A.I.

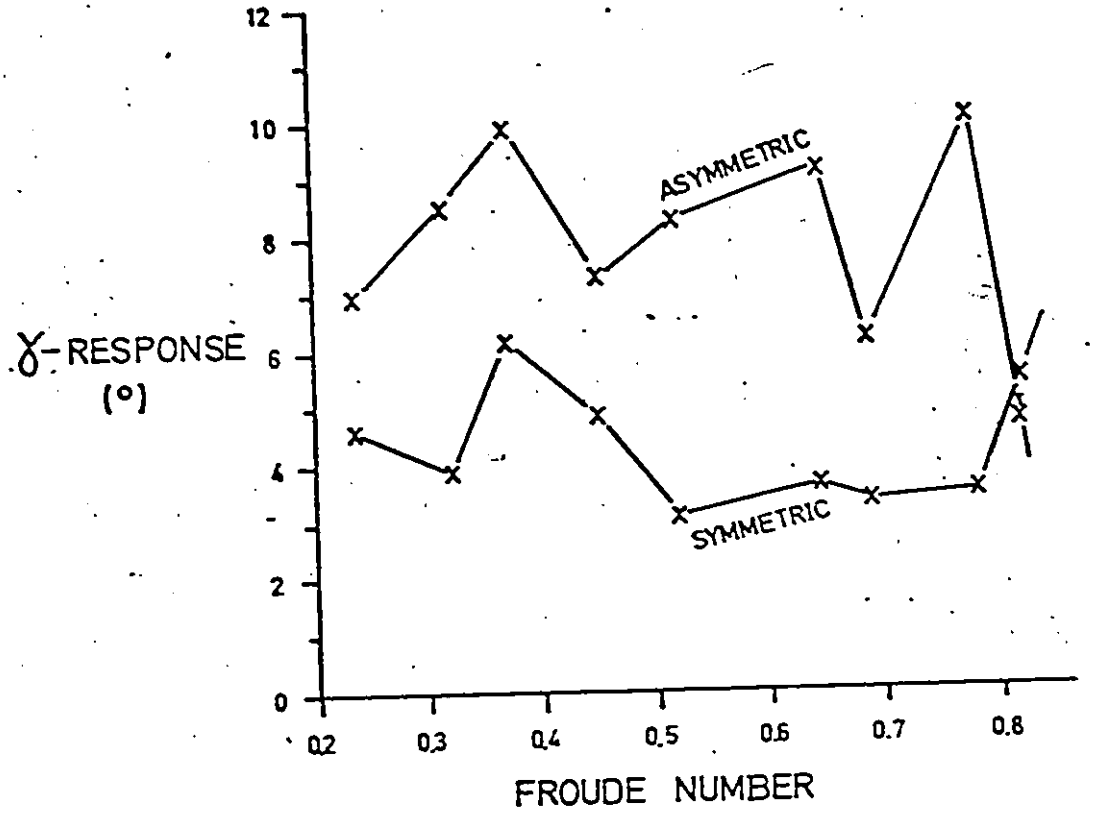

Figure 23: The influence of the composite asymmetry index on the γ-response of each run. Subdivision is based on the median AI value of 0.62.

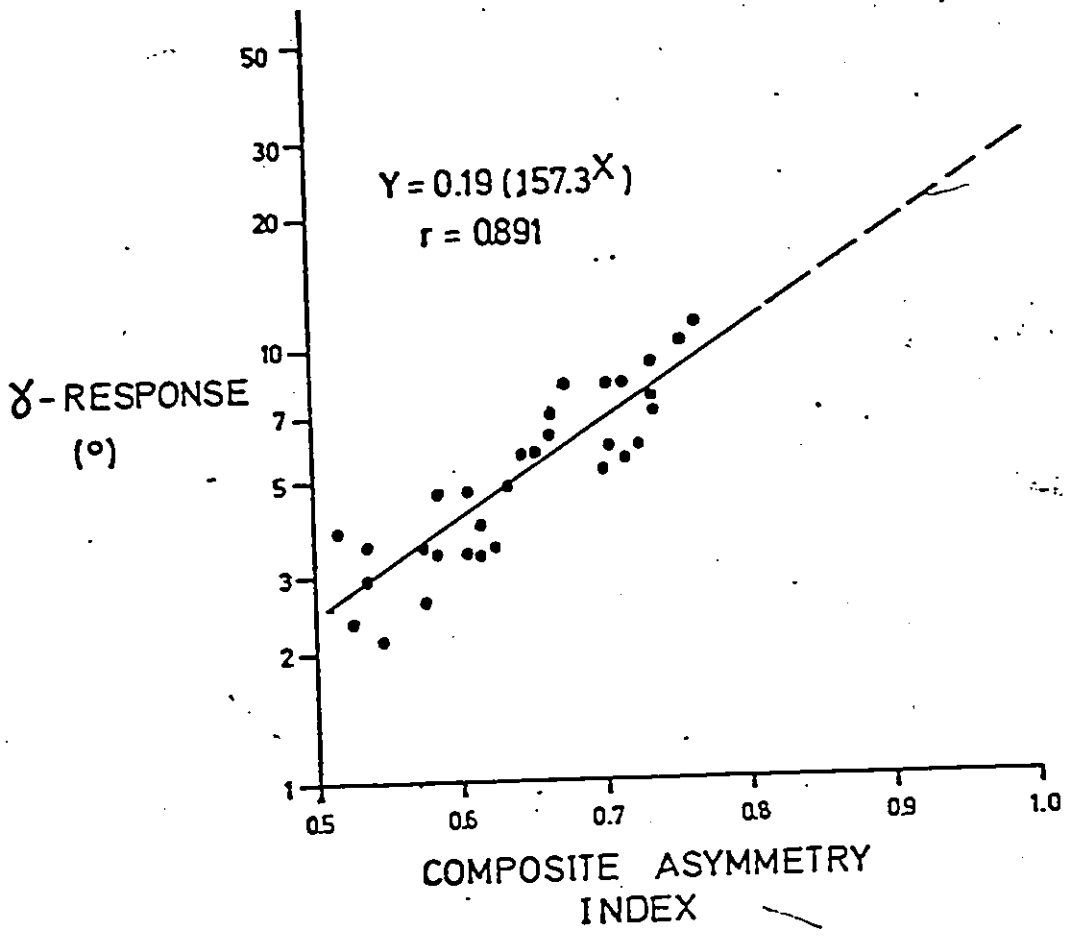

Figure 24: The exponential relationship between the γ-response and the composite AI index. Each point represents the mean a-axis inclination for each clast.

for which r = 0.891. The empirical formula is exponential in its form, but has finite limits owing to the nature of the process variable: a γ-response of 30° is predicted for a clast with maximum asymmetry (AI = 1). A-axis inclination is suggested even under conditions of perfect symmetry (AI = 0.5), but this probably arises from a combination of insufficient data for precise regression analysis, natural randomness in the fluvial system, and imperfections in the initial layout of the clasts on the sandbed.

In spite of these limitations, almost 80% of the observed variability in the γ-response can be explained by the composite asymmetry index. The unexplained portion might in part be due to the oblate clast category, which because of a tendency toward imperfect transverse orientation (Sections 3.411/2) is more susceptible to a-axis inclination.

3.44 Motion parallel to the x flow axis

The only previous laboratory study of upstream motion of large isolate clasts on a sandbed was that of Fahnestock and Haushild (1962), but their work has limited application because their clasts were all highly spherical and well rounded. The present study indicates that roundness of the b-c plane, maximum projection sphericity and

nominal diameter are all important process variables in determining the magnitude of the X-response (Table 17). Increasing values of these parameters relate to increasing amounts of upstream motion accompanying the imbrication process.

High degrees of roundness assist rolling and/or sliding, because surface friction is reduced. For the same reason, high degrees of equidimensionality also favour greater upstream motion. The effect of greater submerged weight is reflected by the moderate value of correlation with nominal diameter.

The X-response is further explained by figure 25. Within the lower-flow regime, the well-rounded group moves upstream 1-1.5cm more than the low roundness group. The distinction is less regular for the subdivisions based on sphericity and size. The effect of the oblate-prolate index seems to reverse from low to high amplitude bedforms: when the host bedforms are ripples or in-phase waves elongate clasts undergo more upstream motion, but in dune runs flat clasts show the greater response. It would therefore seem that these two categories of bedforms are conducive to a rolling and sliding type of motion, respectively. At the regime transition, the plane bed condition essentially eliminates the effect of clast properties. In the upper-flow

TABLE 17: Regression and correlation analyses of the X-response

Parameters

Dependent response variable - X, distance of upstream motion (cm).

Independent process variables d_n, nominal diameter
$\overline{OP}$, oblate-prolate index
ψ_p, maximum projection sphericity
P, roundness of b-c plane

Bivariate Analysis

a) Matrix of Correlation Coefficients

	X	d_n	$\overline{OP}$	ψ_p	P
X	1.000	-0.523(1)	-0.274	-0.720(1)	-0.764(1)
d_n		1.000	-0.003	-0.029	0.319
$\overline{OP}$			1.000	0.486(1)	0.469(1)
ψ_p				1.000	0.684(1)
P					1.000

N.B. (1) denotes significance level in excess of 95%.

b) Regression Equations

$$X = -(2.71 + 0.23d_n)$$
$$X = -(3.97 + 0.030\overline{P})$$
$$X = 0.15 - 0.11\psi_p$$
$$X = -(2.73 + 4.28P)$$

Multivariate Analysis

Function	Correl. Coeff.	% explanation
$X = f(d_n, \psi_p)$	-0.9061	82.1
$X = f(d_n, P)$	-0.8192	67.1
$X = f(\psi_p, \overline{OP})$	-0.8106	65.7

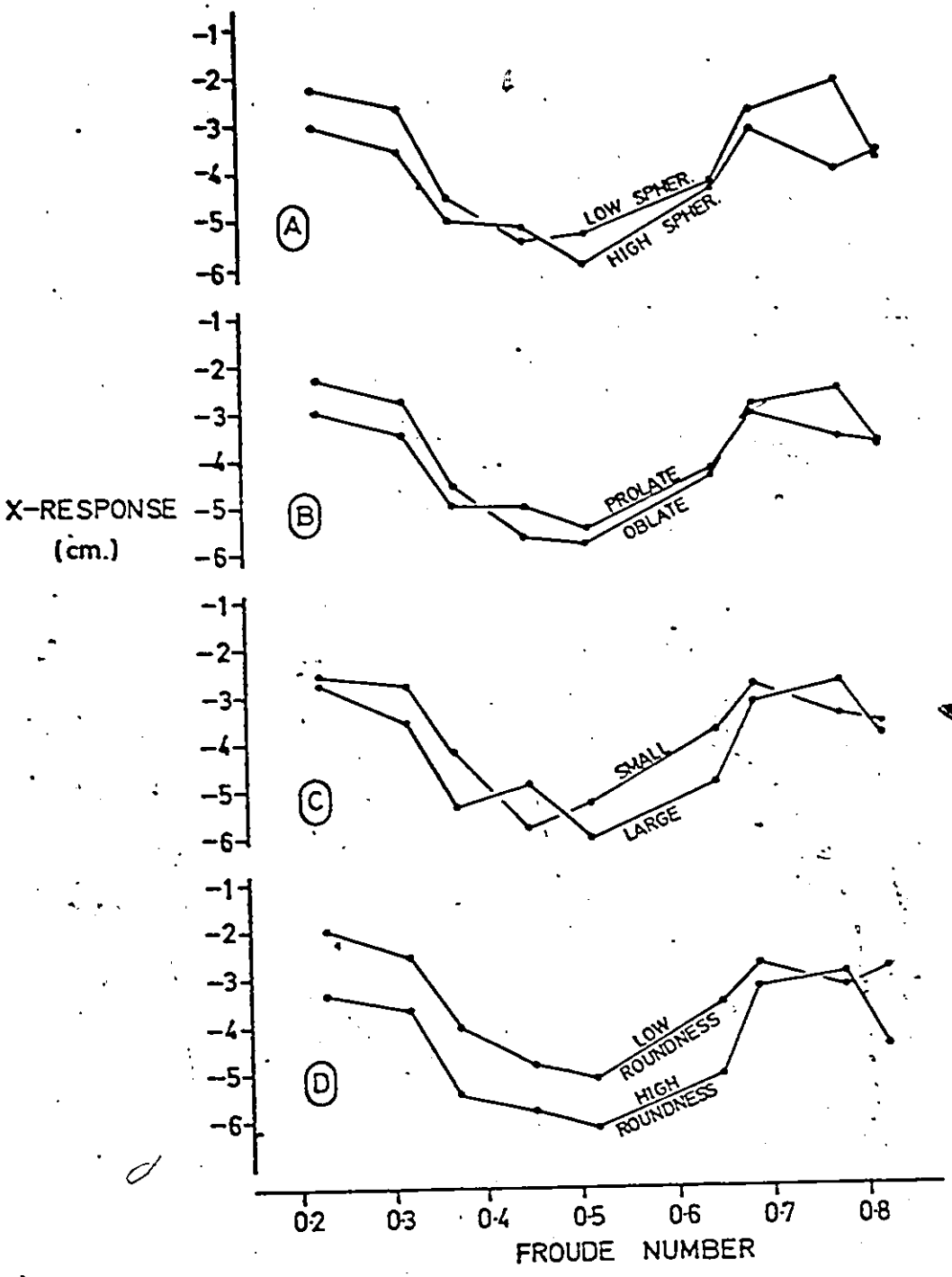

Figure 25: Variable influence of clast properties - A. maximum projection sphericity, B. oblate-prolate index, C. nominal diameter, D. b-c plane roundness - on the X-response with varying Froude Number.

regime, differences in the magnitude of upstream motion between shape, form and size groups are less systematic: this is probably due to imminent transport (i.e. + X response) under conditions of high shear stress. As with the other responses, the influence of clast properties is made possible by the presence of three-dimensional bedforms.

Multivariate analysis indicates that the most accurate descriptive equation for the X-response is one which incorporates sphericity and size. The combination of b-c plane roundness (which has the highest bivariate correlation with the X-response, see Fig. 26) with sphericity or size does not produce better results owing to their interdependence (Table 17). The equation

$$X = 0.142 - 4.93\psi_p - 0.233d_n, \quad r = 0.9061$$

has high accuracy (Fig. 27). The observed magnitude of the X-response is predicted with ± 10% error for 87.1% of the data.

The semi-quantitative study of Fahnestock and Haushild (1962) indicated that an increased amount of upstream movement accompanies the change from ripple beds to dune beds. This observation accords with the findings of the present study, except that as much upstream motion occurs in the upper-flow regime as in ripple runs.

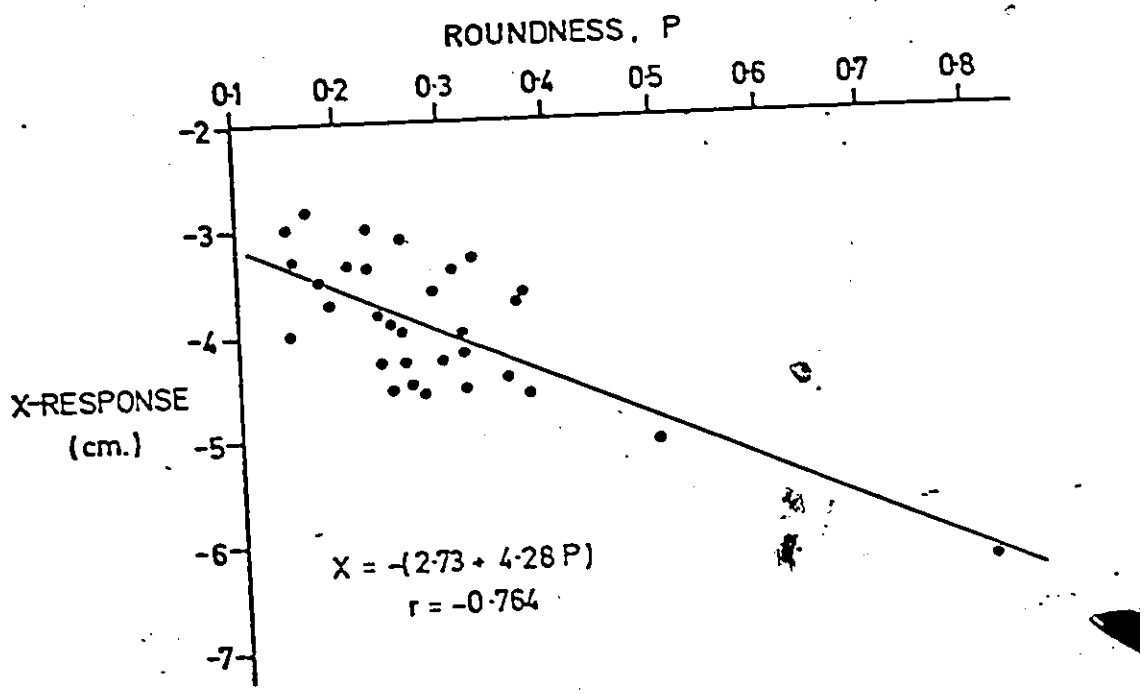

Figure 26: The mean X-response for each clast as a linear function of b-c plane roundness.

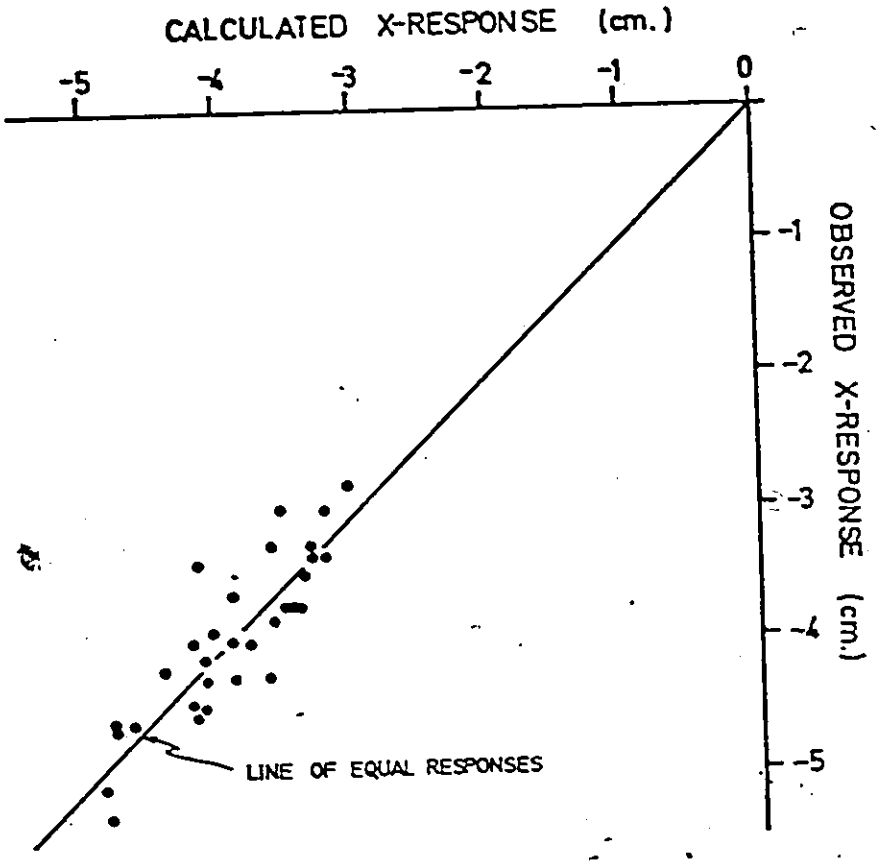

DISTRIBUTION OF ERROR

Percent error (±)	Number of Measurements	Percent Error
0 - 5	16	51.6
5 - 10	11	35.5
10 - 15	3	9.7
15 - 20	1	3.2
	31	100.0

Figure 27: Observed mean X-response compared to those calculated according to the multivariate predictive equation:

$X = 0.142 - 4.93U_{lp} - 0.233d_n$.

3.45 Motion parallel to the y flow axis

The lowering in clast elevation during the imbrication process results from the action of gravity forces in response to current-crescent scour. In comparison to the two other translational responses, the Y-response is of intermediate magnitude. Variability in the amount of downward motion for the whole clast population duplicates that determined for clast #73 alone (Table 19).

Analysis of the Y-response indicates that maximum projection sphericity, nominal diameter and roundness of the b-c plane are all important process variables (Table 18). Increasing values of these clast parameters produce increasing depths of current-crescent scour which in turn raises the potential for downward motion. Their specific role may be briefly described as follows. Localised scour around stationary clasts deepens with increasing value of the particle Reynolds number. For a given clast size, the effective height of roughness elements increases with increasing sphericity, but roundness is a potential compensating influence because high values serve to minimise angular disruption of streamlines. As with the X-response, high degrees of roundness in the plane parallel to flow assist rolling and/or sliding because surface friction is reduced.

TABLE 18: Regression and correlation analysis of the Y-response

Parameters

Dependent response variable - Y, average downward motion, cm.

Independent process variables - ψ_p, maximum projection sphericity
d_n, nominal diameter, cm
P, roundness of b-c plane

Bivariate Analysis

a) Matrix of Correlation Coefficients

	Y	ψ_p	d_n	P
Y	1.000	-0.646(1)	-0.419(1)	-0.642(1)
ψ_p		1.000	-0.029	0.684(1)
d_n			1.000	0.319
P				1.000

N.B. (1) denotes significance in excess of 95%.

b) Regression Equations

$$Y = -(0.99 + 3.4\psi_p)$$

$$Y = -(2.16 + 0.14d_n)$$

$$Y = -(2.14 + 2.76P)$$

Multivariate Analysis

a) Y as a function of ψ_p and d_n

$Y = -(0.12 + 3.48\psi_p + 0.15d_n)$: r = -0.785, 61.6% of the variability in Y-response explained.

b) Y as a function of P and d_n

$Y = -(1.79 + 2.44P + 0.08d_n)$: r = -0.681, 46.4% of the variability in Y-response explained.

Variability in the sand bedform results in comparatively little difference in the effect of clast parameters. In the ripple and antidune phases particularly, low sphericity and large size are conducive to greater downward motion. Within the dune phase the influence of these clast parameters is minimal, and in the case of run EK3D-13 inconsistent.

Although sphericity and roundness have the highest individual correlations with the magnitude of the Y-response, their moderate interdependence causes the most accurate predictive equation to be one which combines sphericity and size (other reasons for excluding roundness were given in the previous section dealing with the X-response). By means of the multivariate equation

$$Y = -(0.12 + 3.48\Psi_p + 0.15d_n),$$

the observed Y-response of the clast population is predicted with 10% error for 71% of the data (Fig. 28).

3.46 Motion parallel to the z flow axis

Lateral motion of clasts during the imbrication process is a minor response and is of minimal sedimentological importance. The majority of clasts (≈60%) keep within 1cm of their original positions with respect to the z flow axis (Fig. 29): the observed maximum response was almost 6cm. The translation of clasts upstream therefore proceeds with close parallelism to the x flow axis.

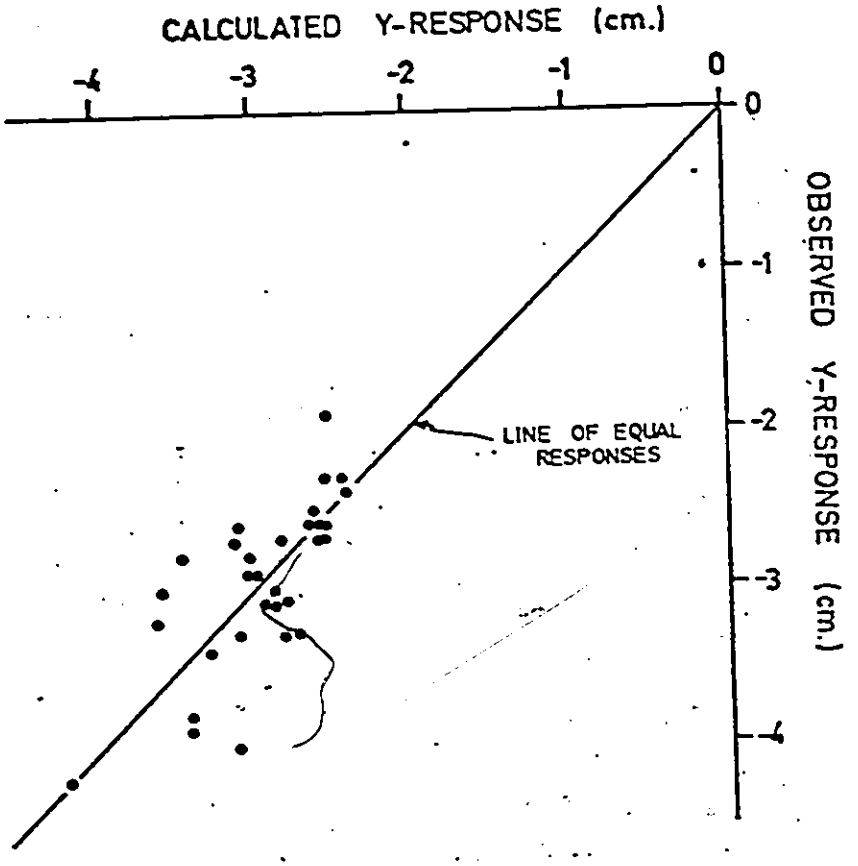

DISTRIBUTION OF ERROR

Percent error (±)	Number of Measurements	Percent Error
0 - 5	17	54.8
5 - 10	5	16.2
10 - 15	5	16.1
15 - 20	4	12.9
	31	100.0

Figure 28: Observed mean Y-response compared to those calculated according to the multivariate predictive equation:

$$Y = -(0.12 + 3.48U_{ip} + 0.233d_n).$$

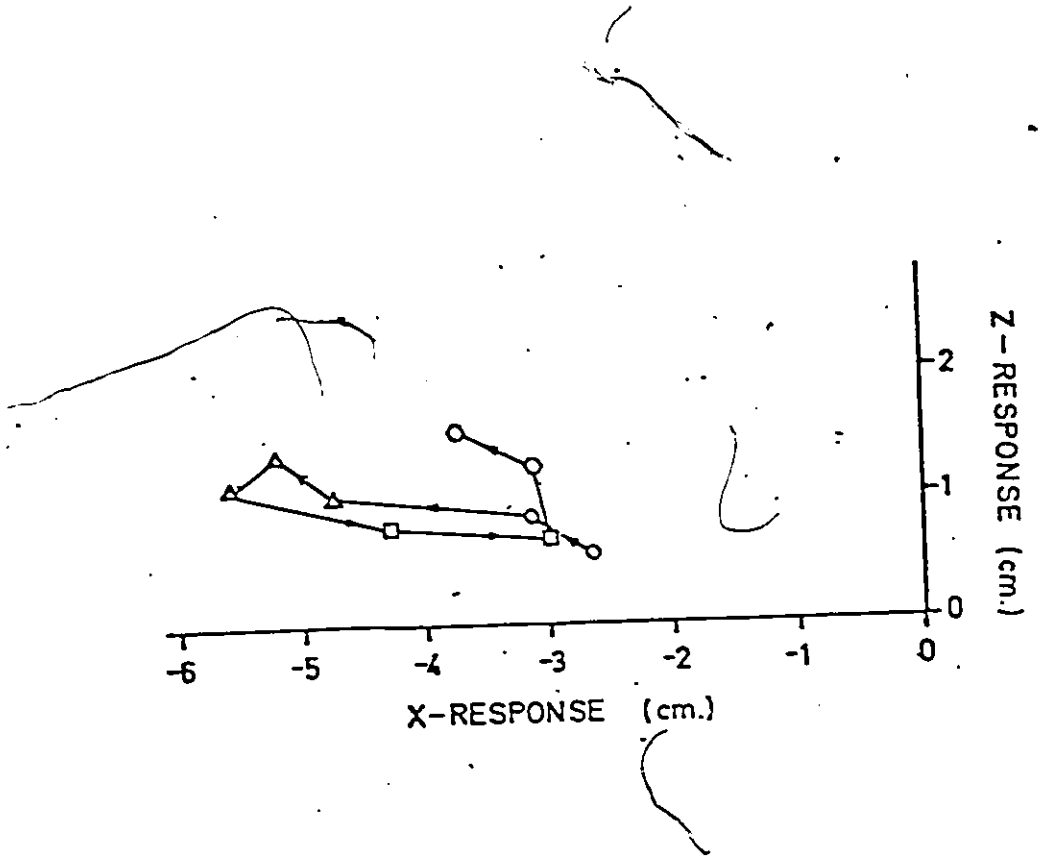

Figure 29: Partial inter-dependence of mean values for each run of the Z-response and X-response.
Refer to figure 15 for explanation of symbols.

The small Z-components of clast translation appear to be an indirect result of the development of the other responses. The magnitudes of upstream and lateral motion are closely interrelated (Fig. 29), the X-response being the dominant variable. Lateral motion is disproportionately large under conditions of high form roughness (i.e. dunes, breaking antidunes). This is probably due to the increased vigour of current-crescent scour as well as to turbulent eddies associated with flow separation. To some extent, the magnitude of the Z-response is also an indirect result of variable clast asymmetry. This parameter has been shown to control the amount of a-axis inclination (Figure 24): as the long axis becomes inclined, the potential for lateral clast motion steadily increases (Fig. 30).

3.47 Magnitude of displacement

Thus far, process-response analysis of translational motion has been conducted according to its three components, which are all closely influenced by the form roughness of the sandbed. In addition, the magnitude of the displacements can be calculated by substituting the X, Y and Z components of displacement for each clast, and in each run, in the formula

$$\vec{if} = (X^2 + Y^2 + Z^2)^{\frac{1}{2}}$$

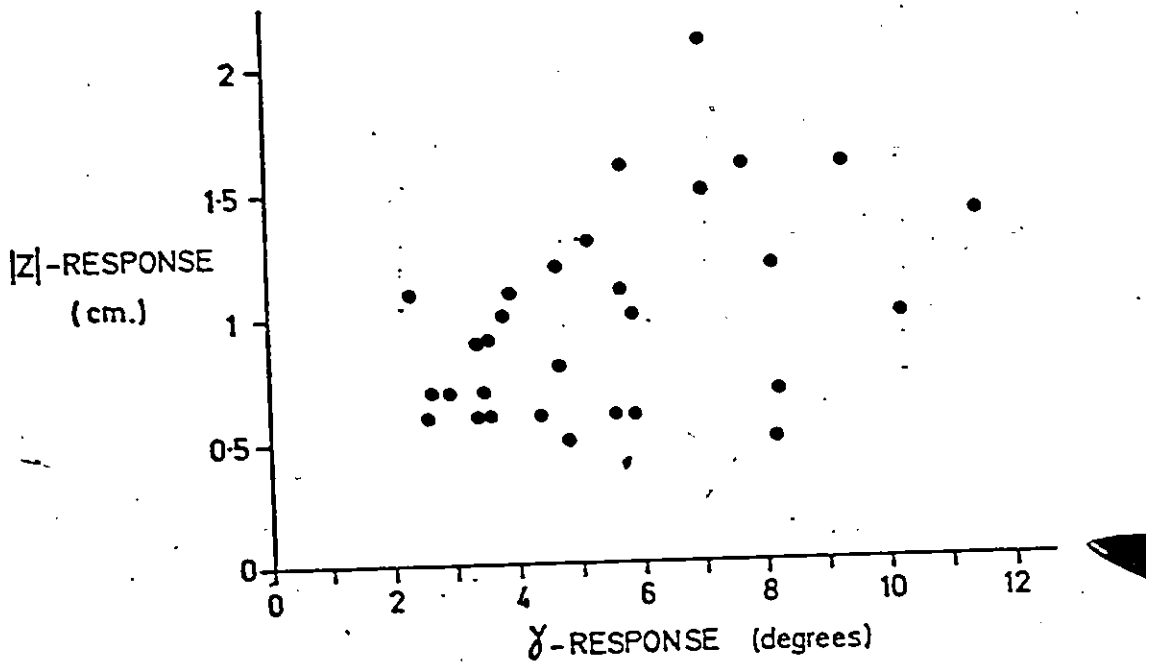

Figure 30: Partial inter-dependence of the mean Z-responses for each clast with those of the γ-response.

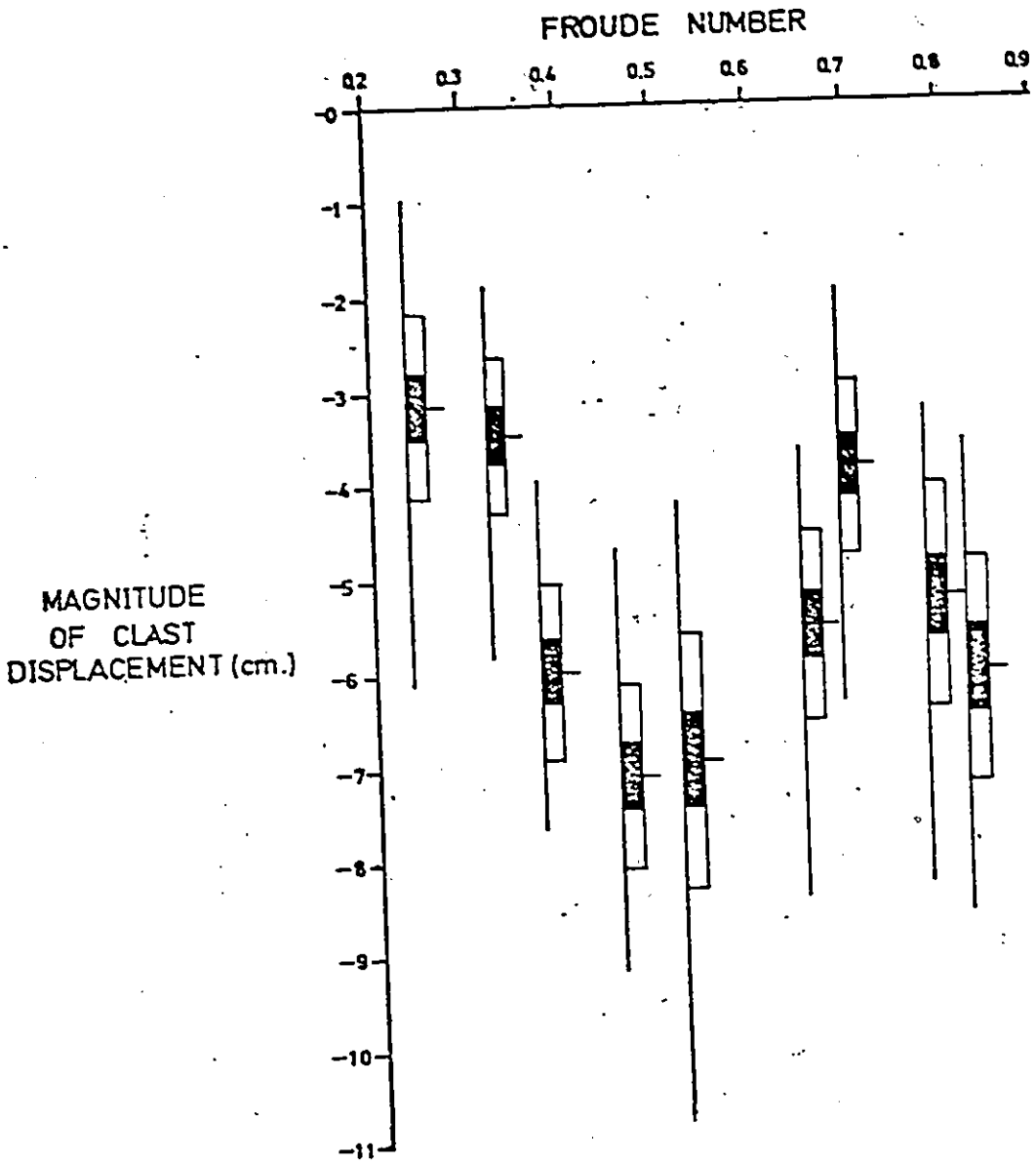

Figure 31: Dice-Diagrams for total displacement vectors at each flume run.

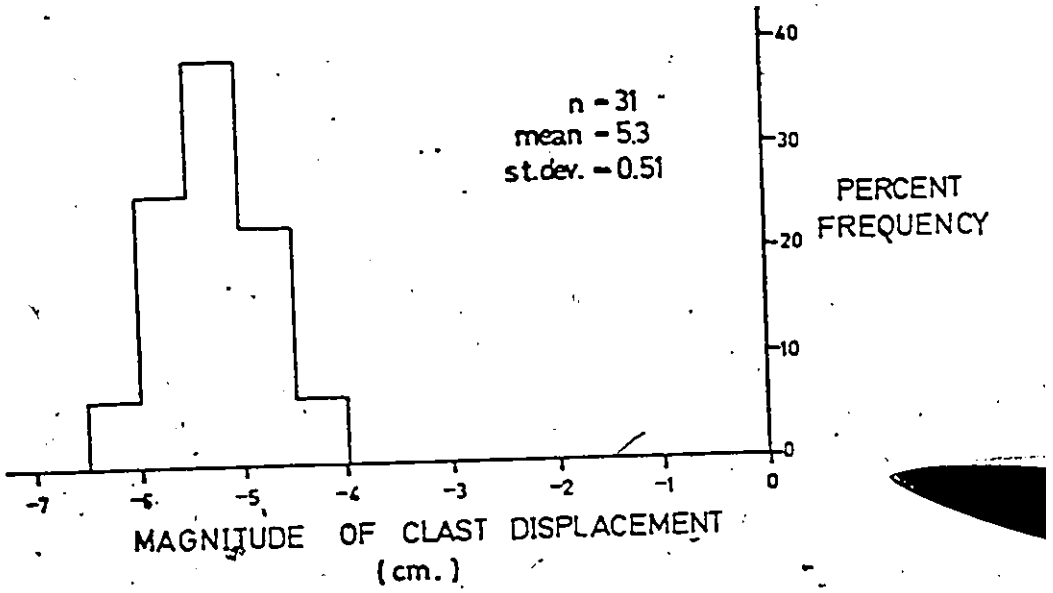

Figure 32: Histogram of mean values for each clast of total displacement.

where $\vec{if}$ denotes the straight-line displacement between the initial and final clast positions.

Figure 31 shows a series of Dice-Diagrams (Fig. 8) representing the distribution obtained from each run. The pattern of variability of the displacement $\vec{if}$ repeats those seen for the individual components (Fig. 9). The standard deviation of the data for each run is remarkably constant at between 0.9 and 1.1cm, but skewness is a more variable statistic of the distributions. An enhanced role of bed roughness is indicated by large and highly significant differences between the values of the various bed phases.

Variability in mean values for each clast falls within a small range of 2.5cm: 87% of the values are within 4.5 and 6.0cm (Fig. 32). In contrast to the three axial components, it was not possible to satisfactorily explain variation in mean values of $\vec{if}$ for each clast. However, the average magnitude of displacement (i.e. 5.26cm) is very similar to mean clast size ($\overline{d_n}$ = 5.59cm).

3.5 Development of the imbrication process

The rate of imbrication, and hence also the duration of the imbrication process, were successfully monitored with the flume's mobile point gauge in seven of the experimental runs. Information of this nature is useful because it potentially enables certain deductions concerning the

rate of aggradation in matrix-supported gravels.

Turbidity prevented direct observation, and it was necessary to exercise extreme care when lowering the point gauge to obtain measurements of clast elevation. The gauge was moved in small increments in the -x, -y and ±z flow axial directions to follow the clast motion in three dimensions. To define the initial rate of development accurately, measurements were taken at ½-minute intervals. The submerged portion of the point gauge which comprises two thin vertical rods and a small horizontal base plate does not significantly disrupt the ambient flow structure nor the scour processes active a few centimetres below the level of measurement.

There are advantages (comparison between different flows) and disadvantages (questionable application to clasts with different size and shape properties) to confining measurement to one clast: however, this was necessary in view of the method used. Manual sensing was found to be easiest with the largest clasts, and so measurement was confined to clast #73 for which d_n = 11.14cm, Ψ_p = -4.42. During some lower flow regime runs, the angle of imbrication was periodically determined by means of a waterproof clinometer: the azimuth of inclination was assumed to be parallel to the x flow axis.

Data of maximum clast elevation (h) plot as a straight-line function of the time elapsed (t) on semi-logarithmic coordinates (Fig. 33), and therefore fit an equation of the form

$$h = a + b(\log t)$$

The constant a merely indicates the initial clast elevation; to facilitate direct comparison of the different rates of development encountered in the experimental runs, the equation is simplified thus.

$$h = b(\log t).$$

Of primary interest is the variability in the coefficient b (Table 19). With the exception of the lowest ripple run (EK3D-14), b is positive, indicating that as imbrication develops, the highest point of the clast traces a downward inclined vector. Processes associated with current-crescent scour are unable to raise a clast's centre of gravity. Imbrication can therefore be attained by the clast either rotating about its centre of gravity, or by undergoing simultaneous translational and rotational motion resulting in a lowering of the centre of gravity. If the clast attained stable imbrication merely by <u>in situ</u> rotation, its elevation would be proportional to the imbrication angle. These two

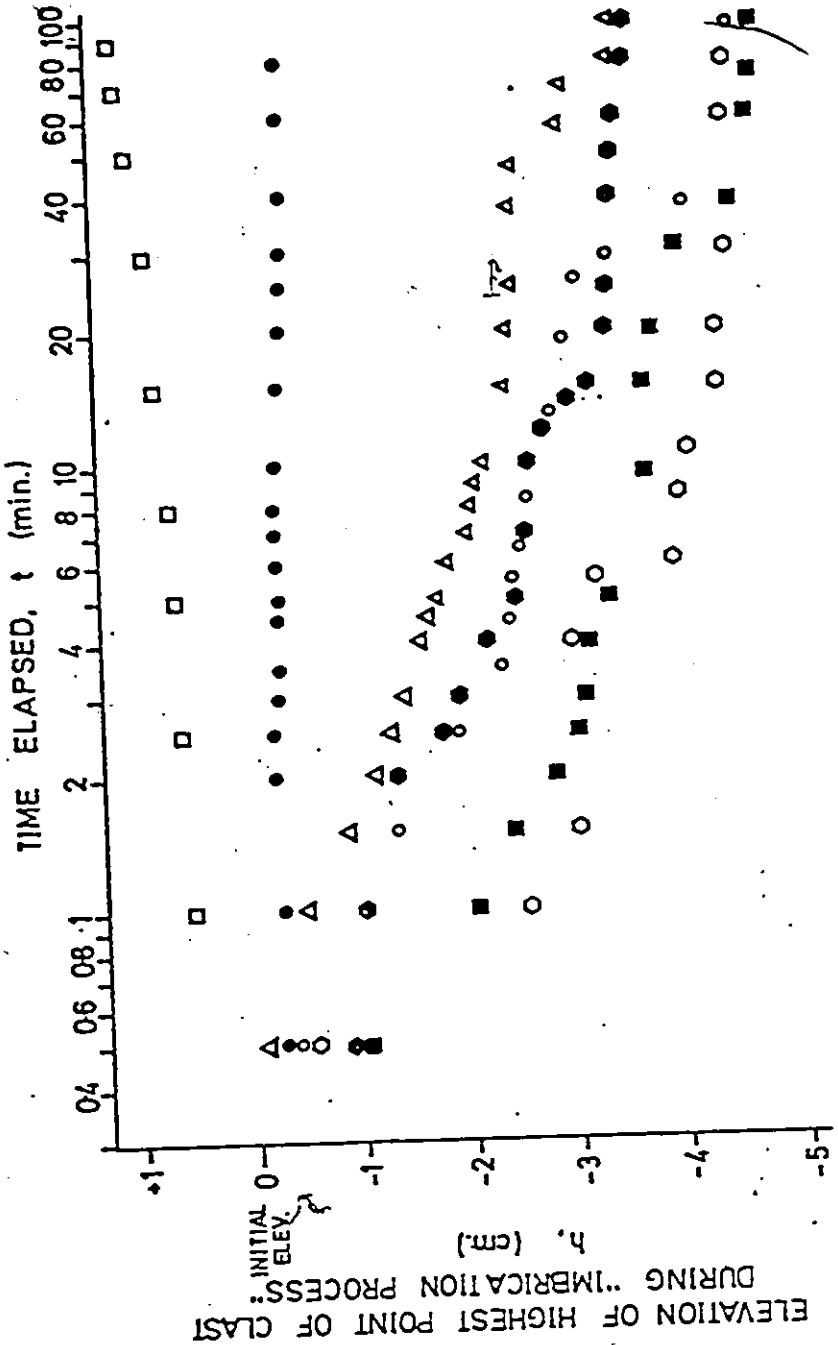

Figure 33: For clast #73, maximum elevation as a semi-logarithmic function of the time elapsed from the beginning of each run. See Figure 34 for explanation of different symbols. The data from Run EK3D-5 are excluded because of insufficient room on plot.

TABLE 19: Values of the coefficient b in the relation h = b(log t)

Run No.	Froude Number	Clast No. 73	
		b-value	correlation coefficient
EK3D-14	0.2377	0.6730	0.9959
-6	0.3236	-0.1353	-0.9457
-8	0.3742	-1.2268	-0.9866
	0.4542	-1.8033	-0.9885
-9	0.6483	-1.4709	-0.9498
-7	0.6894	-1.5072	-0.9792
-5	0.7804	-0.7115	-0.8846
-12	0.8212	-1.7831	-0.9735

variables were found to have negligible correlation, and it was therefore concluded that the clasts attained stable imbrication by combined rotational and translational motion.

One might expect the rate of combined rotational and translational motion (expressed by the coefficient b) to steadily increase from the lower- to the upper-flow regime. There is however, a major discontinuity in this relation owing to the pattern of form roughness variation with increasing Froude Number (Fig. 34). This is similar to the variation of the S, X, Y and Z responses with changing Froude number.

There are several causes of the frequently abrupt fluctuations of the data about the best-fit line:

a) In the ripple phase, low rates of bedform migration together with their low amplitude limit the possible deviation of individual measurements from the best-fit line. In the dune phase, the bedform celerity is higher and the height of the imbricating clast is likely to be less than the bedform amplitude, causing it to be highly susceptible to variations in local bed elevation. In the upper-flow regime, the discontinuous and abrupt shifting of antidunes enables a rapid attainment of stable imbrication: the data obtained from antidune runs comprise a few rapid fluctuations corresponding to the vigorous scour activity and oscillatory motion of the bed waves.

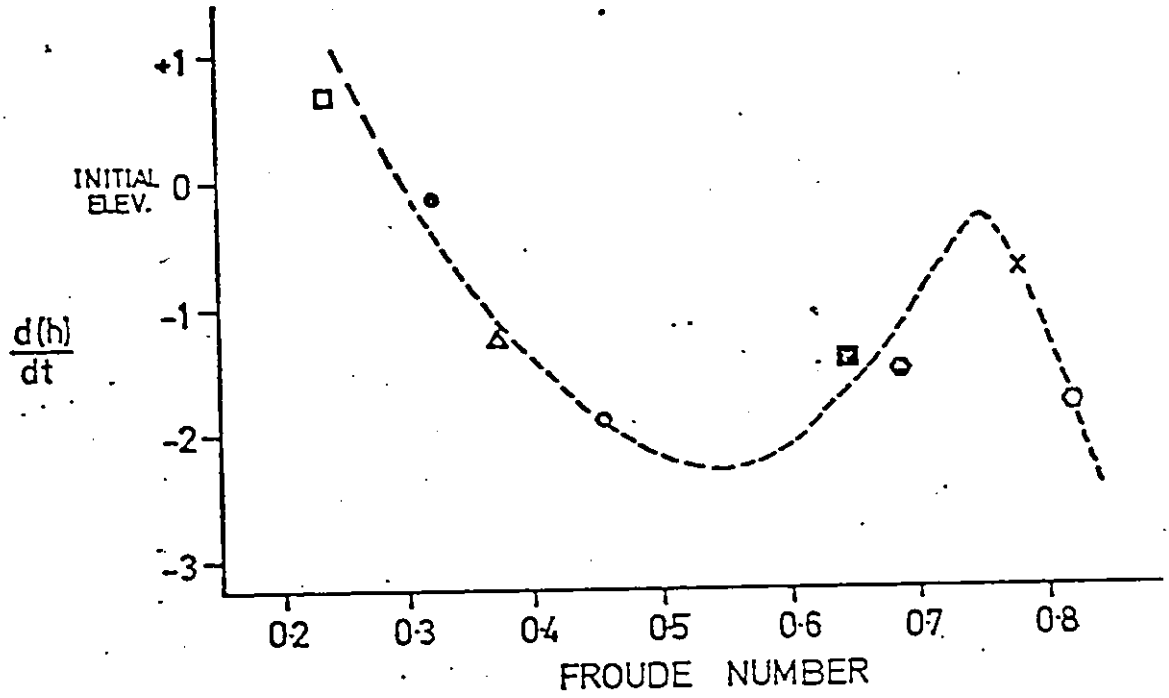

Figure 34: The rate of development of the imbrication process for each experimental run. . The pattern of variability is precisely similar to that of the relief of the sandbed with increasing Froude Number.

b) The imbrication angle steepens in discrete stages, with the steps in its development only occurring when the clast is fully exposed in troughs of migrating bedforms. Once exposed, current-crescent scour is likely to be an unsteady phenomenon owing to "large pulsating changes in the bottom pressure and shear...at the point where the separated flow returns to the bed" (Briggs and Middleton, 1965, p.15). Dunes with relatively large amplitude and wavelength cause the greatest fluctuations. In contrast, the transition plane bed gives rise to continuous development.

c) Fluctuations also result from the discontinuous sliding of the clast into a current-crescent scour. Angles of imbrication are generally below those of sliding friction so that upstream clast motion results from the action of a static torque force which momentarily becomes dynamic in response to underscouring. This produces an increment of combined rotational and translational motion. Measurements with the clinometer indicated that the imbrication angle at which equilibrium area is projected is rapidly attained (within a few minutes) with subsequent translational motion, principally as -x and -y components. This second phase of motion maintains the early-acquired imbrication angle, and the clast is eventually lowered below mean bed elevation. At this point, the cause of current-crescent scour has been eliminated, and the hollow infills with trough cross-laminae and wake bar deposits are eroded.

The semi-logarithmic nature of the relation height versus time is a result of the progressive decline in the degree of turbulence associated with the imbrication process. A particle is a source of 'grain roughness' when the particle Reynolds number exceeds 3.5 (White, 1940; Karcz, 1968). Fully exposed cobbles and boulders exert a large-scale variety of grain roughness, and in response to large Reynolds numbers, are loci of intense energy dissipation: the current-crescent scours around them are symptomatic of flow separation and streamline disruption. Since for a particular clast, the velocity of the intercepted flow is a principal determining factor in the rate of scour (Karcz, 1968) and the magnitude of the velocity declines according to the logarithm of the height (Blatt, Middleton and Murray, 1972, p. 88), it follows that the imbrication process will progressively decelerate as it develops. The limiting value of h with respect to t is an expression of this rather complex feedback mechanism. For these reasons, the particle Reynolds number is eventually reduced to a single figure, and a hydraulically 'smooth' boundary results. The term 'smooth' is used only with respect to grain roughness originating from the clasts - form roughness owing to the sand bedforms remains. Figure 35 illustrates the dependence of the particle Reynolds number on the height of the roughness element for two flow conditions.

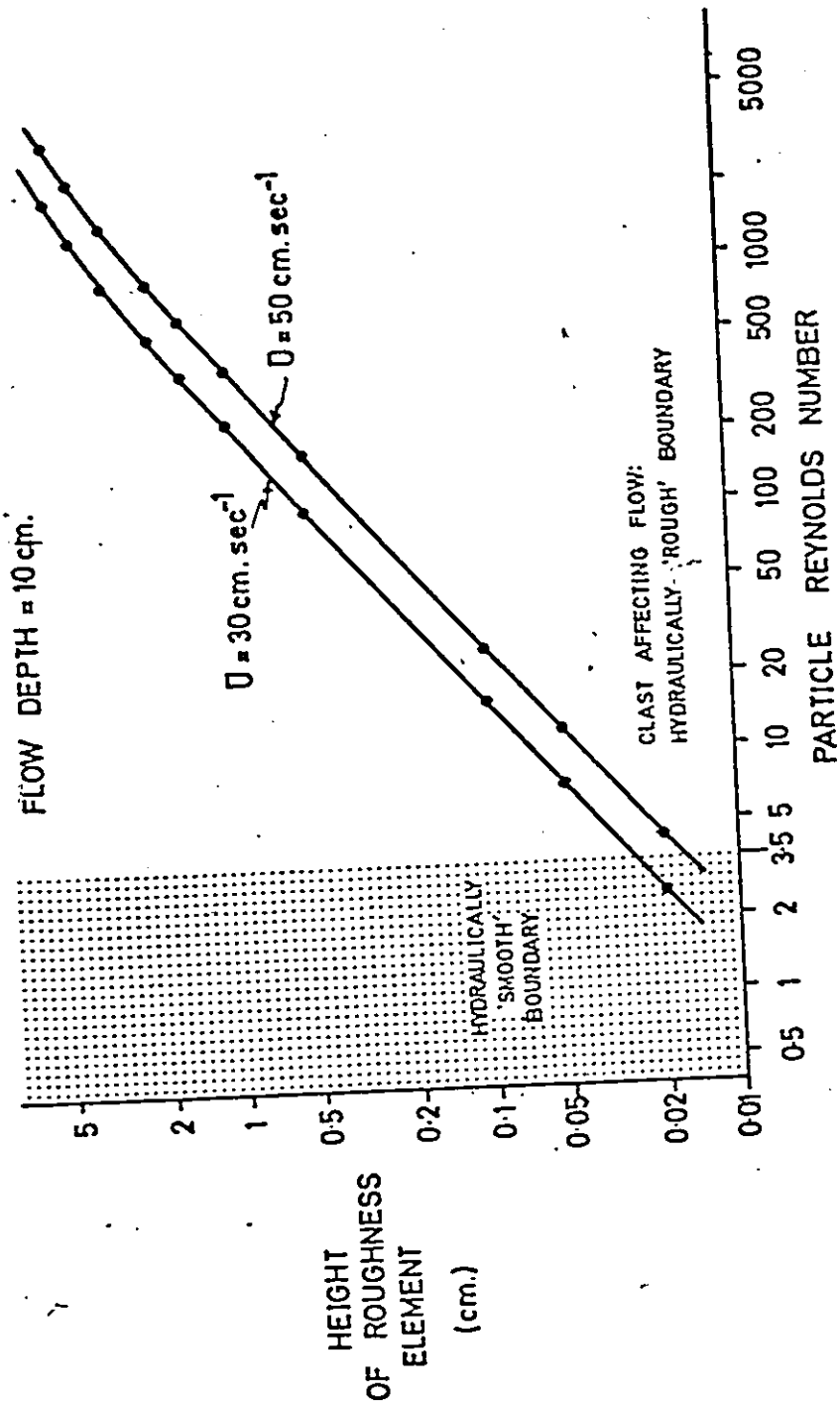

Figure 35: An explanation of hydraulically 'rough' and 'smooth' flow boundaries. With progressive reduction in the height of a clast the particle Reynolds number decreases to below 3.5. The diagram shows that this transition occurs at higher elevations for lower velocities.

The duration of the imbrication process, Δt, was determined from the graphs of four runs spanning the transition and upper-flow regime. The four points plot as a straight line on double logarithmic coordinates indicating that Δt is a power function of Froude number. The regression equation is

$$\Delta t = 7.6(Fr^{-3.5})$$

but it is probable that the absolute values of its coefficient and exponent are dependent on the size and morphology of the clast, and to a much lesser extent on the size distribution of the sand. The above equation predicts that for flows with ripple bedforms, cobble-sized clasts require 300-400min. to attain equilibrium, while in antidune flows, the time required is only about 10min.

The preceding analysis leads to some qualitative statements concerning the deposition of matrix-supported gravels. Upon waning flow, the deposition of scattered large clasts would likely proceed as follows. Initially, the clast would be deposited with its a-b plane parallel to the sand surface — comprising a plane bed or in-phase waves (Fahnestock and Haushild, 1962). Current-crescent scour would immediately commence around the clast thereby initiating the imbrication process. Completion of the process obviously requires that there be a negligible rate of sandbed aggradation, an adequate sandbed thickness and unimpeded motion of the clast.

In cases where matrix-supported gravels do contain well-imbricated clasts, such as the New Red Sandstone fanglomerates of south-west England (Laming, 1966), aggradation must have been relatively slow and/or discontinuous to allow the necessary exposure of the clasts at the flow-bed interface. The present study indicates that for cobble-sized clasts to achieve equilibrium according to the 'stability criterion', at least 10-15min. of exposure are required after deposition. Rates of aggradation would probably involve this duration of exposure for individual bedding planes.

4.0 CLAST TRANSPORT

The transportation of coarse-grained, poorly-sorted bedload is a fundamental sedimentological process for which there is a paucity of experimental data. Important laboratory work has been done by Hjulstrom (1935), Krumbein (1942), Fahnestock and Haushild (1962), Meland and Norrman (1966, 1969) and by Bradley et al. (1972). Transport and depositional velocities are variables which in large part govern the sorting and size attributes of braided river deposits (Walker, 1975) and therefore warrant detailed study.

In a discussion following Krumbein's (1942) paper, Kalinske (1942) deals theoretically with the relationship between the three aspects of clast behaviour. He considers that

$$U_2 = b(U_i - U_1)$$

where U_2 - velocity of clast motion,

U_1 - threshold velocity capable of initiating transport,

U_i - fluid velocity acting on particle,

b - coefficient.

b was found to closely approximate unity, so the equation can be rewritten

$$U_2 = U_i - U_1,$$

indicating that the transport velocity approximates the excess of flow velocity over the threshold velocity. For a given flow condition with a heterogenous bedload, the velocity of individual clast motion depends on the slope of the velocity profile. The formula predicts that when U_i is less than U_1, bedload motion ceases, and that for sand-sized material, U_1 is small and therefore U_2 approximates U_i. However, this formula does not allow for the possibility that motion can be sustained by flow velocities lower than that required to initiate motion (Hjulstrom, 1935).

Kalinske's ideas have not received attention in the sedimentological literature: they imply the important role of the velocity profile in relation to particle size. Moreover, his theory indicates that size is not the only determining factor - an idea that is inherent in most velocity versus particle size plots. Briggs and Middleton (1965, p. 14) stressed that studies of sediment transport should take into account particle size in relation to the velocity profile; they therefore considered that average flow velocity is not a desirable parameter for prediction of particle movement, as is done in Hjulstrom-type diagrams. In the flume, an additional reason against the use of mean velocity is the effect of side-wall resistance (Crickmore, 1970), which if considerable involves an under-estimate of the mean velocity along the centre-line of the flume where clast

transport occurred. To avoid these problems, Froude number was selected as the measure of flow strength in the experiments of transport velocity.

Transport velocity, U_2, can be experimentally investigated, or theoretically analysed, under two different conditions:

i) at a given flow condition (cf. the present experiments) that is competent to transport the available bedload, or

ii) for a given clast size.

4.1 Experimental Method

Three experiments (Runs EK3D-15, -16 and -17) were conducted to investigate the transport velocity of large, non-spherical clasts. Run EK3D-15 was a trial, using a small number of clasts, but because its results reproduced the findings of the subsequent experiments, the process-response analysis utilises the data from all three runs (Table 7, p.35).

The experiments were designed to simulate a typical proximal braided channel in which the ratio of clast size to depth ($d_n/\overline{Y}$) is high. The shallow, fast-moving flows had steep velocity gradients (Fig. 36), which caused high levels of shear to be exerted on the moving particles. High fluid shear was enhanced by means of a hydraulically 'rough' mat

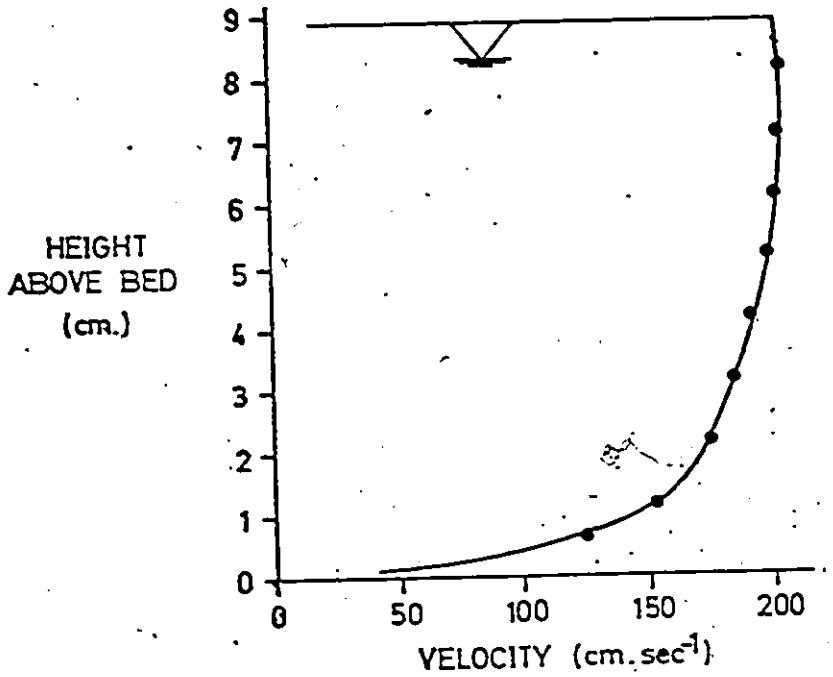

Figure 36: Velocity profile, along the centre-line of the flume, determined by measurements with a pitot tube for Run EK3D-17. $U_* = 10.3$cm/sec., Fr = 0.896, and Re = 74,000. The flow was turbulent over the total depth.

adhered to the otherwise 'smooth' aluminum floor of the flume (described on p.32). The flows were sub-critical and uniform in so far as the water- and bed-surfaces were parallel.

Having obtained the desired flow condition, transport velocities were determined by timing the passage of individual clasts over a 10m. test section centrally located in the flume. Clasts were introduced manually in random orientation at mid-flume just upstream from the test section, and were observed to accelerate rapidly to their full transport velocities. At least three separate velocity determinations were made on each clast to cancel out the random influences of fluid turbulence and irregularities in clast motion. Rarely did the variation in individual measurements exceed 10% of the mean value.

With a view to maximising the statistical significance of process-response analyses, the clast population was selected with a wide variation in morphology throughout its size range. Clasts with high degrees of asymmetry along the a-axis were excluded because of erratic transport paths.

4.2 Types of clast motion

Water recycling the flume is turbid on account of rust development in the end-tank and within the return pipes. However, observation of clast motion in these experiments was possible because of the large particle size relative to flow depth. That particle motion is highly shape-dependent has been shown experimentally (Krumbein, 1942) and in the field (Lane and Carlson, 1954).

Clast orientation during transport was ubiquitously current-normal, despite the random orientation at the point of introduction. Transverse alignment of clast long axes developed even when large, highly elongate clasts were introduced in a current-parallel configuration: the clast was observed to initially wobble in response to strong z-components of fluid motion but within seconds it abruptly turned 90° and started to roll downstream.

The following types of transport were observed:-

a) Rolling, continuous and discontinuous. Rotation about a-axes was generally confined to well-rounded, highly spherical or prolate forms. Highly oblate clasts with minimal angularity were observed to rotate about the circumference of their a-b planes.

b) Sliding. Continuous sliding was confined to oblate clasts, while discontinuous sliding occurred with clasts possessing high angularity in the b-c plane.

c) Saltation, intermittent. This was rarely observed and was confined to smaller clasts and/or to oblate clasts in between periods of sliding motion.

Hendry (1976) regarded rolling of highly oblate clasts about the circumference of their a-b planes as occurring in turbidity currents. Presumably it requires a fairly smooth bed in combination with strong turbulence to raise the

principal plane to the vertical: this hydraulic condition is perhaps rarely encountered in natural channels. It does, however, constitute a very efficient means of transport because of reduced resistance, and in some cases may provide the means by which oblate clasts become very steeply imbricated in contact bedload (Laronne and Carson, 1976). Bradley et al (1972, p. 1278) observed that prolate clasts occasionally developed a "complicated wobble...something between a roll and an end-over-end cartwheel...each end in turn rises up off the bed to where higher velocity flows can impart a strong torque which maintains the wobble".

4.3 Process-response analysis

The primary aim of the analysis is to clarify the influence of clast parameters on transport velocity. Emphasis is given to size (d_n) and to morphology (Table 20). The oblate-prolate index ($\overline{OP}$) was selected as the principal shape variable for the following reasons:-

i) sphericity does not distinguish between oblateness and prolateness,

ii) the greater numerical range of $\overline{OP}$ values, as compared to sphericity, is advantageous from the standpoint of regression analysis, and

TABLE 20: Size and shape properties of the clast populations used in the experiments of transport velocity.

Run #	EK3D-15	EK3D-16	EK3D-17
Nominal diameter, d_n			
mean	7.4cm	6.4cm	7.2cm
range	5.2 - 10.3cm	4.5 - 8.7cm	5.1 - 9.2cm
Max. Proj. Sphericity, Ψ_p			
mean	.54	.39	.62
range	.33 - .86	.27 - .44	.44 - .86
Oblate-prolate index, $\overline{OP}$			
mean	+2.2	-13.5	-.39
range	-9.6 - +17.6	-29.2 - +2.9	-15.1 - +8.6

iii). clast form, as described by the $\overline{OP}$ index, has been considered more important than sphericity in determining the character of large particle motion (Lane and Carlson, 1954: Bradley et al., 1972).

It is acknowledged that other variables such as density, roundness and asymmetry must also exert some control on the clast's transport behaviour.

4.31 Influence of clast size

The plots of U_2 versus d_n all contain a curvilinear relationship with negative gradients (Fig. 37). The higher gradient of the intermediate velocity run is probably due to the lower sphericity and more oblate tendency of its clast population (Table 20).

The curvilinear trends generated by each run's data are satisfactorily fitted by short segments of a least-squares parabola, using the method of Ezekiel and Fox (1950): APL programme PARABOLA (see Appendix for details) was written to furnish the necessary values. Use of a parabola implies that at smaller d_n values, the relationship with U_2 is either fairly constant (corresponding to the vertex portion), or has a positive gradient (corresponding to the left-hand portion).

The experimental studies of Meland and Norrman (1966), involving single spherical glass beads, generated a set of particle velocity versus size plots (their Fig. 4, p. 174) which closely resemble the left-hand portions of parabolic

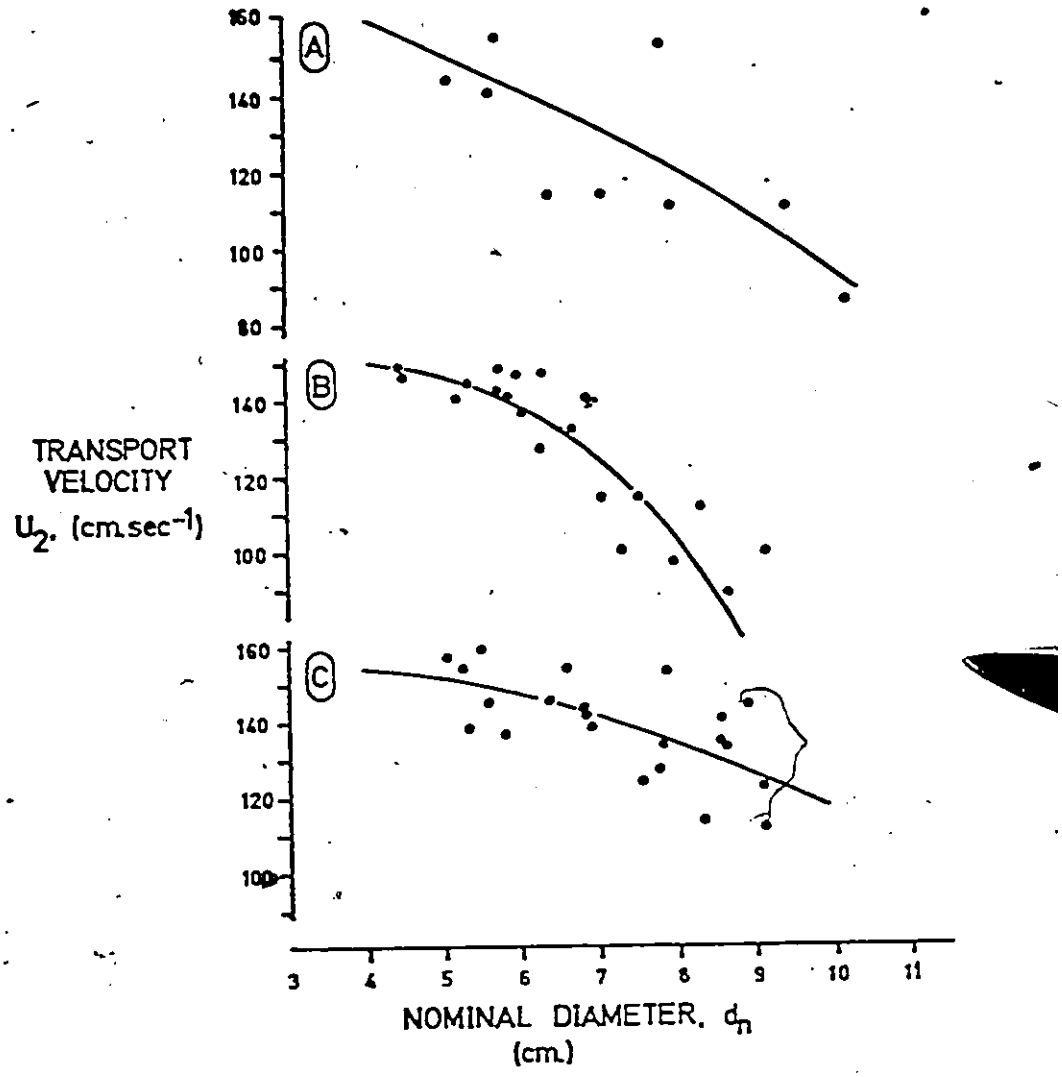

Figure 37: Plots of transport velocity as a curvilinear function of nominal diameter for each experiment. To some extent, variation in the position and curvature of the best-fit parabolas is due to the different size and morphology of the clast populations. A, B and C are the data of runs EK3D-15, -16 and -17, respectively.

functions. Had they used a wider range of sediment size, it seems likely that they would have encountered maximum transport velocities in the intermediate grades. In a later study (Meland and Norrman, 1969) using natural sediment ranging from coarse sand to small pebbles, they found that granule sized sediment generated the maximum transport velocities. Laronne and Carson (1976) found that in a small stream with coarse-grained heterogenous bedload, the medium-sized pebbles showed the greatest mobility. Plots of distance of transport of labelled material versus the logarithm of particle weight (their Fig. 12, p. 83) produced skewed parabola-type functions. Other experimental work with sand to granule sized sediment has generally encountered plots with positive gradient (Gilbert, 1914; Hjulstrom, 1939, p. 13), whereas the studies of Fahnestock and Haushild (1962) and Bradley et al. (1972) using cobble-sized clasts failed to reveal any systematic relationship between transport velocity and size. Although greater mean flow velocities are required for movement of larger clasts (Hjulstrom, 1935), Hjulstrom (1939, p. 13) attributes the more rapid transport of larger clasts to the fact that they intercept higher levels in the velocity profile. A compilation of the available evidence therefore lends support to a parabolic inter-relationship between U_2 and d_n, i.e. steady flow acting on hetergenous bedload generates the maximum transport velocities in an intermediate size grade.

On theoretical grounds however, it would appear that attainment of an optimum size for transport is dependent on certain aspects of the flow and bedload. Presumably, the ideal parabolic relation between U_2 and d_n is confined to conditions in which the clasts are fully immersed, and so flow depth is considered a factor. Degree of immersion is expressed by the $d_n/\overline{Y}$ ratio, and can range from less than 10^{-5} in deep sand-bed rivers to almost 1 in shallow, braided rivers transporting boulders. The clast size at the intersection of the parabola at $U_2=0$ is considered to mark the absolute competence level. U_2 as a function of d_n for all the data combined is shown in figure 38, and to the right the parabola crosses the size-axis at 14.5cm: the actual competence of the experimental flows is probably less than this value because this size of clast exceeds the depth of flow. The parabola suggests that maximum transport velocities are developed by clasts with d_n between 2.5 and 5.5cm. The ambient flow velocities of clasts smaller than this optimum grade are considerably lower (Fig. 36), and larger clast sizes approach the competence level of the flow.

4.32 Influence of clast form

On the curvilinear plots of U_2 and d_n (Fig. 37), it was noticed that high sphericity and/or prolate clasts and low sphericity and/or oblate clasts tend to lie above and

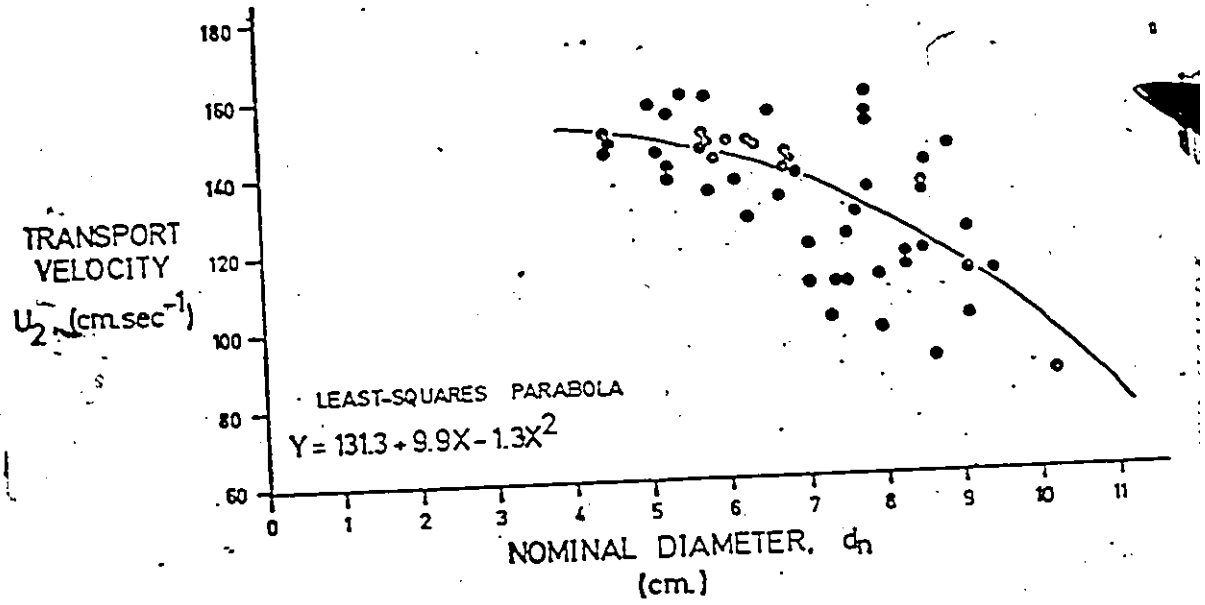

Figure 38: Plot of transport velocity versus nominal diameter for all the data combined (n=52).

below the best-fit line, respectively. This was anticipated from Krumbein's (1942) study in which for a set of hand-moulded bodies of the same nominal diameter the influence of sphericity was clearly illustrated (Fig. 3B, p. 626) and the additional influence of form realised (p. 625). However, variable clast morphology was shown to have a declining effect with increasing mean flow velocity (Fig. 2, p. 625). Bradley et al. (1972) have reviewed the recent literature concerning the influence of form and shape on transport velocity and found little agreement.

To alleviate the potential problem of relatively small clast populations, a special statistical procedure was developed to analyse the influence of clast form on transport velocity. Table 21 illustrates the procedure: the data are first ranked with respect to d_n values, and then proceeding down the matrix in incremental fashion groups of data are subjected to linear regression analysis. By moving incrementally through the ranked data, a relatively large number of equations are produced, which allows accurate quantification of the form influence. The method has been applied both to the data of individual runs, and to grouped data from all three runs. The former gives an indication of the influence of increasing flow while the latter serves to define more clearly the trends related to clast properties.

TABLE 21: An illustration of the two-stage analytical technique used for the data of transport velocity. In the first stage, data are ranked with respect to nominal diameter and then grouped (n=16) in the manner shown. In the second stage, linear regression analyses are performed on each group and assigned value of nominal diameter according to the moving average.

STAGE ONE

	PROCESS		RESPONSE	
RANK (W.R.T. d_n)	d_n	$\overline{OP}$	$\overline{U}_2$	
1	4.52	-29.24	149.7	
2	4.53	-20.16	144.9	
3	4.58	-17.65	147.1	
4	5.10	-5.14	157.0	
5	5.19	3.51	144.9	
6	5.32	3.2	140.8	
7	5.34	2.32	154.6	
8	5.36	7.75	138.9	1
9	5.52	-1.58	159.5	
10	5.66	-1.09	145.6	
11	5.71	-9.24	149.3	
12	5.81	-2.92	148.5	2
13	5.82	3.88	137.0	
14	5.82	3.88	142.9	
15	5.82	3.88	156.3	
16	5.92	0.36	141.2	3
17	6.08	-9.92	147.1	
18	6.16	-11.43	137.0	
19	6.34	-17.54	127.4	
20	6.34	-5.15	147.1	4
21	6.42	3.34	145.6	
22	6.64	5.65	154.6	
23	6.75	-8.97	132.8	
24	6.83	-1.58	143.5	
25	6.89	-0.47	141.4	
26	etc.	etc.	etc.	
27				
etc.				

STAGE TWO REGRESSION ANALYSIS	RANK INTERVAL	$\overline{d}_n$	REGRESSION EQUATION
1	1-16	5.38	$\overline{U}_2 = 146.9 - 0.13\ \overline{OP}$
2	4-20	5.76	$\overline{U}_2 = 145.5 + 0.35\ \overline{OP}$
3	8-24	6.10	$\overline{U}_2 = 146.7 + 0.66\ \overline{OP}$

1a) Run EK3D-15, Fr = 0.683 (Table 22A and Fig. 39A):

In spite of the small number of data pairs, the six regression lines are very consistent. The coefficients average 1.9 with little variation, whereas the intercept values systematically decline from 145 to 120cm.sec^{-1} with the increase in $\overline{d_n}$ from 6.0 to 8.9cm. This set of regression lines indicates that for equal sized clasts, prolate forms move more readily than do oblate forms, and that at a given value of $\overline{OP}$, smaller clasts move with higher velocity than larger ones.

1b) Run EK3D-16, Fr = 0.809 (Table 22B and Fig. 39B):

The influence of size and form is less straightforward in the data from this run. The seven regression lines, of which only the one for $\overline{d_n}$ = 5.8cm is not significant at the 95% level, are characterised by very similar intercepts (≈145cm.sec^{-1}) but coefficients which increase in orderly fashion with increasing clast size, so that the regression lines intersect nearly at a common point. This point is located at $\overline{OP}$ = 0 which indicates that small oblate and large prolate clasts respectively are more readily transported. The regression lines for the smallest d_n values have negligible gradients, indicating a low influence of both size and form.

TABLE 2: Sets of linear regression equations, relating transport velocity to oblate-prolate index at given clast sizes, for each run's data. A, B and C refer to the low-, middle- and high-velocity runs, respectively.

	MEAN CLAST SIZE, d_n (cm)	n	REGRESSION EQUATIONS	CORRELATION COEFFICIENT	SIGNIFICANCE LEVEL *>95% (t-test)	$d_n/\overline{Y}$
						0.66
1)	6.0	4	$\overline{U}_2 = 148.2 + 1.41\ \overline{OP}$	0.81		0.72
2)	6.5	4	$\overline{U}_2 = 149.6 + 1.94\ \overline{OP}$	0.78		0.79
3)	7.1	4	$\overline{U}_2 = 143.7 + 1.98\ \overline{OP}$	0.95	*	0.84
4)	7.6	4	$\overline{U}_2 = 139.8 + 1.88\ \overline{OP}$	0.94	*	0.91
5)	8.2	4	$\overline{U}_2 = 129.6 + 1.72\ \overline{OP}$	0.72	*	0.99
6)	8.9	4	$\overline{U}_2 = 120.2 + 2.03\ \overline{OP}$	0.56		
						0.62
1)	5.3	8	$\overline{U}_2 = 143.5 - 0.20\ \overline{OP}$	-0.72	*	0.67
2)	5.8	8	$\overline{U}_2 = 143.0 + 0.23\ \overline{OP}$	0.30		0.72
3)	6.2	8	$\overline{U}_2 = 144.9 + 0.68\ \overline{OP}$	0.62	*	0.76
4)	6.5	8	$\overline{U}_2 = 145.5 + 1.00\ \overline{OP}$	0.72	*	0.79
5)	6.8	8	$\overline{U}_2 = 145.6 + 1.62\ \overline{OP}$	0.72	*	0.84
6)	7.2	8	$\overline{U}_2 = 145.0 + 2.19\ \overline{OP}$	0.85	*	0.92
7)	7.9	9	$\overline{U}_2 = 128.4 + 1.72\ \overline{OP}$	0.64		
						0.64
1)	5.7	8	$\overline{U}_2 = 151.3 - 1.17\ \overline{OP}$	-0.58		0.69
2)	6.1	8	$\overline{U}_2 = 146.9 - 0.58\ \overline{OP}$	-0.28		0.74
3)	6.6	8	$\overline{U}_2 = 140.8 + 1.71\ \overline{OP}$	0.69	*	0.80
4)	7.1	8	$\overline{U}_2 = 141.3 + 1.29\ \overline{OP}$	0.79	*	0.84
5)	7.5	8	$\overline{U}_2 = 140.7 + 1.56\ \overline{OP}$	0.82	*	0.89
6)	7.9	8	$\overline{U}_2 = 138.7 + 1.35\ \overline{OP}$	0.76	*	0.93
7)	8.3	8	$\overline{U}_2 = 137.4 + 1.13\ \overline{OP}$	0.79		0.98
8)	8.7	8	$\overline{U}_2 = 131.5 + 0.91\ \overline{OP}$	0.44		

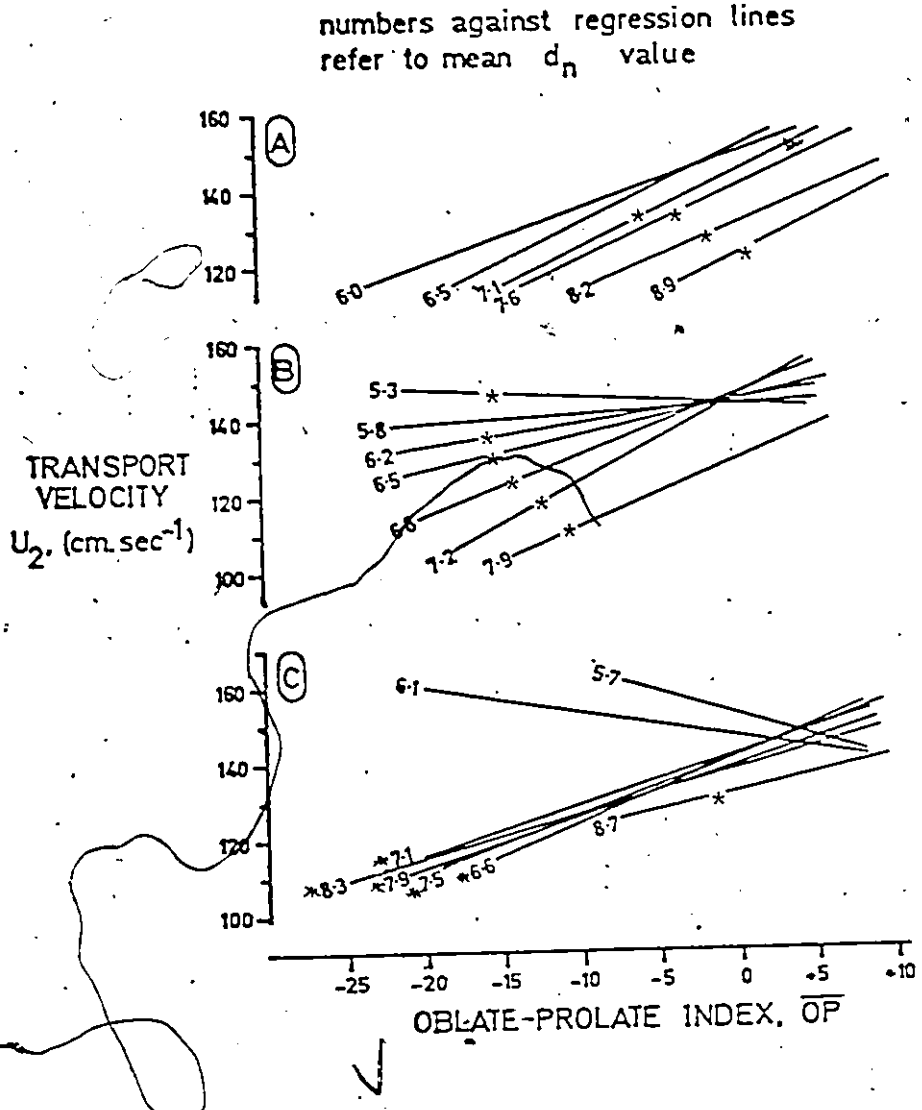

Figure 39: Plots of transport velocity as a function of the oblate-prolate index for each experimental run. The sets of regression lines are according to the series of mean sizes listed in Table 23. A, B and C are the data of runs EK3D-15, -16 and -17, respectively.
* - denotes that the regression line is statistically significant at the 95% confidence level, as indicated in Table 22.

1c) Run EK3D-17, Fr = 0.896 (Table 22C and Fig. 39C):

From this run, five out of the eight regression lines are significant at the 95% level and conspicuous for the lack of variation in both intercept values ($\pm 138 cm.sec^{-1}$) and coefficients (± 1.3). This indicates a negligible role of clast size: the corollary being that form is the predominant process variable, such that prolate clasts generate higher U_2 values compared to oblate ones. Meland and Norrman (1966, p. 173) found that the influence of particle size was at a minimum at high velocities. Advancing a minor trend seen in the intermediate run, the smaller size grades generate regression lines with gradients that range from zero to slightly negative, although these are not significant at the 95% level. The implication is that small clasts are transported more readily if they possess an oblate form: small oblate clasts were observed to occasionally saltate, or roll about the circumference of their a-b planes, and both these types of motion are conducive to high transport velocities.

2) Grouped data from all runs:

The trends shown in figure 39 are clarified by grouping of all the data (Table 23). By doing this, the role of flow velocity is averaged, but the trends are reinforced and the results made more statistically significant. No significant error arises from the averaging of depth, since this parameter only varied by 4mm for the three runs.

TABLE 23: Sets of linear regression equations, relating transport velocity to oblate-prolate index at the given values of clast size to depth ratio.

$d_n/\bar{Y}$	MEAN CLAST SIZE, d_n (cm)	n	REGRESSION EQUATIONS	CORRELATION COEFFICIENT	SIGNIFICANCE LEVEL >95% (t-test)
0.61	5.38	16	$\bar{U}_2 = 146.9 - 0.13\ \overline{OP}$	-0.19	
0.65	5.76	16	$\bar{U}_2 = 145.5 + 0.35\ \overline{OP}$	+0.30	
0.69	6.10	16	$\bar{U}_2 = 146.7 + 0.66\ \overline{OP}$	+0.53	*
0.72	6.42	16	$\bar{U}_2 = 143.9 + 0.90\ \overline{OP}$	+0.74	*
0.77	6.81	16	$\bar{U}_2 = 144.4 + 1.53\ \overline{OP}$	+0.79	*
0.80	7.12	16	$\bar{U}_2 = 140.9 + 1.64\ \overline{OP}$	+0.89	*
0.85	7.52	16	$\bar{U}_2 = 140.4 + 1.89\ \overline{OP}$	+0.88	*
0.89	7.90	16	$\bar{U}_2 = 137.5 + 1.87\ \overline{OP}$	+0.85	*
0.93	8.27	16	$\bar{U}_2 = 134.4 + 2.00\ \overline{OP}$	+0.76	*
0.98	8.70	16	$\bar{U}_2 = 124.4 + 1.93\ \overline{OP}$	+0.61	*

The parameters of the equation

$$\overline{U}_2 = a + b(\overline{OP})$$

vary systematically (Fig. 40). Asymptotic values are rapidly attained as the $d_n/\overline{Y}$ ratio approaches unity. The two curves are precisely fitted by portions of a least-squares parabola, but because of the truncation at $d_n/\overline{Y} = 1$, the quadratic equations are not given. With diminishing value of the $d_n/\overline{Y}$ ratio, limiting values of a and b are also attained. When $d_n/\overline{Y} = 0.6$, b changes sign and rapidly reaches large negative values. Figure 40 is derived from the empirical relations in figure 39 and portrays a complex interrelation between U_2 versus $\overline{OP}$ for varying values of the $d_n/\overline{Y}$ ratio. The reversal of the form effect at small d_n values is probably due jointly to the fact that small clasts are in the zone of steepest velocity gradient and that their oblate form, having relatively high surface area which assists hydraulic lift and retards settling, increases the likelihood of saltation. Lines representing $d_n/\overline{Y}$ ratios less than 0.2 were excluded from figure 40 because of the different type of transport for particles of this size (i.e. quasi-continuous suspension rather than predominantly traction). Boulders which are not fully immersed are loci of intense energy dissipation, and therefore constitute a different hydraulic phenomena (Matthes, 1947).

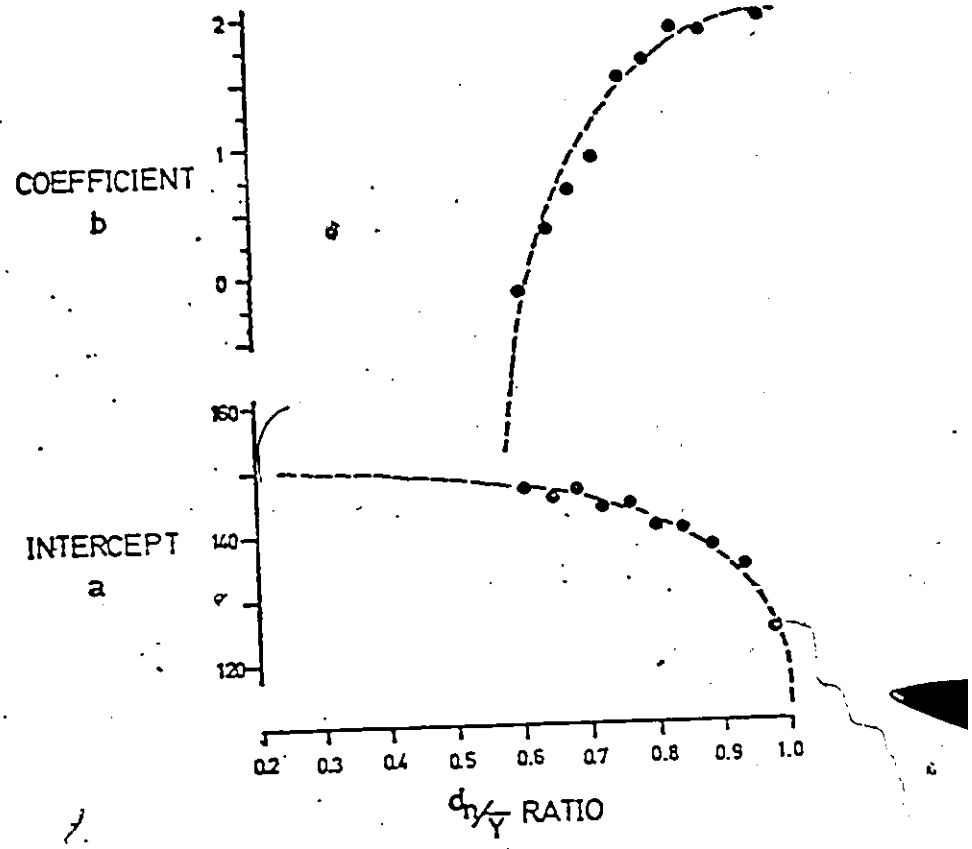

Figure 40: The variation of the parameters of the equation $U_2 = a + b(OP)$ with increasing value of the $d_n/\bar{Y}$ ratio. Plotted values are according to those listed in Table 23. Note that the best-fit lines have limiting values when the ratio equals 1, and that they are extended to lower values of the ratio.

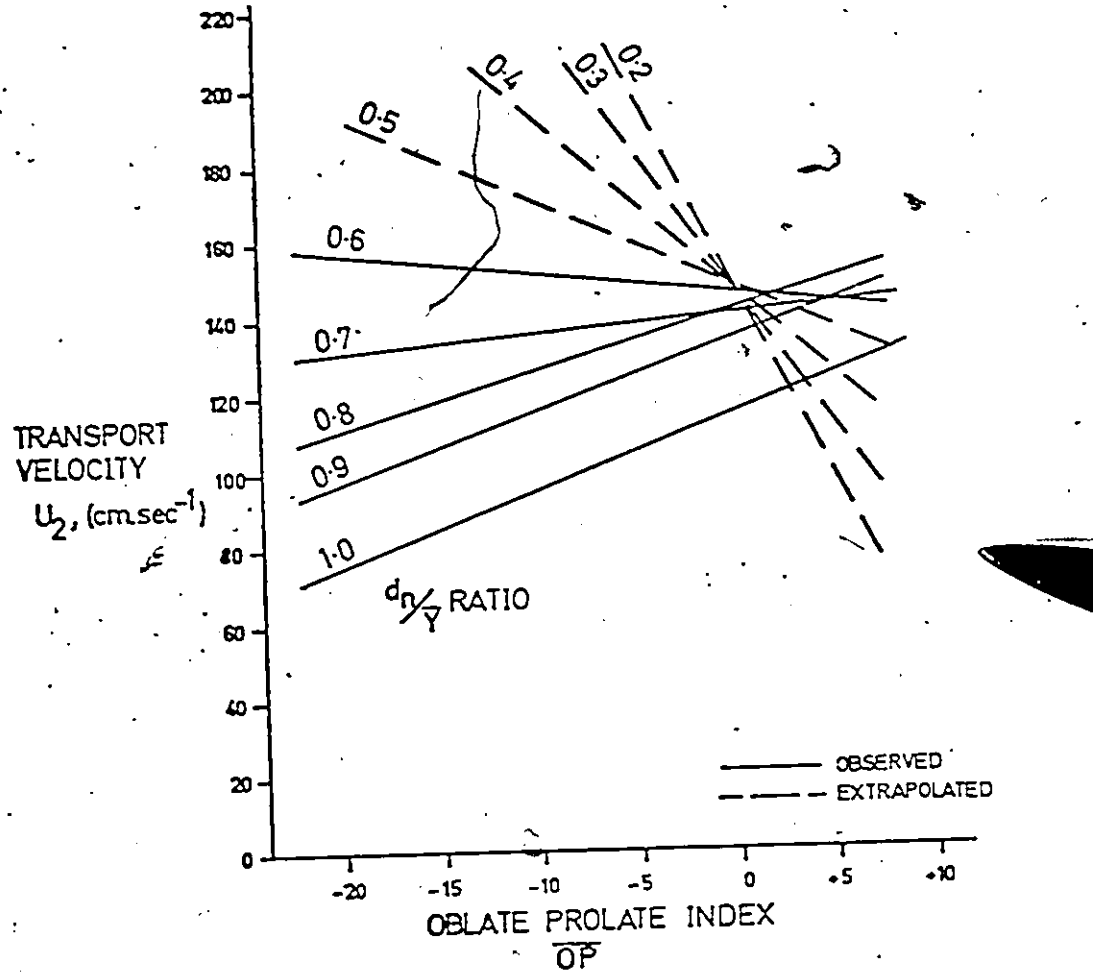

Table 41: Plot of transport velocity as a function of the oblate-prolate index for all the data combined. The parameters for the regression lines at each d_n/Y value are according to the empirical curves in Figure 40.

The experiments of Bradley et al. (1972) strongly suggest that oblate forms are preferentially transported. They attributed this to "an erratic saltation motion which enabled higher-velocity flows away from the bed to take advantage of their large cross-sectional area (p. 1278)...these particles overtake more spherical ones which remain closer to the bed" (p. 1279); elongate forms were found to have intermediate transport velocities.

4.4 Discussion

Previous experimental and field studies of transport velocity of large, non-spherical clasts have given an over-simplistic view of the relation with size. The present experiments extend the findings of Meland and Norrman (1969) and Laronne and Carson (1976) that intermediate grades in the size distribution of the available bedload may be transported with the highest velocities. For coarse-grained sediment, this 'optimum size' largely depends on the $d_n/\overline{Y}$ ratio: in the present experiments, large pebbles with $d_n/\overline{Y}$ ratio between 0.3 and 0.6 were inferred to be the optimum size. Larger clast sizes with higher values of this ratio generate a negatively-sloped segment on a U_2 versus d_n plot, and this is considered to be the right-hand portion of a parabola with limits at $d_n \rightarrow 0$ and at $U_2 \rightarrow 0$. The former is interpreted as the transport velocity of small pebbles, while the latter is an indication of the competence level, or the condition $d_n/\overline{Y} = 1$.

The degree of oblateness/prolateness exerts a strong control over U_2, particularly at high flows, as well as over the type of motion at low values of $d_n/\overline{Y}$. The present data support the finding of Bradley et al. (1972) that transport velocities are as much related to morphology as to size.

It would also appear that the steep velocity gradients which typify shallow, high-velocity flows in braided channels are highly effective in moving a large range of clast sizes with a relatively small variation in transport velocity.

In natural channels, a host of factors which include unsteadiness and non-uniformity of the flow, clast interactions, armouring of the bed surface, preferred clast fabric and secondary flow systems associated with small- and large-scale bedforms hinder the precise prediction of transport velocity (Laronne and Carson, 1976). Many of these factors are not amenable to laboratory study, and at present it is only possible to appraise their collective influence in a qualitative way. Considerable progress could be made by improving the level of understanding of the basic relationship in bedload transport, i.e. the motion of a particular clast on a flat bed under conditions of steady, uniform flow. The present experiments have been directed towards this objective.

Inter-relationships between transport velocity and size which are neither parabolic, nor recognisable segments of a parabola, are probably due to an insufficient range of clast sizes. The size distribution of the available bedload relative to the competence level is considered to determine to what degree a concave-downward relation is developed (i.e. left-hand positively sloped segment, vertex, or negatively-sloped right-hand segment).

Preferential transport of a certain size of the available bedload is a possible mechanism for local and progressive size-sorting in a fluvial system; viz. "the conclusion is inescapable that the bulk of sorting is effected during active transport and that comprehension of layering and sequences in sedimentary deposits requires understanding of sediment behaviour during transport" (Meland and Norrman, 1969, p. 143).

5.0 TRANSVERSE RIBS

Transverse ribs have been reported from coarse-grained braided systems with longitudinal bars, or from single channel, high gradient streams. In these fluvial environments channels are conspicuous for their high velocity and shallow nature (such that $d_n/\bar{Y}$ ratios are high).

Since their initial description by McDonald and Banerjee (1971) from the Peyto outwash plain in western Alberta, 'transverse ribs' have been recognized on proglacial fans bordering the Gulf of Alaska (Boothroyd, 1972; Gustavson, 1974; Boothroyd and Ashley, 1975), and from a small stream near Sherbrooke, Quebec (Laronne and Carson, 1976). Also referred to as 'clast stripes' by Boothroyd (1972), they are "a series of regularly spaced pebble, cobble or boulder ridges orientated transverse to flow" (McDonald and Banerjee, 1971, p. 1290). They have also been reported from streams in the Himalayas, from alluvial fans in southern Nevada and in numerous locations in the Canadian and Colorado Rockies (McDonald, pers. comm., 1972).

Transverse ribs were observed on the Spring Creek fan, (Plates 2, 3, 4 &5), but are conspicuously absent in the neighbouring Donjek River outwash. On the alluvial fan surface, ribs contain the largest percentiles of the available bedload and are located in riffle portions of abandoned

Plates 2 and 3 depict occurrences of transverse ribs in channels: see upper part of Table 27 for details of measurements.

Plate 2: Rib sequence #4. An upstream view of the coarsest and best defined transverse rib sequence located on the fan. The b-axis of the largest boulder is 47cm. A 4-year old poplar on the right-bank indicates that the reach is essentially abandoned on the intermediate berm - however, recent high stage flow in the active tract has partially dissected the inter-rib sediment which comprises cross-bedded sands and laminated silty-clays. As the channel shallows toward the left-bank, the ribs show an abrupt transition to a cellular pattern. Shovel for scale.

Plate 3: Rib sequence #1. An upstream view of a channel reach containing 8 fairly well-defined ribs. Partly concealed along the right-bank by wind blown sediment and material collapsed from the bank, there is evidence that this rib sequence is in the process of being preserved in the stratigraphic record of the alluvial fan deposits. Immediately to the right of the shovel less coarse bar material has (?)prograded laterally towards the right-bank over part of the rib sequence. Spacing varies from 36 to 102cm, suggesting that more than one generation of ribs is present.

PLATE 2

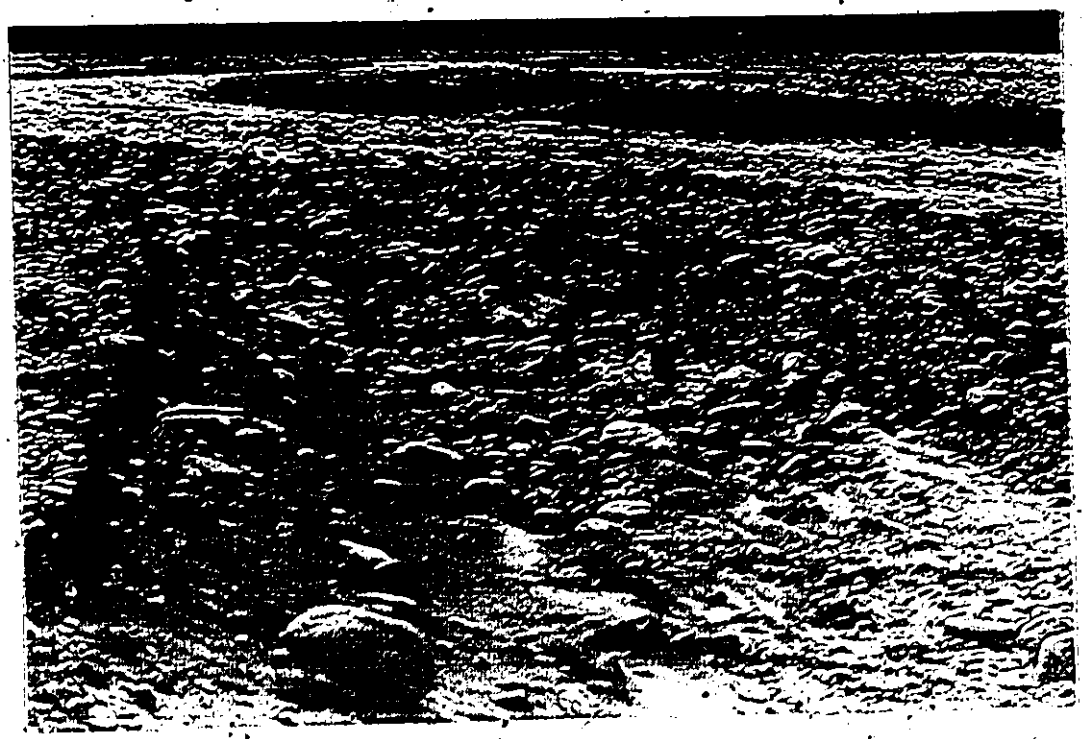

PLATE 3

Plate 4 depicts an occurrence of transverse ribs on the surface of a longitudinal bar: see lower part of Table 27 for details of measurements. Plate 5 illustrates the typical features of individual ribs.

Plate 4: Rib sequence #5. A series of ill-defined pebbly ribs on an inclined bar surface. Flow was from right to left; the staff is 4.5ft (1.37m.) long. Laterally, away from the vicinity of the staff, the ribs bifurcate and become indistinct, and eventually display transition to an unribbed surface.

Plate 5: View of one well-defined rib in rib sequence #1 (see Plate 3). Flow was from the upper left in the orientation of the staff. Note the current-normal alignment of the rib, as well as of the component clasts, and the imbrication of oblate and bladed cobbles on its upstream side. The rib is made conspicuous by the subsequent deposition of sand with current-crescents in the inter-rib areas.

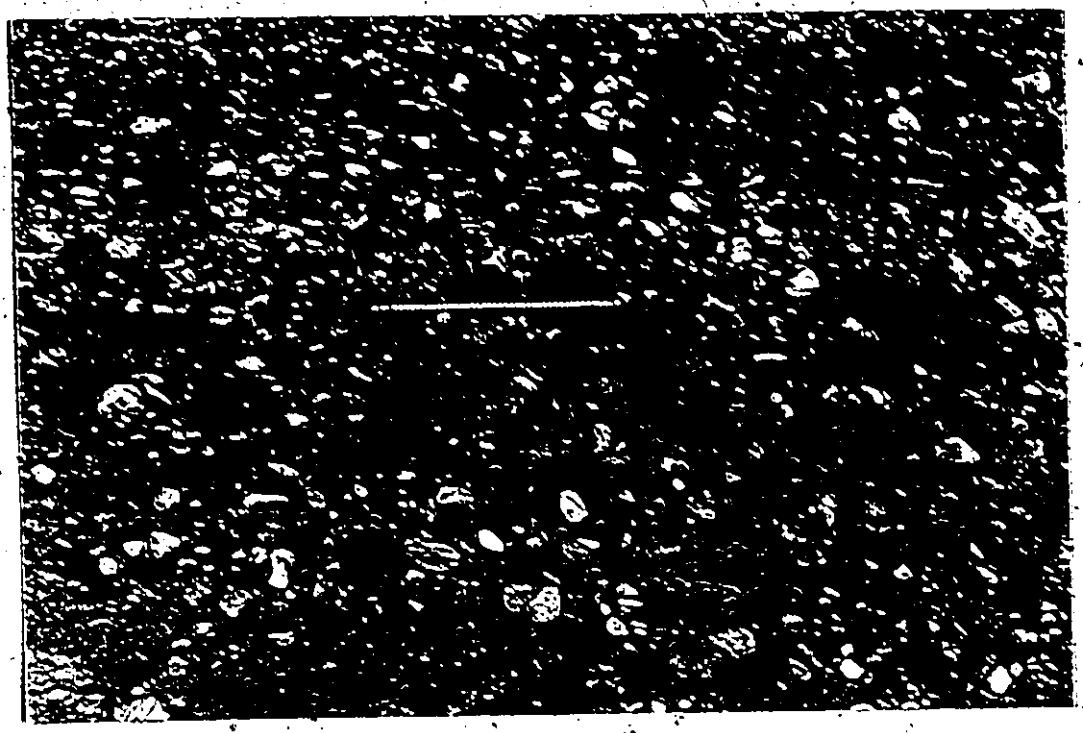

PLATE 4

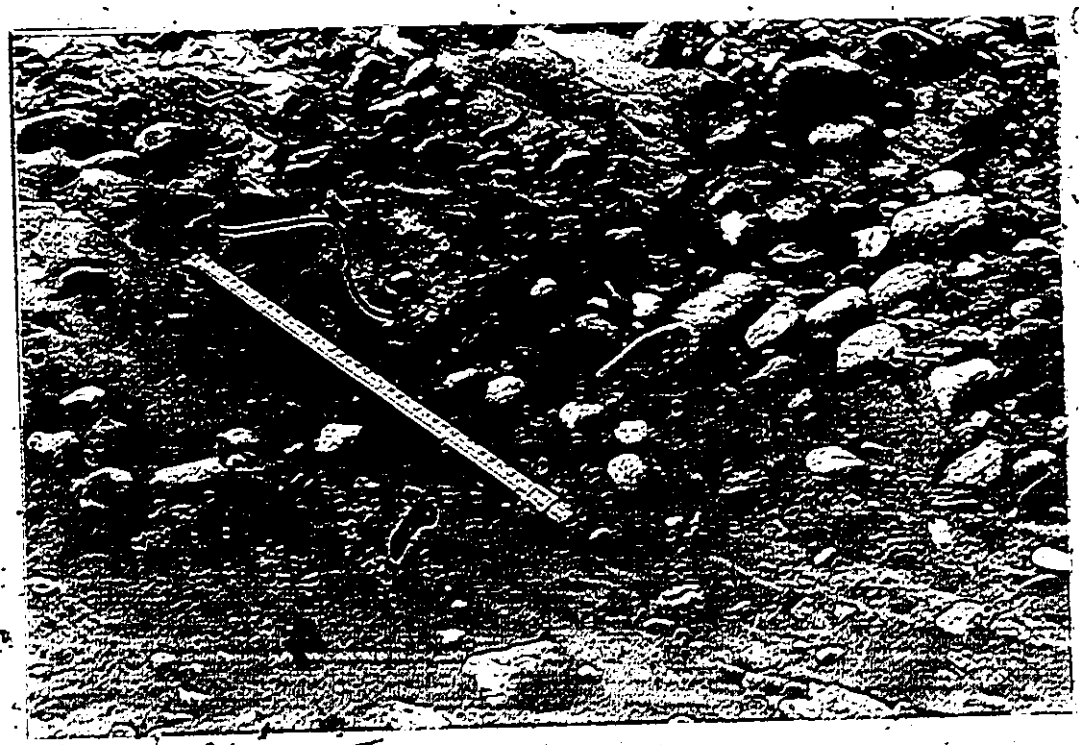

PLATE 5

anabranches or on inclined surfaces of longitudinal bars. The within-channel category is both coarser grained and more abundant. Twelve rib sequences were found and measured using the standard parameters of McDonald and Banerjee (1971). The data is summarised in Table 24 and inter-related graphically in figure 42.

5.1. Field characteristics

Incorporating all the findings of the various field studies, the characteristic properties of transverse ribs may be summarised as follows (an asterisk denotes evidence from Spring Creek, not recorded elsewhere):-

A) Relationship between the rib parameters (McDonald and Banerjee, 1971, p. 1290):-

Positive correlations between

i) spacing and clast size,

ii) rib width and clast size, and

iii) spacing and rib width.

B) Overall features of a rib sequence:-

i) number of ribs comprising one sequence may reach 16 (*),

ii) spacing between ribs is generally uniform,

iii) rib width is generally uniform,

iv) current-normal orientation of each rib,

v) upstream decrease in spacing, if any, is accompanied by a slight reduction in clast size (*),

TABLE 24: Values of transverse ribs parameters obtained from Spring Creek. The rib sequences are classified according to their occurrence within channels or on the surfaces of longitudinal bars: underlining of averages denotes the micro-environment with the greater value of the response element.

#	S_b	b_{max}	$\overline{S}$	$\overline{W}$
Within channels:				
1	0.0320	18.8	57.8	46.4
2	0.0203	22.3	99.0	90.6
3	0.0349	19.3	75.2	41.2
4	0.0233	30.9	137.8	110.7
7	0.0116	24.4	74.9	83.4
8	0.0204	26.9	88.9	77.1
AVERAGE	0.0238	<u>23.8</u>	<u>88.9</u>	<u>74.9</u>
On longitudinal bars:				
5	0.0291	14.3	45.8	67.5
6	0.0087	22.6	88.9	80.4
9	0.0291	17.8	82.6	49.1
10	0.0495	12.8	31.3	33.0
11	0.0146	19.8	92.3	57.2
12	0.0408	2.6	20.6	15.3
AVERAGE	<u>0.0286</u>	15.0	60.3	50.4

N.B. Explanation of the symbols used in this table is given on p. x-xiii.

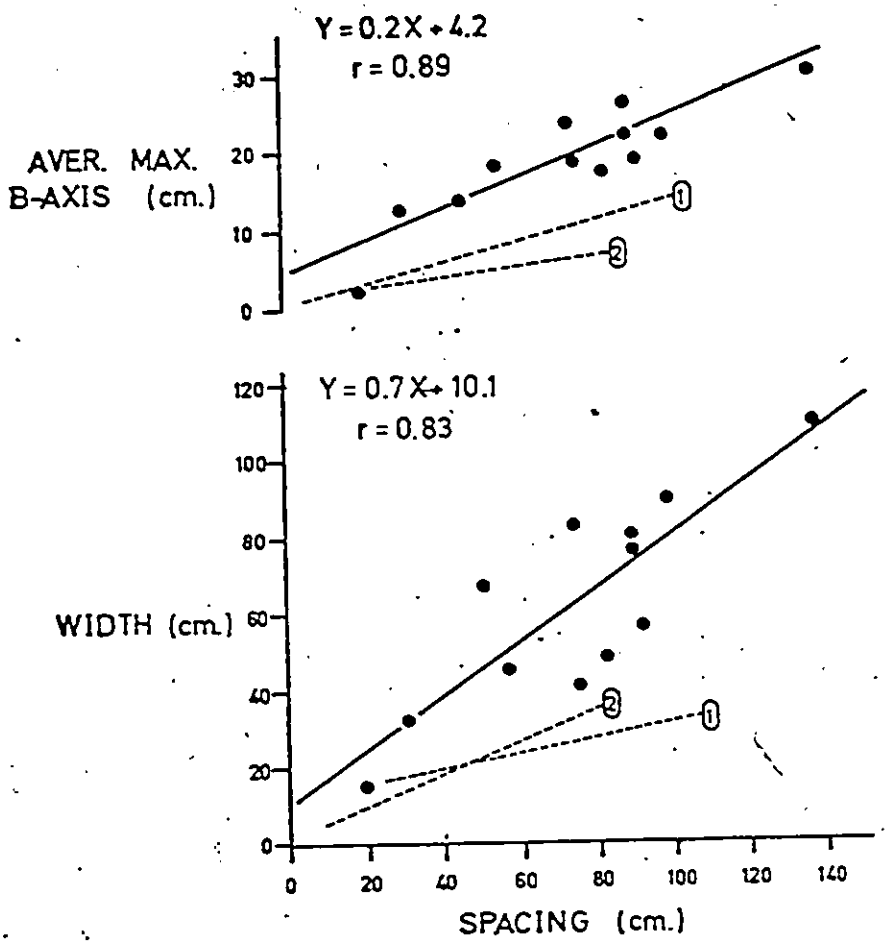

Figure 42: Inter-relationship of transverse rib data from Spring Creek. The regression lines of another study are shown for comparison.

vi) occasional 'transition' of within-bar ribs to a 'flat bed' (Figure 15B, Boothroyd and Ashley, 1975) and/or to a 'cellular structure' (Boothroyd, 1972) and/or to 'stone cells' (Gustavson, 1974),

vii) tendency for gentle convexity downchannel at points of channel widening (McDonald, pers. comm., 1972).

viii) occasional bifurcation of individual ribs at channel margin, and

ix) unlike within-channel ribs, ribs on bar surfaces contain similarly sized material to the inter-rib areas (*).

C) Features of individual ribs:-

i) clast population displays prominent imbrication and current-normal orientation (Plate 3), and

ii) larger, less transportable, clasts tend to be located on the downstream side (*).

The inter-relationships between spacing, width and clast size are more apparent when data from different localities are treated separately (see Fig. 42). This indicates that some variable(s) characteristic of the local environment influences rib development. The inter-relationships for the Spring Creek data have higher slopes than those derived from other data.

5.2 Analysis of Process

Transverse ribs are not amenable to direct field study. As with many other bedforms, it is a relatively easy matter to envisage processes by which the bedform is maintained, but the initial formation from a flat bed is at best poorly understood.

5.21 Hydraulic jump

Flume experiments by McDonald (pers. comm. 1972) have shown that transverse ribs can be formed by an upstream migrating hydraulic jump. He observed clasts being deposited in rib-like fashion in the transition zone where super-critical flow abruptly changes to sub-critical flow. The development of well-defined ribs largely depends on the bedload transport rate and on the size distribution of the bedload. Individual ribs were observed to form in seconds, after which the ribs further downstream become 'fossilized' in the less competent sub-critical flow. Formed in this way, the spacing of ribs reflects the dimensions of the hydraulic jump.

The formation of transverse ribs by a hydraulic jump requires that super-critical flow conditions (i.e. Froude Number greater than unity) be fairly widespread in the field. On the Spring Creek fan, rib sequences were found in inactive, vegetated channels and in channels abandoned as recently as the day before. Extensive reconnaissance of the channels together with careful and prolonged observations failed to locate the stepping hydraulic jump condition. One possible hydraulic jump was observed in a distal meandering channel

on the fan surface during a high, almost bankfull flow: this is interpreted, however, as a 'pseudo-meander' (Hickin, 1972) - a rare fluvial event in which flow is maintained at the critical to super-critical condition.

In general, super-critical flows are rarely developed by natural flows because at Froude Numbers around 0.4 - 0.55 'spill resistance' becomes operative (Leopold et al., 1969). This type of resistance, created by chaotic deformation of the flow around large clasts in transport, involves a sufficient degree of energy loss to inhibit further rise in Froude Number. Highly competent, shallow flows in which the ratio $d_n/\overline{Y}$ commonly approaches unity (see Fig. 26, Fahnestock, 1963) undergo such intense internal deformation that, instead of the flow being locally super-critical around large isolate roughness elements, the average condition for the flow approaches a critical or even sub-critical condition. This was observed by the author on Spring Creek fan, by Fahnestock (1963, p.27) on the White River, and by Church (1972, p.72) on the Lewis River.

5.22 Antidunes

The apparent rarity of super-critical flow in natural flows warrants enquiry into a possible second cause for the formation of transverse ribs. The argument that follows in no

way invalidates the findings of McDonald - it merely searches for a more common flow condition which is also capable of depositing a sequence of transverse ribs.

This study supports, and extends, the viewpoint of Boothroyd (1972) that ribs are "relict antidune bedforms". The term 'antidune' was introduced by Gilbert (1914) to describe the upstream migration of these bedforms. The term 'standing wave' is often used interchangeably with 'antidune', but the former was introduced to describe the appearance of the water surface. For gravelly bedloads, the term 'in-phase wave' might theoretically be preferable because upstream migration and/or antidune cross-bedding would be difficult to recognise with this calibre of bedload. However, Kennedy (1963) suggested that the term 'antidune' be applied to all bedforms which are in-phase with surface waves. Once 'ribs' of coarse gravel are established on the bed, the undulations on the water-surface are essentially 'anchored', unlike the morphollogically similar phenomena in sand-bed rivers where modification proceeds almost continuously. It is considered that the tight-settled nature of rib material prevents migration of rib sequences. Gustavson (1974) distinguished between three morphological types of surface waveforms from his study of meltwater streams draining Malaspina Glacier:-

i) so-called 'rooster-tails', upstream-breaking variety, conical in three-dimensional form, often forming trains;

ii) same as i), except for considerable lateral extent which approaches channel width; and

iii) reticulate or checkerboard pattern of upstream-breaking waves.

Types ii) and iii) were found to be most common. Gustavson postulated that transverse ribs and stone cells are developed by linear and reticulate waveforms respectively.

McDonald and Banerjee (1971) indicate in their Table 2 (p. 1288) that the "characteristic flow regime" of the "largest active channels in late afternoon" on the Peyto outwash plain is "standing waves on the water surface". By definition, if there are standing waves on the water-surface, then there must be co-existing in-phase waves on the bed (Allen, 1970, p. 81). Peyto outwash is composed of sand and pebbly-sand with maximum clast size around 16cm.

The development of standing waves and upstream-breaking waves is common within proximal reaches of braided systems: most are located in riffle portions, but at high flows (whether as a diurnal or seasonal peak) they are also fairly abundant in pool sections.

According to the theoretical analysis of Kennedy (1963), a Froude Number of 0.844 constitutes a lower limit for antidunes, but a later three-dimensional analysis by Reynolds (1965) indicated this limit to be somewhat lower at 0.7. The present flume data finds precise agreement with the latter figure.

The preservation potential of antidune bedforms in sand is low on account of destruction during falling stage (Middleton, 1965) Only one field study has reported antidune bedding from a pebbly sandstone (Hand et al., 1969), and in sandstones upper-flow regime bedforms have been recognized by Jopling and Walker (1968).

Reports of antidune bedding in sand from the proglacial braided environment are rare, despite many reports of undulatory water wave forms. Fahnestock (1963, p. 28) stated "antidunes are observed when discharge increased markedly in a channel with predominantly sandy bed materials"; although sediment traps, designed to sample the larger size fractions, indicated median diameters of 2.5cm. Langbein (1942, p. 618) stated: "the effect of sediment load (particularly the finer sizes) is to decrease the kineticity required for the formation for sand waves...the critical slope...is reduced by fines and increased hydraulic radius...accordingly, sand waves could be expected to be frequent flood-adjuncts under conditions of steep slopes and fine sediments." Flume

experiments by Fahnestock and Haushild (1962, p. 1433) showed that rolling clasts tend to be deposited beneath the crests of breaking antidune waves. In the field, Fahnestock (1963, p. 27) observed boulders rolling silently on a sand bed during the antidune phase: coarser bedloads on Spring Creek are easily identified by a din of clashing boulders.

In the reconnaissance run EK3D-18 (see Table 7 for hydraulic details), 122 clasts were introduced singly at 5 second intervals at the upstream end of the flume in random orientation. Deposition at the downstream end was induced by a low, coarse-mesh barrier; which occupied 0.8 of the flow depth. Upstream from the barrier, the bed formed a short sequence of imperfect transverse ribs. Because the clasts were numbered, it was possible to compare the entry order with the order of deposition. The Spearman's rank correlation coefficient (Walpole, 1968) for this data, is 0.920 which indicates that the bed did not simply develop by progressive addition of material at its upstream margin. The majority of clasts were initial rib material, but some smaller and more transportable clasts were subsequent additions to rib material after passing the rib(s) already formed upstream. Transverse ribs were observed to lie beneath the crests of a quasi-stable antidune wave train. T. Day (pers. comm., Oct. 1976) has also observed ribs forming beneath antidunes during some recent flume experiments at the G.S.C.

Abrupt upstream migration of the surface waveform

occurred when the width of the rib undergoing formation becomes too great: the distance of each migration was constant (80-90cm). The new wave form was stabilised in its position by larger, less transportable clasts becoming stationary in the lower velocity zone of the crest which then acted as a locus for deposition of ensuing clasts. Clasts comprising each rib showed contact imbrication and current-normal orientation.

Kennedy's (1961) equation, relating wavelength to flow velocity,

$$\overline{U}^2 = \frac{g.L}{2.\pi}$$

may involve some error because it is assumed that:-

i) the in-phase system is two-dimensional;

ii) the profile of bed and water waves are sinusoidal, but this only holds true for waves of very small amplitude (Hand, 1969a);

iii) the bed and water surfaces are parallel; and

iv) the wave system is stationary (if breaking does occur, calculated wavelengths will be low (Kennedy, 1963).

Despite these limitations, Forbes (1973) found a definite functional relationship between flow velocity and antidune wavelength very similar to the above equation.

According to the theoretical analysis of Hand (1969), antidunes do not develop when the mean flow depth, $\overline{Y}$, exceeds the value of $(\lambda/2.\pi)$. In addition, the criterion for maximum

steepness for a free water wave is when the ratio of the water wave height over the wavelength reaches the value of 0.142. Owing to high values of the $d_n/\bar{Y}$ ratio in ribbed reaches, it appears probable that the accompanying water waves would attain height to wavelength ratios close to the maximum figure.

Downstream from an obstruction, like a large boulder, undulatory water waves are sometimes present: presumably, this case can be identified by the fact that the wave amplitude uniformly declines distally from the point of propagation. Elsewhere in a coarse-grained environment, undulatory water waves are presumably associated with antidune waves (or 'ribs') on the bed surface, thereby making them antidunes in the proper sense of the term. Coarse-grained antidune deposits may either be composed of:-

i) sand or pebbly sand over which an 'isolate bedload' of cobbles and boulders is transported and temporarily becomes stationary beneath wave crests, but reverts to a plane or dune bed during falling stage, leaving no evidence of former antidunes, or

ii) cobble to boulder bedloads in which individual clasts are isolate and arrive singularly at the site of potential rib formation - because the largest percentiles of the bedload are involved, lower stage flows are incapable of modification and therefore evidence remains as transverse ribs on the bed, and attests to former antidune flows.

5.3 Discussion

The underlying theory of the hydraulic jump and in-phase wave hypotheses for the formation of transverse ribs have similarities and differences.

The similarities are as follows. Both invoke:-

i) 'growth' of the ribbed sequence in the upstream direction (this of course is to be anticipated since as a depositional product, each rib acts as an effective barrier to coarse bed-load transport - the only, somewhat unrealistic, alternative is that the whole sequence be formed instantaneously);

ii) a water disturbance migrating upstream in discrete steps;

iii) that, once a rib has been formed, those 'fossilised' downstream stablise a train of in-phase waves with wavelength and amplitude conditioned by the spacing and height of the in-phase transverse ribs;

and both recognise that:-

iv) ribs are not an 'equilibrium' bedform (e.g. ripples) because they are neither produced, or maintained, all at the same time - once produced, the clasts comprising a rib are stationary; and

v) clast supply rate is an important factor.

The differences are as follows:-

i) Flow is not necessarily super-critical in the antidune wave hypothesis; and

ii) the two models differ in the mechanism which initiates the formation of the first downstream-placed rib.

The latter difference warrants considerable attention. Two possible 'triggering mechanisms' are proposed here:-

i) Random, or 'chance' deposition of a larger, less transportable clast which forces ensuing clasts in a similar trajectory to be also deposited. This would lead to 'contact imbrication' (or so-called 'shingling) which would subsequently serve as an 'anchor' for an in-phase wave - initially the waveform could be of the 'rooster-tail' variety. (Boothroyd, 1972) but lateral propagation would presumably occur as more clasts became stationary in this lower velocity flow field.

ii) Langbein and Leopold (1968) showed that incohesive bedloads (without size limitations) subject to unidirectional flow frequently develop 'kinematic waves' (Lighthill and Whitham, 1955). The kinematic waves are manifested by bedforms on all scales. In brief, it may be stated that "fairly regular waves can be generated by a random process....particles are subject to the condition that, where particles happen to be far apart, they are more easily moved than when the particles are close....thus, the movements will tend to collect the particles into groups that have wave-like form" with "characteristic lengths and heights" (p. 14). Of possible relevance to this study is the observation that "the lengths {or 'spacing'} of such wave patterns would be proportional to the mean concentration and speed" (p. 15). In an experiment

on particle transport, Lighthill and Whitham observed that "as the rate of feed was increased, the size of groups increased, and the average speed decreased so that ultimately a point was reached where a group became so large that a jam formed and all motion halted" (p. 15). Groups were observed to form rather quickly.

It is possible that the imposition of kinematic waves on clast transport could abruptly trigger formation of the initial rib. Thereafter, the effect would be to 'anchor' a standing wave over the first-formed rib and ensuing clasts would then be subject to 'dynamic waves' - in this case, antidunes - which are uniquely determined by mean flow velocity, although Langbein and Leopold (1968) remark that their speed could be inferred from kinetic properties of the flux-concentration curve.

Development of kinematic waves occurs in both the x and y flow axial directions (at least for sandy sediment; Lighthill and Whitham, 1955, p. 19), and it is considered that this might provide an explanation for the 'stone cells' (Gustavson, 1974) which thus far have only been observed in pebbly material.

5.4 Reconstruction of the Paleoflow Regime

For the purposes of paleohydraulic determinations, transverse ribs are more conveniently analysed according to the average values of spacing, width and clast size, rather than viewing each rib individually. This method assumes that hydraulic conditions in the reach were essentially constant during the period of rib formation: this provides a convenient working hypothesis.

Assuming that transverse ribs are deposited as antidune waves, mean wavelength of the water waves ($\overline{\lambda}$) can be deduced from average spacing ($\overline{S}$) and width ($\overline{W}$) by means of the formula:

$$\overline{\lambda} = \overline{S} + \overline{W} \qquad \ldots\ldots\ldots(1)$$

With wavelength empirically determined, Kennedy's (1961) equation

$$\overline{U}^2 = \frac{g \cdot \lambda}{2 \cdot \pi}$$

can be rearranged in the form

$$\overline{U} = \left(\frac{g \cdot \lambda}{2 \cdot \pi}\right)^{\frac{1}{2}} \qquad \ldots\ldots\ldots(2)$$

thus enabling mean flow velocity of the ribbed reach to be calculated. For $\overline{U}$, 'mean' should be interpreted as both an average velocity in the flow cross-section, but also a time-average velocity in the reach during rib formation.

Kennedy's equation states that the wavelength of the bed and water waves is dependent only on $\bar{U}$; Allen (1970, p. 82) reports that this simple relation is closely paralleled by both field and laboratory (e.g. Forbes, 1973) studies. There are, however, some field studies which have detected a partial dependence of wavelength on other hydraulic variables. For example, Nordin (1964) found a positive linear relation between mean depth, $\bar{Y}$, and antidune wavelength given by the simple relation

$$\lambda = 4.2\bar{Y}$$

For Spring Creek anabranches containing ribs, wavelength appears to be less dependent on $\bar{Y}$ (see page 175 for method of determination), viz.

$$\lambda = 39(\bar{Y}^{0.352}), \quad r = 0.865$$

As Nordin (1964, p. 12) points out, the existence of a relation between these two variables does not serve to reject the theory of Kennedy (1961) that wavelength is independent of depth. Instead, the existence of such a relation "merely indicates that the velocity-depth relation was reasonably stable" (Nordin, 1964, p. 12): the particular at-a-station hydraulic geometry that characterises braided channels offers support to Nordin's viewpoint.

The particle size versus shear stress relation compiled by Baker and Ritter (1975) enables mean depth, $\bar{Y}$, to be determined given a representative particle size, d, and channel slope, S. They carefully standardised all the available data and arrived at the following relation:

$$d(mm) = 65(\tau^{0.54}), \quad r = 0.92 \qquad \ldots\ldots\ldots(3)$$

where τ is the boundary shear stress, given by Du Boys' (1879) formula. The correlation coefficient indicates that 85% of the observed variability in particle size is accounted for by variation in boundary shear stress.

The Du Boys equation for boundary shear stress is given as

$$\tau(kg.m^{2}) = \rho_f.R.S_e \qquad \ldots\ldots\ldots(4)$$

but this can be simplified without introduction of significant error. In braided channels with coarse-grained bedload, high width to depth ratios enable the hydraulic radius R to be closely approximated by the average depth $\bar{Y}$. In addition, γ_f does not generally show significant departures from the standard value of $1000kg.m^{-3}$: Østrem (1975) finds that maximum concentrations of suspended sediment in proglacial outwash streams of Norway are 12 grams per litre. The only possible source of error rests with the assumption that slope of the channel bed accurately reflects the slope of the energy grade line. In paleohydraulic studies, the paleoflow system

is necessarily assumed to be in equilibrium with water and bed surfaces parallel. On Spring Creek, it is considered that channel reaches containing ribs do not display any pronounced lack of parallelism: in contrast, ribbed inclined surfaces of longitudinal bars would likely be non-parallel with the water surface.

Substituting the simplified Du Boys relation in equation 3, and rearranging it to make flow depth the subject, we obtain

$$\overline{Y}(cm.) = \left(\frac{d}{65(1000^{0.54})\ (S^{0.54})}\right)^{1.852}(100) \quad \ldots.(5)$$

By substitution of the values of clast size (b_{max} for d) and bed slope (Table 27) in equation 5, an estimate of paleodepth for each rib sequence is obtained.

The values of mean flow velocity and depth may also be substituted in the formulae

$$Fr = \frac{\overline{U}}{(g.\overline{Y})^{\frac{1}{2}}} \qquad \text{and} \qquad Re = \frac{\overline{U}.\overline{Y}}{\upsilon}$$

to yield estimates of Froude Number and Reynolds Number for the rib-forming flows. The standard value for kinematic viscosity at 5°C. (i.e. 0.01519) has been employed in the computations of Reynolds Number: allowances have not been made for suspended or dissolved material in the Spring Creek flows.

From studies of upper-flow regime flow on the Rio Grande, Nordin (1964) found that antidune wavelength is 3 to 6 times the flow depth. Using the values of extrapolated wavelength calculated by means of equation 1, and computed values of flow depth (on the basis of the particle size versus boundary shear stress relation of Baker and Ritter (1975)), the in-phase waves of Spring Creek had an average wavelength to depth ratio of 4.38. Nordin states that lateral extent of in-phase waves "averages about 1½ times the wavelength and has never been observed to exceed 3 times the wavelength" (p. 11). This latter relation might enable an approximate estimate of channel width to be made which, in conjunction with the estimates of depth and velocity, then permits estimation of paleo-discharge.

An approximate relationship between the three parameters (i.e. width, spacing and clast size) of transverse ribs may be calculated as follows:-

Equation 11 (see p.182) is the best-fit relation between paleo-velocity and clast size, viz.

$$\bar{U} = 49(b_{max}^{0.381})$$

Also, a re-arrangement of Kennedy's (1961) formula relating antidune wavelength to velocity leads to equation 2. Equating the right-hand sides of these two equations for a given

value of $\overline{U}$, and assigning values to the constants g and π, leads to

$$12.49(\overline{\lambda}^{\frac{1}{2}}) = 49(b_{max}^{0.381})$$

But since $\overline{\lambda}=(\overline{S}+\overline{W})$, rib spacing is given by the formula

$$\overline{S} = 15.36(b_{max}^{0.762}) - W \quad \ldots\ldots\ldots(6)$$

Also $$\overline{\lambda} = 15.36(b_{max}^{0.762}) \quad \ldots\ldots\ldots(7)$$

Thus if transverse ribs were to be recognised in a fluvial succession, and spacing and/or width were readily apparent, wavelength could be obtained just from data on size, and thereafter estimates of paleoflow could be made in the above-described manner.

Table 25 contains values for each paleoflow variable calculated on the basis of the antidune hypothesis for transverse ribs. The results are more informative when they are grouped according to whether the ribs were developed within channels or on bars. Support for the in-phase wave origin for transverse ribs stems from the fact that average values of each paleoflow variable are appropriate for the braided stream environment of Spring Creek.

As expected, rib-forming flows in channels have greater depths and higher velocities than those over bars. Accordingly, channels prossess antidune waves which are larger, both with respect to the water-surface (i.e. wave

Table 25: Values of paleoflow parameters computed on the basis of transverse rib measurements (see Table 24): see text for details. Underlining of averages denotes the micro-environment with the greater value of the inferred process element.

#	$\bar{\lambda}$	$\bar{H}_w$ (max)	$\bar{Y}$	$\bar{U}$	Fr	Re
Within channels:						
1	104.2	14.8	22.2	127.5	0.86	186,340
2	189.6	26.9	48.0	172.0	0.79	543,515
3	116.4	16.5	21.5	134.7	0.93	190,655
4	248.5	35.3	77.1	196.1	0.72	999,407
7	158.3	22.5	99.7	157.2	0.50	1,031,787
8	168.0	23.9	68.0	160.9	0.62	720,290
AVERAGE	<u>164.2</u>	<u>23.3</u>	<u>56.1</u>	<u>158.2</u>	<u>0.74</u>	<u>732,047</u>
On longitudinal bars:						
5	113.3	16.2	14.8	132.9	1.10	129,488
6	169.3	24.0	115.5	162.6	0.48	1,236,359
9	131.7	18.7	22.3	143.3	0.97	210,375
10	64.3	9.1	7.1	100.2	1.21	46,835
11	149.5	21.2	53.6	152.7	0.66	538,823
12	35.9	5.1	-	-	-	-
AVERAGE	125.6	17.8	42.7	138.3	<u>0.88</u>	540,141

N.B. Explanation of the symbols used in this table is given on p. x-xiii.

amplitude, length and steepness) and to the bed-surface (i.e. rib coarseness, spacing and width). Channel flows are also more turbulent. Because flow over bars tends to be shallower and owing to the locally steeper slopes associated with the longitudinal bars, the Froude Numbers of rib-forming flows over bars are greater than those within channels.

The analysis of paleoflow conditions indicates that the flow was super-critical for only two of the measured ribbed sequences. In channels, the computations indicate that transverse ribs may be formed by flows with Froude Number as low as 0.5. Since ribs contain the largest calibre of bedload, it is instructive to abstract the highest flow condition from the results of the foregoing analysis of paleoflow conditions. Table 25 indicates that maximum mean velocities approach $2m.sec^{-1}$ and maximum mean depths slightly exceed 1m. These values are realistic maxima for the braided stream environment of Spring Creek: at-a-station hydraulic geometry for the main channel at the fanhead indicates that mean velocities of $2m.sec^{-1}$ are developed by flows having a discharge of approximately $13m^3.sec$.

5.5 Clast Transport and Competence

Antidunes are characterised by lower levels of competence beneath the wave crest than beneath the wave trough. Forbes (1973) found a 20% reduction in surface velocity over wave crests.

Mean flow velocity, as computed from rib parameters, is assumed to be representative of a flow which was marginally competent to transport the clasts in the ribs. However, due to either impeded transport by already deposited clasts or to an excessive 'low' in velocity peturbations, it must also be considered representative of a flow that deposited the clasts. Certainly, it reflects conditions of transport and deposition, rather than entrainment.

Using the observed clast size data in conjunction with the computed values of paleo-velocity, the relationship between particle size and velocity was determined. For the data (n = 12) from Spring Creek, the relation is

$$\overline{U} = 48.3(b_{max}^{0.372}), \quad r = 0.923 \qquad \text{.....(8)}$$

The rib sequences (n = 22) measured by McDonald and Banerjee (1971) yield the relation

$$\overline{U} = 38.7(b_{max}^{0.439}), \quad r = 0.935 \qquad \text{.....(9)}$$

In view of the close similarity of equations 8 and 9, the two groups of data were combined for the purposes of obtaining a statistically more significant relationship:

$$\overline{U} = 39.3(b_{max}^{0.436}), \quad r = 0.954 \qquad \text{.....(10)}$$

The above regression lines are all enclosed by the envelope of data compiled by Novak (1973) (Fig. 43), whose particle size and velocity data (n=112) were subjected to the

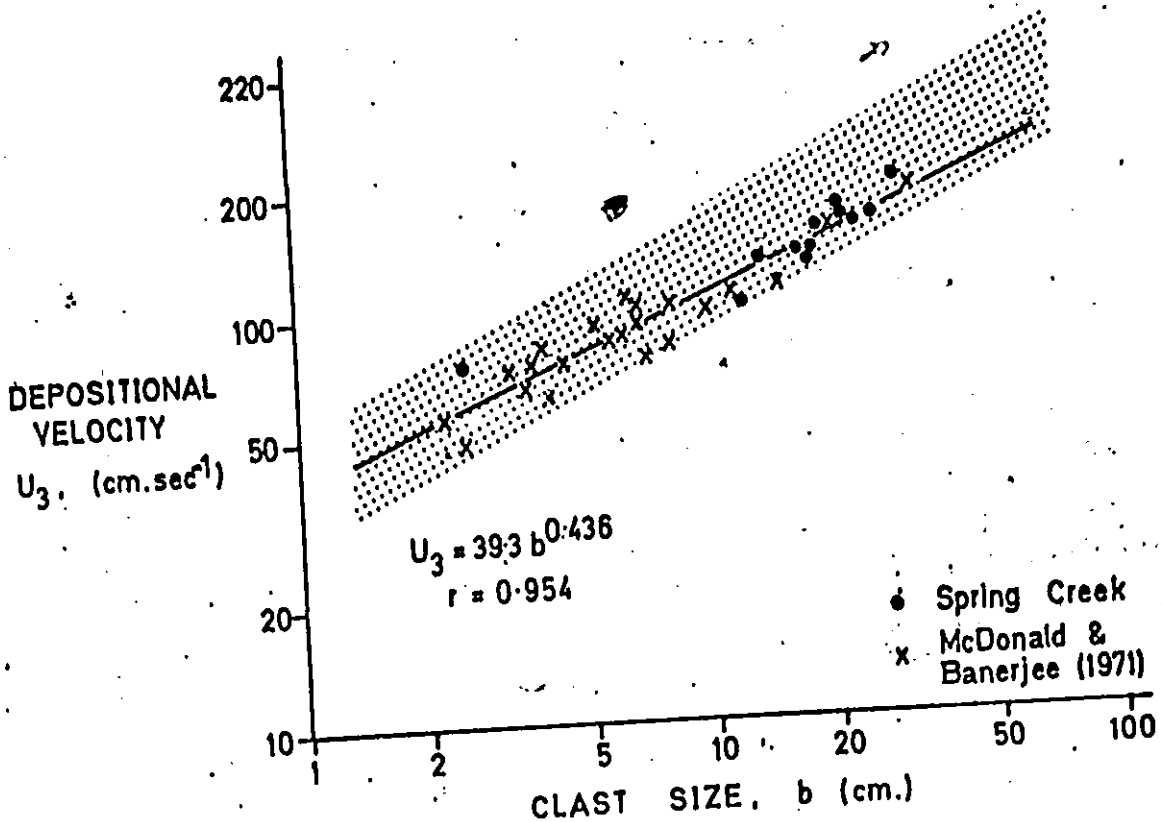

Figure 43: The data of depositional velocity versus clast size based on paleoflow calculations from transverse rib data. All the data are enclosed by the envelope compiled by Novak (1973) shown by the stippled zone.

same regression analysis, and yielded the following relation

$$\overline{U} = 49.0(d^{0.381}), \quad r = 0.825 \qquad \ldots\ldots(11)$$

Equation 11 is very similar to that derived from the ribbed sequences of Spring Creek (equation 8). The relation deduced from McDonald and Banerjee's (1971) data gives a somewhat steeper line than the ones referred to above.

It is interesting to note that the best-fit equation of Novak's (1973) data supports the findings of Nevin (1946) and Malde (1968) that particle size varies as the 2.6 power of velocity, since equation 11 can be re-stated thus -

$$d = \left(\frac{\overline{U}}{49}\right)^{2.62} \qquad \ldots\ldots(12)$$

Most of the scatter in these graphs relating velocity to particle size derives from unsatisfactory description of clast size. The intermediate b-axis is not a very precise measure for inequidimensional clasts (see Section 2.51). In addition, the graphs neglect the effect of clast shape which has been shown to have a considerable effect on entrainment (Lane and Carlson, 1954), transport velocities (the present study; Krumbein, 1942) and on deposition (Helley, 1969).

It is reasonable to assume that in the absence of any consistent change in clast size through a rib sequence, flow conditions were essentially constant. Presumably competence levels of the paleoflow are reflected by the largest clast in

each rib, rather than the average of the ten largest ones. In view of the fact that successive ribs are added in the upstream direction, an upstream detrease in maximum (or perhaps median) clast size would probably reflect waning flow, and vice versa. However, inference on the basis of particular clast sizes may be a little tenuous, owing to the interplay of at least two variables: these pertain to bedload transport and are

i) availability of each size grade to the reach undergoing rib formation, and

ii) the random nature of the processes involved.

Information on clast size and rib spacing should be sought collectively since, according to the antidune wave hypothesis, both these parameters are velocity-dependent. Changes in one would likely be accompanied by changes of similar magnitude in the other.

5.6 Comment

The antidune hypothesis for the formation of transverse ribs receives support from the study of paleoflow on three accounts.

i) Pairs of measured clast size and computed paleo-velocity data are in close agreement with the relations for fluvial competence established by other, more direct, sedimentological studies (i.e. Novak, 1973; Baker and Ritter, 1975).

ii) The geometry of the standing wave train has been computed from transverse rib data and is in close agreement with the findings of other studies (e.g. Nordin, 1964; Hand, 1969).
iii) Values of paleo-depth, -velocity and -Froude Number are in the same range as those encountered in the proglacial braided stream environment. Rib-forming flows are generally sub-critical, relatively shallow and highly competent because of their high velocity.

It therefore appears that sequences of transverse ribs are of considerable use in paleoflow reconstruction. They have yet to be recognised in ancient or recent successions and it may be assumed that ribs have a low preservation potential. Alternatively, they might be widely preserved but difficult to recognise.

Perhaps paleoflow reconstruction based on transverse ribs will find most application in modern environments, such as Spring Creek. Proglacial braided streams are not generally amenable to direct hydrologic or hydraulic studies and so ribs assume considerable importance by supplying this information indirectly.

6.0 SUMMARY & CONCLUSIONS

Flume experiments on coarse-grained sedimentation have shown that individual clast response to steady, subcritical flow varies according to a complex assemblage of process variables. The empirical relations of process and response enable certain conclusions to be made about the paleo-environment of gravel sedimentation.

Clasts isolate on a sand bed undergo combined rotation and translation in response to current-crescent scour. Motion is dependent both on the degree of form roughness associated with sand bedforms as well as on the size and shape characteristics of the individual clasts. Imbrication to moderate angles is the dominant response, and its development to a stable configuration determines the duration of current-crescent scour. Clast stability appears to be attained when the projection area reaches a value that closely approximates the square of the nominal diameter, although the development of imbrication which satisfies this criterion is limited to the sandbeds with minimal form roughness. Ripple, dune and antidune bedforms do not allow full development of the imbrication process. Since the sand bedform co-existing with pebble deposition is likely to be in the transition or upper-flow regime, it follows that the 'equilibrium area' concept is a potentially useful tool for the recognition of hydrodynamic stability in ancient deposits. Monitoring of the imbrication process reveals that the required duration of

clast exposure rapidly decreases with the onset of the upper-flow regime, such that for matrix-supported gravels in which clast motion on the bed is unimpeded, the contained clasts will likely conform to the stability criterion. A theoretical analysis of the imbrication process indicates that hydrodynamically 'smooth' boundaries require less downward translation in lower velocity flows.

The three axial components of clast translation from the initial position on the bed surface to that of a streamlined, imbricated configuration have magnitudes which are highly dependent on the degree of form roughness of the sandbed, as well as on a small assemblage of clast properties. Orientation of elongate clasts is ubiquitously current-normal even when they were initially laid with a-axes parallel to flow. Oblate clasts are more susceptible to form roughness of the sand bed, and therefore tend toward imperfect alignment.

Experiments designed to clarify the role of clast size and shape properties on transport velocities produced complex results. Some unexpected types of clast motion occurred, including the rolling of highly oblate clasts about the circumference of their a-b planes, but a-axes were consistently aligned transverse to flow in spite of their random orientation at the point of introduction. Data of mean transport velocity versus size are only moderately correlated and produce negatively-sloped curvilinear relations: the majority of previous laboratory studies encountered lines with positive

gradient. It is therefore considered that for a wide range of clast sizes subjected to competent flow the complete relation approximates a convex-upward parabola, such that maximum transport velocities are developed by an intermediate size grade. This offers an explanation for the local and progressive size sorting which typifies coarse-grained fluvial systems. Unsteady, non-uniform flow, armouring of the bed by coarse lag deposits and imbricated tight-settled, contact bedloads are among the factors which would inhibit a consistent relation between transport velocity and clast parameters. A more complete explanation of the experimental data is afforded by a multivariate approach: this statistical analysis indicates that the influence of clast form (expressed as the oblate-prolate index) varies systematically in relation to the clast size to flow depth ratio. In a given flow, it appears that for clasts with low values of this ratio oblate forms are transported more readily because of their susceptibility to hydraulic lift into faster moving levels of the velocity profile. For larger clasts, on the other hand, prolate forms are more rapidly transported, presumably because of the high shear exerted in the lower levels of the flow profile. To some extent, the study of the influence of clast properties on transport velocity of single particles raised more questions than it has answered; clearly, previous investigations of the process-response relationships which govern large clast transport have been somewhat over-simplified.

Transverse ribs were studied because their explanation by an upstream-migrating hydraulic jump did not appear to be a viable mechanism for their widespread development in Spring Creek, where supercritical flows are very rarely attained. Observations in a reconnaissance run prompted a detailed enquiry of the possibility that antidune waves of subcritical flow could form the ribs observed in the field. Using this hypothesis, 'fossilised' ribs replicate the geometry of the former train of antidune waves. Moreover, using established relations of tractive force and transport velocity as a function of clast size, the coarseness of the rib material can be compared with the mean flow velocities computed from the average wavelength of the antidune waves. This analysis produced good results, and a mathematical procedure is outlined for the reconstruction of the paleoflow regime using the measurable geometrical attributes of the rib sequence. It appears that rib development may be triggered by the formation of kinematic waves during bed-load transport.

Where present, transverse ribs are conspicuous features of cobble-boulder deposits, both from the standpoint that they are the only within-channel bedform and because they involve the coarsest percentiles of the available bedload. Therefore, they reflect the highest flow events, and this makes the set of empirical equations for determination of the paleoflow regime a potentially useful addition to sedimentology.

Since 1970, there has been a rapid surge of interest in coarse-grained sediments and conglomeratic rocks. Proximal fluvioglacial systems have been the subject of thorough field investigations, while recent studies of submarine fan deposits have clarified the genesis and properties of resedimented conglomerates. In both environments, considerable significance has been attached to clast fabrics, both in terms of the current-normal or -parallel a-axis orientations and the characteristics of imbrication. This laboratory study has attempted to quantitatively define the stability associated with imbrication in flows where transverse alignment of clasts is the stable configuration. The proposed theory clarifies the hitherto confusing role of clast properties as well as the results of the more detailed previous studies. It is considered that the improved state of knowledge at the matrix-supported end-member of the coarse-grained sediment spectrum also aids interpretation of the more abundant clast-supported type of deposit.

It was frequently found that available field data is of insufficient detail to enable a precise and/or full application of experiment results. In particular, this applies to descriptions of the size, morphology and fabric of the clasts as well as the flow characteristics of the fluvial

environment. It is of course acknowledged that there are often practical reasons why collections of this type of data are not possible. However, it is strongly recommended that the detail of field investigations be improved wherever feasible. It is only via this course that experimental work will realise its full potential in our understanding of coarse-grained sedimentary environment.

On the basis of the present findings, it is recommended that future studies of coarse-grained sedimentation include the following aspects:

1) A more thorough verification should be made of the conformity of fluvial clasts to an ellipsoidal geometry. This geometric similarity is potentially useful because it allows close approximation of clast volume (and thereby also of nominal diameter) and computation of projection area.

2) The present experimental study has described the attainment of clast stability in matrix-supported deposits using the ellipsoidal portion of the clast population. The study could be extended to current-normal clasts in fluvial clast-supported deposits as well as to submarine resedimented conglomerates and river flood deposits in which current-parallel orientation appears to be characteristic.

3) The present findings on the rate of aggradation and the attainment of equilibrium clast response in matrix-supported deposits should be field tested.

4) Further work is required on the movement of large, non-spherical clasts, particularly with regard to 'optimum size grades for transport'. A possible field approach would be to compare the sorting and size attributes of the bedload in abandoned channels with those predicted on the basis of prior hydrometric observations.

5) More field measurements of transverse rib sequences are required to clarify the inter-relationships between rib parameters in different fluvial environments, and to further investigate the merit of the antidune hypothesis as an explanation for their origin. The latter could perhaps be investigated by detailed monitoring of the hydraulic development of channels and longitudinal bars which are observed during flows to have undulatory surface wave forms. The empirical equations for calculation of paleoflow parameters could then be tested using rib sequences exposed on bar surfaces or within channels as a result of avulsion and/or falling stage.

7.0 REFERENCES

ALLEN, J.R.L., 1966, On bedforms and paleocurrents: Sedimentology, v. 6, p.153-190.

_____, 1970, Physical processes of sedimentology: George Allen & Unwin Ltd., 248pp.

_____, 1973, Phase differences between bed configuration and flow in natural environments, and their geological relevance: Sedimentology, v. 20, p.323-329.

BAKER, V.R. & RITTER, D.F., 1975, Competence of rivers to transport coarse bedload material: Geol. Soc. Amer. Bull., v. 86, p.975-978.

BECKER, G.F., 1893, Finite homogenous strain, flow and rupture in rocks: Geol. Soc. Amer. Bull., v. 4, p.53-54.

BLATT, H., MIDDLETON, G.V. & MURRAY, R., 1972, Origin of sedimentary rocks: Prentice-Hall Inc., N.J., 634pp.

BLUCK, B.J., 1967, Deposition of some Upper Old Red Sandstone conglomerates in the Clyde area: a study in the significance of bedding: Scottish Jour. Geol., v. 3, p.139-167.

BOOTHROYD, J., 1972, Coarse-grained sedimentation on a braided outwash fan, northeast Gulf of Alaska; ONR Tech. Rep. No. 6-CRD, Univ. of South Carolina, 127pp.

_____ & ASHLEY, G.N., 1975, Processes, bar morphology, and sedimentary structures on braided outwash fans, northeastern Gulf of Alaska: S.E.P.M. Spec. Pub. No. 23, p.193-222.

BRADLEY, W.C., FAHNESTOCK, R.K. & ROWEKAMP, E.T., 1972, Coarse sediment transport by flood flows on Knik River, Alaska: Geol. Soc. Amer. Bull., v. 83, p.1261-1284.

BRIGGS, L.,& MIDDLETON, G.V., 1965, Hydromechanical principles of sediment structure formation: S.E.P.M. Spec. Pub. No. 12, p.5-16.

BROCK, E.J., 1974, Coarse sediment morphometry: a comparative study: Jour. Sed. Petrology, v. 44, p.663-672.

CAILLEUX, A., 1938, La deposition individuelle des galets dans les formations detritiques: Rev. Geogr. Phys. et Geol. Dynam., v. 11, p.669-707.

_____, 1945, Distinction des galets marins et fluviatiles: Soc. Geol. France Bull., v. 15, p.375-404.

CANT, D.J., & WALKER, R.G., 1976, Development of a braided-fluvial facies model for the Devonian Battery Point Sandstone, Quebec: Can. Jour. Earth Sci., v. 13, p.102-119.

CHURCH, M., 1972, Baffin Island sandurs: Canada Geol. Surv. Bull., no. 216, 205pp.

CLIFTON, H.E., 1973, Pebble segregation and bed lenticularity in wave-worked versus alluvial gravel: Sedimentology, v. 20, p.173-188.

CRICKMORE, M.J., 1970, Effect of flume width on bed-form characteristics: A.S.C.E., Jour. Hydraul. Div., v. 96, Proc. Paper 7077, p. 854-859.

CROWELL, R.H. & SLESNICK, W.E., 1968, Calculus with analytic geometry: W.W. Norton & Co. Inc., N.Y. 727pp.

CURRAY, J.R., 1956, The analysis of two-dimensional orientation data: Jour. Geol., v. 64, p.117-131.

DAVIES, I.C. & WALKER, R.G., 1974, Transport and deposition of resedimented conglomerates; The Cap Enrage Formation, Cambro-Ordovician, Gaspe, Quebec: Jour. Sed. Petrology, v. 44, p.1200-1216.

DOBKINS, J.E. & FOLK, R.L., 1970, Shape development on Tahiti-Nui; Jour. Sed. Petrology, v. 40, p.1167-1203.

DOEGLAS, D.J., 1962, The structure of sedimentary deposits of braided rivers: Sedimentology, v. 1, p.167-190.

DU BOYS, P.D.F., 1879, Le Rhône et le riviére lit affouillable: Annales des ponts et chaussées, v. 18, ser. 5, p.141-195.

DYER, K.R., 1970, Grain-size parameters for sandy-gravels: Jour. Sed. Petrology, v. 40, p.616-620.

DZULYNSKI, S., & SANDERS, J.E., 1962, Current marks on firm mud bottoms: Connecticut Acad. Sci. Trans., v. 42, p.57-96.

EINSTEIN, H.A., 1950, The bed-load function for sediment transportation in open channel flows; U.S. Dept. Agriculture, Soil Conservation Service Tech. Bull. 1026, 71pp.

EYNON, G. & WALKER, R.G., 1974, Facies relationships in Pleistocene outwash gravels, southern Ontario; a model for bar growth in braided rivers: Sedimentology, v. 21, p.43-70.

EZEKIEL, M., & FOX, K.A., 1959, Methods of correlation and regression analysis - linear and curvilinear: John Wiley and Sons Inc., N.Y., 548pp.

FAHNESTOCK, R.K., 1963, Morphology and hydrology of a glacial stream - White River, Mount Rainier, Washington: U.S. Geol. Surv. Prof. Paper 422-A, 70pp.

_____, 1973, Knik and Matanuska Rivers, Alaska - a contrast in braiding: in 'Fluvial Geomorphology', ed. M. Morisawa, Pub. in Geomorphology, State Univ. N.Y., Binghampton, p.200-250.

_____, & HAUSHILD, W.L., 1962, Flume studies of the transport of pebbles and cobbles on a sandbed: Geol. Soc. Amer. Bull., v. 73, p.1431-1436.

FLEMING, N.C., 1965, Form and function of sedimentary particles: Jour. Sed. Petrology, v. 35, p.381-390.

FOLK, R.L. & WARD, W.C., 1957, Brazos River Bar; a study in the significance of grain size parameters: Jour. Sed. Petrology, v. 27, p.3-26.

FORBES, D.L., 1973, Alluvial sedimentation on plane beds and in-phase waves: M.A. Thesis, Univ. of Toronto, 58pp.

GALAY, V.J., 1967, Observed bedforms of bed roughness in an unstable gravel river: Proc. 12th Congr. Int. Assoc. Hydraulic Research, Ft. Collins, Colo., p.85-95.

GARG, S.P., AGRAWAL, A.K., & SINGH, P.H., 1971, Bed load transportation in alluvial channels: A.S.C.E., Jour. Hydraulics Div., v. 97, Proc. Paper 8091, p.653-664.

GIBBONS, G.S., 1969, Planar sections through imbricate-type fabrics: Jour. Geol., v. 77, p.339-346.

GIBBS, R.J., MATTHEWS, M.D. & LINK, D.A., 1971, The relationship between sphere size and settling velocity: Jour. Sed. Petrology, v. 41, p.7-18.

GILBERT, G.K., 1914, The transportation of debris by running water: U.S. Geol. Surv. Prof. Paper 86, 263pp.

GRIFFITHS, J.C., 1967, Scientific method in analysis of sediments: McGraw Hill Co., N.Y., 508pp.

GUSTAVSON, T.C., 1974, Sedimentation of gravel outwash fans, Malaspina Glacier foreland, Alaska: Jour. Sed. Petrology, v. 44, p.374-389.

HAND, B.M., 1969, Antidunes as trochoidal waves: Jour. Sed. Petrology, v. 39, p.1302-1309.

_____, WESSELL, J.M. & HAYES, M.O., 1969, Antidunes in the Mount Toby Conglomerate (Triassic), Massachusetts: Jour. Sed. Petrology, v. 39, p.1310-1316.

HARMS, J.C. & FAHNESTOCK, R.K., 1965, Stratification, bed-forms, and flow phenomena (with an example from the Rio Grande): S.E.P.M. Spec. Pub. No. 12, p.84-115.

HELLEY, E.J., 1969, Field measurement of the initiation of large particle motion in Blue Creek, near Klamath, California: U.S. Geo. Surv. Prof. Paper 562-G, 19pp.

HENDRY, J.E., 1976, The orientation of discoidal clasts in resedimented conglomerates, Cambro-Ordovician, Gaspe, eastern Quebec: Jour. Sed. Petrology, v. 46, p.48-55.

HICKIN, E.J., 1972, Pseudo-meanders and point dunes - a flume study: Amer. Jour. Sci., v. 272, p.762-799.

HJULSTROM, F., 1935, Studies of the morphological activity of rivers as illustrated by the River Fyris: Geol. Instit. Univ. Uppsala Bull., v. 25, p.221-527.

_____, 1939, Transportation of detritus by moving water: in 'Recent Marine Sediments', ed. P.O. Trask, Amer. Assoc. Petrol. Geol., p.5-31.

IMBRIE, J., 1956, Biometrical methods in the study of invertegrate fossils: Amer. Mus. Nat. Hist. Bull., v. 108, p.211-252.

JAMIESON, T.F., 1860, On the Drift and rolled gravel on the North of Scotland: Quart. Jour. Geol. Soc., v. 16, p.347-371.

JOHANSSON, C.E., 1963, Orientation of pebbles in running water. A laboratory study: Geog. Annaler, v. 45, p.85-112.

_____, 1965, Structural studies of sedimentary deposits: Geol. Fören. Stockholm Förh., v.87, p.3-61.

JOHNSTON, W.A., 1922, Imbricated structure in river gravels: Amer. Jour. Sci., v. 4, p.387-390.

JOPLING, A.V., & WALKER, R.G., 1968, Morphology and origin of ripple-drift cross-lamination, with examples from the Pleistocene of Massachusetts: Jour. Sed. Petrology, v. 36, p.971-984.

KALINSKE, A.A., 1942, Discussion of 'Settling-velocity and flume-behaviour of non-spherical particles' by W.C. Krumbein: Amer. Geophys. Union, Pt. 2, p.623-633.

KARCZ, I., 1968, Fluviatile obstacle marks from the wadis of the Negev (southern Israel): Jour. Sed. Petrology, v. 38, p.1000-1012.

_____, 1973, Reflections on the origin of small-scale longitudinal stream-bed scours: in 'Fluvial Geomorphology', ed. M. Morisawa, Pub. in Geomorph., State Univ. N.Y., Binghamton, N.Y., p.149-171.

KATZUNG, G., 1971, Zur fluviatilen gerolleinregelung (English summary): Zeitshrift fur angewadte geol, v. 17, p.39-47.

KELLING, G., & WILLIAMS, P.F., 1967, Flume studies of the orientation of pebbles and shells: Jour. Geol., v. 75, p.243-267.

KENNEDY, J.F., 1961, Stationary waves and antidunes in alluvial channels: W.M. Keck Lab. Hydraul. & Water Res., Calif. Inst. Tech. Rep. KH-R-2, 146pp.

_____, 1963, Mechanics of dunes and antidunes in erodible bed channels: Jour. Fluid Mechanics, v. 16, p.531-544.

KOSTER, E.H., 1974, Flume studies of isolate gravel fabric: Geol. Surv. Canada Rep. Activities, Apr.-Oct. 1973, G.S.C. Paper 74-1, p.95-97.

KRUMBEIN, W.C., 1939, Preferred orientation of pebbles in sedimentary deposits: Jour. Geol., v. 47, p.673-706.

_____, 1940, Flood gravel of San Gabriel Canyon, California: Geol Soc. Amer. Bull., v. 51, p.639-676.

_____, 1941a, Measurement and geological significance of shape and roundness of sedimentary particles: Jour. Sed. Petrology, v. 11, p.64-72.

_____, 1941b, The effects of abrasion on the size, shape and roundness of rock particles: Jour. Geol., v. 49, p.482-520.

_____, 1942, Settling-velocity and flume-behaviour of non-spherical particles: Amer. Geophys. Union Trans, v. 23, p.621-632.

_____, 1968, Statistical methods in sedimentology: Sedimentology, v. 10, p.7-23.

KUENEN, Ph.D., 1956, Experimental abrasion of pebbles, 1. Rolling by current: Jour. Geol., v. 64, p.336-368.

LAMING, D.J.C., 1966, Imbrication, paleocurrents and other sedimentary features of Lower New Red Sandstone, Devonshire, England: Jour. Sed. Petrology, v. 36, p.940-959.

LANE, E.W., & CARLSON, E.J., 1954, Some observations on the effect of particle shape on the movement of coarse sediments: Amer. Geophys. Union Trans., v. 35, p.453-462.

LANGBEIN, W.B., 1942, Hydraulic criteria for sand waves: Amer. Geophys. Union Trans., v. 23, p.615-618.

_____ & LEOPOLD, L.B., 1964, Quasi-equilibrium states in channel morphology: Amer. Jour. Sci., v. 262, p.782-794.

_____, 1968, River channel bars and dunes - Theory of kinematic waves: U.S. Geol. Surv. Prof. Paper 422-L, 20pp.

LARONNE, J.B., & CARSON, M.A., 1976, Interrelationships between bed morphology and bed-material transport for a small, gravel bed channel: Sedimentology, v. 23, p.67-86.

LEOPOLD, L.B. WOLMAN, M.G., & MILLER, J.P., 1964, Fluvial processes in geomorphology; W.H. Freeman & Co., San Francisco, 522pp.

LIGHTHILL, M.J., & WHITHAM, G.B., 1955, On kinematic waves - 1. Flood movement in long rivers: Proc. Royal Soc. London, v. 229, Ser. A, p.281-316.

MALDE, H., 1968, The catastrophic Late Pleistocene Bonneville flood in the Snake River plain, Idaho: U.S. Geol. Surv. Prof. Paper 596, 12pp.

MARTINI, I.P., & OSTLER, J., 1973, Ostler lenses - possible environmental indicators in fluvial gravels and conglomerates: Jour. Sed. Petrology, v. 43, p.418-422.

MATTHES, H.A., 1947, Macroturbulence in natural streamflow: Amer. Geophys. Union, v. 28, pt. 2, p.255-262.

McDONALD, B.C., 1972, The Geological Survey of Canada sedimentation flume; Geol. Sur. Canada Paper 71-46, pp.

_____ & BANERJEE, I., 1971, Sediments and bedforms on a braided outwash plain: Can. Jour. Earth Sci., v. 8, p.1282-1301.

_____ & LEWIS, C.P., 1973, Geomorphic and sedimentological processes of rivers and coasts, Yukon Coastal Plain: Environment-Social Committee, Northern Pipelines Task Force on Northern Oil Devel., Rep. No.73-39, 245pp.

MELAND, N., & NORRMAN, J.O, 1966, Transport velocities of single particles in bed-load motion: Geogr. Annal., v. 48, Ser. A, p.165-182.

_____, 1969, Transport velocities of individual size fractions in heterogenous bedload: Geogr. Annal., v. 51, Ser. A., p.127-144.

MEYER-PETER, E., & MÜLLER, R., 1948, Formula for bed-load transport: Int. Assoc. Hydraulic Structures Research, Stockholm, v. 3, p.39-65.

MIALL, A.D., 1974, Paleocurrent analysis of alluvial sediments: a discussion of directional variance and vector-magnitude: Jour. Sed. Petrology, v. 44, p.1174-1185.

MIDDLETON, G.V., 1965, Antidune cross-bedding in a large flume: Jour. Sed. Petrology, v. 35, p.922-927.

NEVIN, C., 1946, Competency of moving water to transport debris: Geol. Soc. Amer. Bull., v. 57, p.651-674.

NORDIN, C.F., 1964, Aspects of flow resistance and sediment transport, Rio Grande near Bernalillo, New Mexico: U.S. Geol. Surv. Prof. Paper 1498-H, 41pp.

NOVAK, I.D., 1973, Predicting coarse sediment transport: the Hjulstrom curve revisited: in 'Fluvial Geomorphology', ed. M. Morisawa, Pub. in Geomorph., State Univ. N.Y., Binghamton, p.13-25.

ØSTREM, G. 1975, Sediment transport in glacial meltwater streams: S.E.P.M. Spec. Pub. No. 23, p.101-122.

PEABODY, F.E., 1947, Current crescents in the Triassic Moenkopi Formation: Jour. Sed. Petrology, v. 17, p.73-76.

POTTER, P.E., & PETTIJOHN, F.J., 1963, Paleocurrents and basin analysis: Springer-Verlag, N.Y., 296pp.

PURCELL, E.J., 1965, Calculus with analytic geometry: Appleton-Century-Crofts, Div. Meredith Pub. Co., N.Y., 843pp.

REYNOLDS, A.J., 1965, Waves on the erodible bed of an alluvial channel: Jour. Fluid Mechanics, v. 22, p.113-133.

RICHARDSON, E.V., SIMONS, D.M., & POSAKONY, G.J., 1961, Sonic depth sounder for laboratory and field use: U.S. Geol. Surv. Circular 450, 7pp.

RICHARDSON, P.D., 1968, The generation of scour marks near obstacles: Jour. Sed. Petrology, v. 38, p.965-970.

RICHTER, K., 1936, Ergebnisse und aussichten der gerufeforschung im pommerschen diluvium: Geol. Rundschau, v. 27, p.196-206.

ROUSE, H., 1950, Engineering Hydraulics: John Wiley, New York, 1039pp.

RUBEY, W.W., 1933, Settling velocities of gravel, sand and silt: Amer. Jour. Sci., v. 25, p.325-338.

RUST, B.R., 1972a, Pebble orientation in fluvial sediments: Jour. Sed. Petrology, v. 42, p.384-388.

_____, 1972b, Structure and process in a braided river: Sedimentology, v. 18, p.221-245.

_____, 1975, Fabric and structure in glaciofluvial gravels: S.E.P.M. Spec. Pub. No. 23, p.238-248.

SAMES, C.W., 1966, Morphometric data of some recent pebble associations and their application to ancient deposits: Jour. Sed. Petrology, v. 34, p.73-83.

SEDIMENTARY PETROLOGY SEMINAR, 1965, Gravel fabric in Wolf Run: Sedimentology, v. 4, p.273-283.

SENGUPTA, S., 1966, Studies on orientation and imbrication of pebbles with respect to cross-stratification: Jour. Sed. Petrology, v. 30, p.302-309.

SHAPIRO, A.H., 1961, Shape and Flow: the fluid dynamics of drag: Anchor Books, Doubleday & Co. Inc., N.Y., 186pp.

SIMONS, D.B., & RICHARDSON, E.V., 1962, The effect of bed roughness on depth-discharge relations in alluvial channels: U.S. Geol. Surv. Water Supply Paper 1498-E, 26pp.

SNEED, E.D., & FOLK, R.L. 1958, Pebbles in the Lower Colorado River, Texas - a study in particle morphogenesis: Jour. Geol., v. 66, p.114-150.

SOKAL, R.R., 1965, Statistical methods in Systematics: Biol. Revue, v. 40, p.337-391.

SOUTHARD, J.B., 1975, Bed configurations: Chap. 2 in 'Depositional environments as interpreted from primary sedimentary structures and stratification sequences', S.E.P.M. Short Course No. 2, Dallas, 1975.

STEEL, R.J., 1974, New Red Sandstone floodplain and piedmont sedimentation in the Hebridean Province, Scotland: Jour. Sed. Petrology, v. 44, p.336-357.

TEISSEYRE, A.K., 1976, Pebble fabric in braided stream deposits with examples from recent and "frozen" Carboniferous channels (Intrasudetic Basin, Central Sudetes): Geol. Sudetica, v. 10, nr. 1, p.7-56.

TWENHOFEL, W.H., 1932, Treatise on sedimentation: 2nd. ed., Baltimore, Williams and Wilkins, 926pp.

UNRUG, R., 1957, Recent transport and sedimentation of gravels in the Dunajec Valley (Western Carpathians): Acta Geol. Polonica, v. 7, p.217-257.

WADELL, H., 1932, Volume, shape and roundness of rock particles: Jour. Geol., v. 40, p.443-451.

WALKER, R.G., 1975, Conglomerates: sedimentary structures and facies models: Chap. 7 in 'Depositional environments as interpreted from primary sedimentary structures and stratification sequences', S.E.P.M. Short Course No. 2, Dallas, 1975.

WALPOLE, R.E., 1968, Introduction to statistics: MacMillan Co./Collier-MacMillan London Ltd., 365pp.

WHITE, C.M., 1940, The equilibrium of grains on the bed of a stream: Roy. Soc. London, Proc., Ser. A., v. 174, p.332-328.

WHITE, W.S., 1952, Imbrication and initial dip in a Keweenawan conglomerate bed: Jour. Sed. Petrology, v. 22, p.189-199.

WILLIAMS, E.M., 1965, A method of indicating pebble shape with one parameter: Jour. Sed. Petrology, v. 35, p.993-996.

WILLIAMS, P.F., & RUST, B.R., 1969, The sedimentology of a braided river: Jour. Sed. Petrology, v. 39, p.649-679.

WOLMAN, M.G., & BRUSH, L.M., 1961, Factors controlling the size and shape of stream channels in coarse non-cohesive sands: U.S. Geol. Surv. Prof. Paper 282-G, 28pp.

YANG, C.T., 1973, Incipient motion and sediment transport: A.S.C.E., Jour. Hydraul. Div., v. 99, Proc. Paper 10067, p.1679-1704.

ZINGG, T., 1935, Beitrage zur schotteranalyse: Schweiz. min. pet. Mitt., v. 15, p.39-140.

8.0 APPENDICES

8.1 Projection area of ellipsoidal clasts

8.11 Development of equations for calculation of the area projected by symmetric triaxial ellipsoids

References: Purcell (1965), and Crowell and Slesnick (1968). The mathematic theory is presented in three sections.

8.111 Long axis aligned normal to flow: the effect of imbrication

Before imbrication develops, the ellipsoid is in standard position (i.e. its axes are coincident with those of the flow) and is given by the equation

$$S.x'^2 + T.y'^2 = 1 \qquad \ldots\ldots\ldots(1)$$

where $S = \frac{4}{b^2}$ and $T = \frac{4}{c^2}$.

For an imbricated configuration, the axial reference frame of the ellipsoid rotates in the vertical plane about the origin of the flow axial reference frame to an acute angle αi. A point P on the perimeter of the rotated ellipse therefore has two sets of coordinates, (x,y) and (x', y') corresponding to the axial reference frames of the flow and ellipsoid respectively. They are inter-related by the parametric equations

$$x' = x.\cos\alpha + y.\sin\alpha \qquad \ldots\ldots\ldots(2)$$

$$y' = -x.\sin\alpha + y.\cos\alpha \qquad \ldots\ldots\ldots(3)$$

Substitution of equations 2 and 3 into equation 1 yields

$$S(x^2.\cos^2\alpha + 2.x.y.\sin\alpha.\cos\alpha + y^2.\sin^2\alpha) +$$
$$T(x^2.\sin^2\alpha - 2.x.y.\sin\alpha.\cos\alpha + y^2.\cos^2\alpha) = 1 \quad ....(4)$$

Equation 4 can be rearranged in the form

$$J.x^2 + K.x.y + L.y^2 = 1 \quad .....(5)$$

where $J = S.\cos^2\alpha + T.\sin^2\alpha$ .....(6)

$K = \sin 2\alpha.(S - T)$ .....(7)

$L = S.\sin^2\alpha + T.\cos^2\alpha$ .....(8)

To obtain the y-coordinates of the maximum point of the rotated ellipse, it is necessary to differentiate eq. 5 with respect to x as follows:

$$2.J.x + K.x\frac{dy}{dx} + K.y + 2.L.y\frac{dy}{dx} = 0 \quad .....(9)$$

Setting $\frac{dy}{dx} = 0$, eq. 9 becomes

$$2.J.x + K.y = 0 \text{ therefore } x = -\frac{K.y}{2.J} \quad .....(10)$$

Eq. 10 is then substituted into eq. 9 to give an equation for y:

$$Y = (L - \frac{K^2}{4.J})^{-0.5} \quad .....(11);$$

In the text, y-values are denoted by b' because in terms of absolute values, $c \leq b' \leq b$. The area of the projected ellipse is determined by the simple formula

$$A_p = \frac{\pi.a.b'}{2} \quad .....(12).$$

8.112 No imbrication: the effect of variable orientation

Before imbrication develops, the ellipsoid is in standard position and is given by the equation

$$R.x'^2 + S.y'^2 = 1 \qquad \text{.....(13)}$$

where $R = \frac{4}{a^2}$.

For an ellipsoid with its principal plane horizontal, the axial reference frame rotates in an horizontal plane so as to make an acute angle β_i with the axial reference frame of the flow.

Substitution of eqs. 2 and 3 into eq. 13 yields

$$R(x^2.\cos^2\beta + 2.x.y.\sin\beta.\cos\beta + y^2.\sin^2\beta) + S(x^2.\sin^2\beta - 2.x.y.\sin\beta.\cos\beta + y^2.\cos^2\beta) = 1 \qquad \text{....(14)}$$

Eq. 14 can be rearranged in the form

$$J_*.x^2 + K_*.x.y + L_*.y^2 = 1 \qquad \text{.....(15)}$$

where $J_* = R.\cos^2\beta + S.\sin^2\beta$ .....(16)

$K_* = \sin2\beta.(R - S)$ .....(17)

$L_* = R.\sin^2\beta + S.\cos^2\beta$ .....(18).

Tooobtain the x-coordinate of the maximum point of the rotated ellipse, it is necessary to differentiate eq. 15 with respect to y as follows:

$$2.J_*.x\frac{dx}{dy} + K_*.x + K_*.y\frac{dx}{dy} + 2.L_*.y = 0 \qquad \text{.....(19)}$$

Setting $\frac{dx}{dy} = 0$, eq. 19 becomes

$$K_* . x + 2 . L_* . y = 0,$$

therefore $$x = \frac{-K_* . x}{2 . L_*} \qquad \ldots\ldots\ldots(20)$$

Eq. 20 is then substituted into eq. 19 to give an equation for x:

$$x = \left(J_* - \frac{K_*^2}{4 . L_*}\right)^{-0.5} \qquad \ldots\ldots\ldots(21)$$

In the text, x-values are denoted a' because in terms of absolute values, $b \leq a' \leq a$. The area of the projected ellipse is determined by the simple formula

$$A_p = \frac{\pi . a' . b}{2} \qquad \ldots\ldots\ldots(22).$$

8.113 Variable imbrication: variable orientation

If the ellipsoidal axes are rotated in both the vertical and horizontal planes, eqs. 11 and 21 must be used jointly so that:

$$A_p = \pi . a' . b' \qquad \ldots\ldots\ldots(23).$$

8.12 Development of equations for calculation of the required angle of imbrication for projection of a given area by a triaxial symmetric ellipsoid

The mathematic theory is presented in two sections:

8.121 Long axis aligned normal to flow

Given A_p, the required y-value, i.e. b', is found by means of eq. 12.

Eq. 11 may be restated thus

$$\frac{1}{y^2} = L - \frac{K^2}{4.J} \qquad \ldots\ldots(24)$$

Multiplication of the numerator by (4.J) yields

$$\frac{4.J}{y^2} = 4.J.L - K^2 \qquad \ldots\ldots(25).$$

Eqs. 6, 7 and 8 are then substituted into eq. 25 to give

$$\frac{4(S.\cos^2\alpha + T.\sin^2\alpha)}{y^2} = 4(S.\cos^2\alpha + T.\sin^2\alpha)(S.\sin^2\alpha + T.\cos^2\alpha - 4.\sin^2\alpha.\cos^2\alpha.(S - T)^2 \qquad \ldots\ldots(26);$$

this equation can be restated in terms of $\sin\alpha$ by means of the Pythagorean identity, $\sin^2\alpha = 1 - \cos^2\alpha$, and simplified by dividing by 4. Thus eq. 6 leads to

$$\frac{S.(1 - \sin^2\alpha) + T.\sin^2\alpha}{y^2} = S.T.\sin^4\alpha + S.T.(1 - 2.\sin^2\alpha + \sin^4\alpha) + 2.S.T.\sin^2\alpha.(1 - \sin^2\alpha)$$

which reduces to

$$(T - S).\sin^2\alpha = S.T.y^2 - S$$

Therefore

$$\sin^2\alpha = \frac{S.T.y^2 - S}{T - S}$$

which therefore leads the formula

$$\alpha = \arcsin\left(\frac{S.T.y^2 - S}{T - S}\right)^{0.5} \qquad \ldots\ldots(27)$$

8.122 Long axis aligned parallel to flow

Given A_p, the required y-value, i.e. a', is found by means of eq. 22.

Using an exactly similar procedure to the one in the preceding section, it can be shown that for current-parallel orientation of the ellipsoid

$$\alpha = \arcsin\left(\frac{y^2.R.T - R}{T - R}\right)0.5 \qquad \ldots\ldots\ldots(28).$$

8.2 APL computer programmes written for stasticial analyses of the flume data

The programmes appear alphabetically as follows:-

ALPHA

BIVARIATEANALYSIS

EXPONENTIALREGRESSION

FOLKMUSIC

FULLIMBRIC

FULLLOGREG

HYDRAULIC

LOGREG

MULTREG

PARABOLA

SCAT

SEMICIRC

Each listing is preceded by a short explanatory note on the programme function.

```
PROGRAMME ***ALPHA*** COMPUTES THE REQUIRED ANGLE OF IMBRICATION TO PROJECT A GIVEN AREA FOR SYMMETRIC TRIAXIAL
ELLIPSOIDS WITH EQUAL NOMINAL DIAMETER UNDER CONDITIONS OF BOTH CURRENT-NORMAL AND CURRENT-PARALLEL ORIENTATION.

∇ ALPHA
[1] 'PRODUCT OF AXIAL DIMENSIONS'
[2] VOL←□
[3] 'ROWS OF DATA: A-AXIS, B-AXIS (CM.)'
[4] Y←□
[5] 'MATRIX DIMENSIONS OF DATA TABLE (ROWS × COLUMNS)'
[6] X←□
[7] 'AREA OF ELLIPSE TO BE PROJECTED (SQ. CM.)'
[8] AL←□
[9] U←X[1]⍴0
[10] UU←⍳X[1]
[11] W←X[1]⍴0
[12] WW←⍳X[1]
[13] H←X⍴Y
[14] ' '
[15] 'A-AXIS     B-AXIS     C-AXIS     COORDINATES FOR SPHERICITY-FORM DIAGRAM     IMBRIC. ANGLE     IMBRIC. ANGLE'
[16] '                                (C÷A)          [(A-B)÷(A-C)]          A-AXIS TRANSVERSE     A-AXIS PARALLEL'
[17] '*************************************************************************************************************
*'
[18] C1←0
[19] B1:C1←C1+1
[20] A←H[C1;1]
[21] B←H[C1;2]
[22] C←(VOL÷(H[C1;1]×H[C1;2]))
[23] DUH←(C÷A)
[24] DUHHY←((A-B)÷(A-C))
[25] R←(A÷2)*¯2
[26] S←(B÷2)*¯2
[27] T←(C÷2)*¯2
[28] YVAL←((2×AL)÷(A×3.14159))
[29] YYVAL←((2×AL)÷(B×3.14159))
[30] SIN1←((((YVAL*2)×S×T)-S)÷(T-S))*.5
[31] TEST1←SIN1≥1
[32] →(TEST1=0)/35
[33] SINONE←90
[34] →36
[35] SINONE←(¯1○SIN1)×57.29583
[36] SIN2←((((YYVAL*2)×R×T)-R)÷(T-R))*.5
[37] TEST2←SIN2≥1
[38] →(TEST2=0)/41
[39] SINTWO←90
[40] →43
[41] SINTWO←(¯1○SIN2)×57.29583
[42] U[C1]←SINONE
[43] SUMONE←+/U
[44] MEANONE←SUMONE÷X[1]
[45] SDONE←((+/((SINONE-MEANONE)*2))÷(X[1]))*.5)
[46] W[C1]←SINTWO
[47] SUMTWO←+/W
[48] MEANTWO←SUMTWO÷X[1]
[49] SDTWO←(((+/((SINTWO-MEANTWO)*2))÷(X[1]))*.5)
[50] ' ';A';'     '¦B¦'     '¦C¦'     '¦DUH¦'     '¦DUHHY¦'     '¦SINONE¦'     '¦SINTWO
[51] →(C1<X[1])/B1
[52] ' '
[53] 'FOR IMBRICATION, A-AXES TRANSVERSE TO FLOW:'     '¦MEANONE
[54] ⍞←'MEAN ALPHA     '¦SDONE
[55] ⍞←'STANDARD DEVIATION'
[56] 'FOR IMBRICATION, A-AXES PARALLEL TO FLOW:'     '¦MEANTWO
[57] ⍞←'MEAN ALPHA     '¦SDTWO
[58] ⍞←'STANDARD DEVIATION
```

PROGRAMME ***BIVARIATEANALYSIS*** COMPUTES THE PARAMETERS FOR A LINEAR BIVARIATE SCATTER, INCLUDING
THE LEAST-SQUARES REGRESSION EQUATION, CORRELATION COEFFICIENT AND CONFIDENCE LIMITS FOR THE Y-PREDICTION.

```
∇ BIVARIATEANALYSIS
[1] 'VECTOR OF XY PAIRS'
[2] V←⍞
[3] 'MATRIX DIMENSIONS OF DATA TABLE (ROWS × COLUMNS)'
[4] DIM←⍞
[5] 'TYPE T VALUE GIVEN COORDINATES (ALPHA=0.025;NO-2 D.F.)'
[6] TALPHA←⍞
[7] M←DIM⍴V
[8] NO←(⍴V)÷2
[9] SUMX←+/M[;1]
[10] SUMY←+/M[;2]
[11] SUMXY←+/M[;1]×M[;2]
[12] SUMXSQ←+/M[;1]*2
[13] SUMYSQ←+/M[;2]*2
[14] MEANX←SUMX÷NO
[15] MEANY←SUMY÷NO
[16] B←(((NO×SUMXY)-(SUMX×SUMY))÷((NO×SUMXSQ)-((SUMX)*2)))
[17] A←MEANY-(B×MEANY)
[18] R←((NO×SUMXY)-(SUMX×SUMY))÷((((NO×SUMXSQ)-((SUMX)*2))×((NO×SUMYSQ)-((SUMY)*2)))*.5)
[19] SXSQ←(((NO×SUMXSQ)-(SUMX*2))÷(NO×(NO-1)))
[20] SX←SXSQ*.5
[21] SYSQ←(((NO×SUMYSQ)-(SUMY*2))÷(NO×(NO-1)))
[22] SY←SYSQ*.5
[23] K←B*2
[24] J←((NO-1)×(SYSQ-(SXSQ×K)))
[25] SSQ←J÷(NO-2)
[26] S←SSQ*.5
[27] LCLALPHA←(A-(((TALPHA×S)×(SUMXSQ*.5))÷(SX×((NO×(NO-1))*.5))))
[28] UCLALPHA←(A+(((TALPHA×S)×(SUMXSQ*.5))÷(SX×((NO×(NO-1))*.5))))
[29] SSE←((NO-1)×(SYSQ-(SXSQ×(B*2))))
[30] T←((R×((NO-2)*.5))÷((1-(R*2))*.5))
[31] ' '
[32] ⍞←'SAMPLE SIZE                    ';NO
[33] ⍞←'MEAN OF X VALUES               ';MEANX
[34] ⍞←'MEAN OF Y VALUES               ';MEANY
[35] ' '
[36] 'REGRESSION EQUATION HAS THE FORM  Y = A + B(X) WHERE:-'
[37] ⍞←'INTERCEPT, A                   ';A
[38] ⍞←'COEFFICIENT, B                 ';B
[39] ⍞←'CORRELATION COEFFICIENT        ';R
[40] ⍞←'SUM SQUARE RESIDUAL ERRORS     ';SSE
[41] ⍞←'STUDENTS T-VALUE               ';T
[42] 'CONFIDENCE LIMITS FOR Y ESTIMATE'
[43] ⍞←'Y-INTERCEPT FOR UPPER LINE     ';UCLALPHA
[44] ⍞←'Y-INTERCEPT FOR LOWER LINE     ';LCLALPHA
∇
```

PROGRAMME ***EXPONENTIALREGRESSION*** COMPUTES THE PARAMETERS FOR A LINEAR (X) - LOG (Y) BIVARIATE SCATTER, INCLUDING THE LEAST-SQUARES REGRESSION LINE, CORRELATION COEFFICIENT AND ITS SIGNIFICANCE.

```
∇ EXPONENTIALREGRESSION
[1] 'VECTOR OF XY PAIRS'
[2] V←⍞
[3] 'MATRIX DIMENSIONS OF DATA TABLE (ROWS ×COLUMNS)'
[4] DIM←⍞
[5] NO←(⍴V)÷2
[6] M←DIM⍴V
[7] SUMX←+/M[ ;1]
[8] SUMLOGY←+/10⍟M[ ;2]
[9] SUMXLOGY←+/(M[ ;1]×(10⍟M[ ;2]))
[10] SUMXSQ←+/M[ ;1]*2
[11] SUMLOGYSQ←+/((10⍟M[ ;2])*2)
[12] MEANX←SUMX÷NO
[13] MEANLOGY←SUMLOGY÷NO
[14] B←(((NO×SUMLOGY)-(SUMX×SUMLOGY))÷((NO×SUMXSQ)-((SUMX)*2)))
[15] D←10*B
[16] A←MEANLOGY-(B×MEANX)
[17] C←10*A
[18] R←((NO×SUMXLOGY)-(SUMX×SUMLOGY))÷((((NO×SUMXSQ)-((SUMX)*2))×((NO×SUMLOGYSQ)-((SUMLOGY)*2)))*.5)
[19] T←((R×((NO-2)*.5))÷((1-(R*2))*.5))
[20] ' '
[21] ⍞←'SAMPLE SIZE                    ';NO
[22] ⍞←'MEAN OF X VALUES               ';MEANX
[23] ⍞←'MEAN OF Y VALUES               ';10*MEANLOGY
[24] ' '
[25] 'REGRESSION EQUATION HAS THE FORM Y = C(D*X) WHERE:-'
[26] ⍞←'Y-AXIS INTERCEPT WHEN X=0, C   ';C
[27] ⍞←'COEFFICIENT RAISED TO POWER X  ';D
[28] ⍞←'CORRELATION COEFFICIENT        ';R
[29] ⍞←'STUDENTS T-VALUE               ';T
∇
```

PROGRAMME ***POLKMUSIC*** COMPUTES VALUES OF MAXIMUM PROJECTION SPHERICITY (SNEED AND FOLK, 1958)
AND OBLATE-PROLATE INDEX (DOBKINS AND FOLK, 1970) FOR A CLAST POPULATION GIVEN THEIR TRIAXIAL DIMENSIONS

```
∇ POLKMUSIC
 [1] 'VECTOR OF DATA - CLAST NUMBER/A-AXIS/B-AXIS/C-AXIS'
 [2] V←⍞
 [3] 'MATRIX DIMENSIONS OF DATA TABLE (ROWS ×COLUMNS)'
 [4] X←⍞
 [5] U←X[1]⍴0
 [6] SEX←⍉X[1]
 [7] W←X[1]⍴0
 [8] WEX←⍉X[1]
 [9] N←X⍴V
 [10] ' '
 [11] ' '
 [12] 'CLAST NO:          MAX. PROJ. SPHERICITY          OBLATE-PROLATE INDEX'
 [13] '*********************************************************************'
 [14] ' '
 [15] C1←0
 [16] B1:C1←C1+1
 [17] A←N[C1;2]
 [18] B←N[C1;3]
 [19] C←N[C1;4]
 [20] FS←((C*2)÷(A×B))
 [21] S←FS*.333333
 [22] OP←(((((A-B)÷(A-C))-.5)÷(C÷A))×10)
 [23] U[C1]←S
 [24] SUMS←+/U
 [25] MEANS←SUMS÷X[1]
 [26] SDS←(((+/((S-MEANS)*2))÷(X[1]))*0.5)
 [27] W[C1]←OP
 [28] SUMOP←+/W
 [29] MEANOP←SUMOP÷X[1]
 [30] SDOP←(((+/((W-MEANOP)*2))÷(X[1]))*0.5)
 [31] '  ';N[C1;1];'                    ';S;'          ';OP
 [32] →(C1<X[1])/B1
 [33] ' '
 [34] ⍞←'MEAN SPHERICITY      ';MEANS
 [35] ⍞←'STANDARD DEV     ';SDS
 [36] ' '
 [37] ⍞←'MEAN O-P INDEX   ';MEANOP
 [38] ⍞←'STANDARD DEV     ';SDOP
∇
```

```
PROGRAMME ***FULLIMBRIC*** COMPUTES THE AREA PROJECTED BY A SYMMETRIC TRIAXIAL ELLIPSOID
GIVEN THE ANGLE OF IMBRICATION AND THE DEVIATION OF THE LONG AXIS FROM CURRENT-NORMAL ORIENTATION.

∇ FULLIMBRIC
[1] 'RUN NUMBER'
[2] NO←⎕
[3] 'ROWS OF DATA:  CLAST NO. / A-AXIS / B-AXIS / C-AXIS / ALPHA / BETA '
[4] V←⎕
[5] 'MATRIX DIMENSIONS OF DATA TABLE'
[6] X←⎕
[7] N←X⍴V
[8] ' '
[9] ' '
[10] '     CLAST NUMBER:          ALPHA              BETA (AZIMUTH              ELLIPTICAL AREA'
                                  (A-B DIP):         DEVIATION OF A-AXIS):      PROJECTED (CM.*2):'
[11] '
[12] '*****************************************************************************************'
[13] ' '
[14] C1←0
[15] B1:C1←C1+1
[16] A←N[C1;2]
[17] B←N[C1;3]
[18] C←N[C1;4]
[19] ALPHA←N[C1;5]
[20] BETA←N[C1;6]
[21] R←(1÷((A÷2)*2))
[22] S←(1÷((B÷2)*2))
[23] T←(1÷((C÷2)*2))
[24] RAD←(ALPHA×○1)÷180
[25] RADIAN←(BETA×○1)÷180
[26] J←((S×((2○RAD)*2))+(T×((1○RAD)*2)))
[27] K←((S-T)×(1○(2×RAD)))
[28] L←((S×((1○RAD)*2))+(T×((2○RAD)*2)))
[29] YVALUE←((1÷(L-((K*2)+(4×J))))*.5)
[30] JJ←((R×((2○RADIAN)*2))+(S×((1○RADIAN)*2)))
[31] KK←((R-S)×(1○(2×RADIAN)))
[32] LL←((R×((1○RADIAN)*2))+(S×((2○RADIAN)*2)))
[33] XVALUE←((1÷(JJ-((KK*2)+(4×LL))))*.5)
[34] PA←(3.141593×YVALUE×XVALUE)
[35] '          ',N[C1;1];'          ';N[C1;5];'          ';N[C1;6];'          ';PA
[36] →(C1<X[1])/B1
∇
```

```
PROGRAMME ***FULLLOGREG*** COMPUTES THE PARAMETERS FOR A LOG - LOG BIVARIATE SCATTER, INCLUDING
THE LEAST SQUARES REGRESSION LINE, CORRELATION COEFFICIENT AND ITS SIGNIFICANCE.

∇ FULLLOGREGRESSION
 [1] 'VECTOR OF XY PAIRS'
 [2] V←⍞
 [3] 'MATRIX DIMENSIONS OF DATA TABLE (ROWS × COLUMNS)'
 [4] DIM←⍞
 [5] NO←(⍴V)÷2
 [6] N←DIM⍴V
 [7] SUMLOGX←+/10⍟N[ ;1]
 [8] SUMX←+/N[ ;1]
 [9] SUMLOGY←+/10⍟N[ ;2]
[10] SUMY←+/N[ ;2]
[11] SUMLOGXLOGY←+/((10⍟N[ ;1])×(10⍟N[ ;2]))
[12] SUMXY←+/N[ ;1]×N[ ;2]
[13] SUMLOGXSQ←+/((10⍟N[ ;1])*2)
[14] SUMXSQ←+/N[ ;1]*2
[15] SUMLOGYSQ←+/((10⍟N[ ;2])*2)
[16] SUMYSQ←+/N[ ;2]*2
[17] MEANX←SUMX÷NO
[18] MEANY←SUMY÷NO
[19] J←SUMLOGX*2
[20] LOGC←(((SUMLOGY×SUMLOGXSQ)-(SUMLOGX×SUMLOGXLOGY))÷((NO×SUMLOGXSQ)-J))
[21] D←(((NO×SUMLOGXLOGY)-(SUMLOGX×SUMLOGY))÷((NO×SUMLOGXSQ)-((SUMLOGX)*2))×((NO×SUMLOGYSQ)-((SUMLOGY)*2)))*.5)
[22] R←((NO×SUMLOGXLOGY)-(SUMLOGX×SUMLOGY))÷((((NO×SUMLOGXSQ)-((SUMLOGX)*2))×((NO×SUMLOGYSQ)-((SUMLOGY)*2)))*.5)
[23] C←10*LOGC
[24] T←((R×((NO-2)*.5))÷((1-(R*2))*.5))
[25] ' '
[26] ⍞←'MEAN OF X VALUES          ';MEANX
[27] ⍞←'MEAN OF Y VALUES          ';MEANY
[28] ⍞←'SAMPLE SIZE               ';NO
[29] ' '
[30] 'REGRESSION EQUATION HAS THE FORM  Y = C(X*D), WHERE THE COEFFICIENT C IS THE Y-VALUE WHEN X=1 AND'
[31] 'WHERE THE EXPONENT D IS THE SLOPE OF THE LINE, I.E. ARCTAN OF THE ANGLE:-'
[32] ⍞←'COEFFICIENT, C            ';C
[33] ⍞←'EXPONENT, D               ';D
[34] ⍞←'CORRELATION COEFFICIENT   ';R
[35] ⍞←'STUDENTS T-VALUE          ';T
∇
```

PROGRAMME ***HYDRAULIC*** COMPUTES THE VALUES OF CERTAIN FLOW VARIABLES
FROM MEASURED FLOW VARIABLES FOR EACH FLUME RUN.

```
∇ HYDRAULIC
 [1] 'FLUME RUN NUMBER:'
 [2] RUN←⍞
 [3] ' '
 [4] 'MEASURED DISCHARGE (LITRES/SEC):'
 [5] Q←⍞
 [6] 'MEASURED MEAN DEPTH (CM):'
 [7] Y←⍞
 [8] 'MEASURED SLOPE (METRE/METRE):'
 [9] S←⍞
 [10] ' '
 [11] MFV←(1000×Q)÷(76.68×Y)
 [12] MSV←(980.6×Y×S)*.5
 [13] MBST←MSV*2
 [14] FR←(MFV÷((980.6×Y)*.5))
 [15] RE←(MFV×Y)÷.01003
 [16] MAN←((Y*.66666)×(S*.5))÷MFV
 [17] ' '
 [18] 'CALCULATED FLOW VARIABLES:'
 [19] ⍞←'MEAN FLOW VELOCITY (CM/SEC)          ';MFV
 [20] ⍞←'MEAN SHEAR VELOCITY (CM/SEC)         ';MSV
 [21] ⍞←'MEAN BED SHEAR STRESS (DYNES/CM*2)   ';MBST
 [22] ⍞←'FROUDE NUMBER                        ';FR
 [23] ⍞←'REYNOLDS NUMBER                      ';RE
 [24] ⍞←'MANNING ROUGHNESS COEFFICIENT        ';MAN
∇
```

PROGRAMME ***LOGREG*** COMPUTES THE PARAMETERS FOR A LOG (X) - LINEAR (Y) BIVARIATE SCATTER, INCLUDING THE LEAST-SQUARES REGRESSION EQUATION, CORRELATION COEFFICIENT AND ITS SIGNIFICANCE.

```
∇ LOGREG
 [1] 'VECTOR OF XY PAIRS'
 [2] V←⍞
 [3] 'MATRIX DIMENSIONS OF DATA TABLE (ROWS × COLUMNS)'
 [4] DIM←⍞
 [5] M←DIM⍴V
 [6] NO←(⍴V)÷2
 [7] SUMX←+/M[ ;1]
 [8] MEANX←SUMX÷NO
 [9] SUMY←+/M[ ;2]
 [10] MEANY←SUMY÷NO
 [11] SUMLOGX←+/10⍟M[ ;1]
 [12] MEANLOGX←SUMLOGX÷NO
 [13] SUMYLOGX←+/(M[ ;2]×(10⍟M[ ;1]))
 [14] SUMLOGXSQ←+/((10⍟M[ ;1])*2)
 [15] SUMYSQ←+/M[ ;2]*2
 [16] B←((SUMYLOGX-(NO×MEANY×MEANLOGX))÷(SUMLOGXSQ-(NO×(MEANLOGX*2))))
 [17] A←MEANY-(B×MEANLOGX)
 [18] R←((NO×SUMYLOGX)-(SUMLOGX×SUMY))÷((((NO×SUMLOGXSQ)-((SUMLOGX)*2))×((NO×SUMYSQ)-((SUMY)*2)))*.5)
 [19] T←((R×((NO-2)*.5))÷((1-(R*2))*.5))
 [20] ' '
 [21] ⍞←'SAMPLE SIZE                    ';NO
 [22] ⍞←'MEAN OF X VALUES               ';MEANX
 [23] ⍞←'MEAN OF Y VALUES               ';MEANY
 [24] ' '
 [25] 'REGRESSION EQUATION OF THE FORM  Y = A + B(LOGX), WHERE:-'
 [26] ⍞←'Y-AXIS INTERCEPT, A            ';A
 [27] ⍞←'COEFFICIENT, B                 ';B
 [28] ⍞←'CORRELATION COEFFICIENT        ';R
 [29] ⍞←'STUDENTS T-VALUE               ';T
∇
```

PROGRAMME ***MULTREG*** COMPUTES THE VALUES REQUIRED FOR SOLVING SIMULTANEOUS EQUATIONS FOR A MULTIVARIATE ANALYSIS INVOLVING THREE INDEPENDENT VARIABLES ACCORDING TO THE METHOD OF EZEKIEL AND FOX (1959).

```
∇ MULTREG
[1] 'ROWS OF DATA:  X1 (DEPENDENT VARIABLE) AND X2, X3, X4 (INDEPENDENT VARIABLES)'
[2] DATA←⍞
[3] 'MATRIX DIMENSIONS (ROWS × COLUMNS)'
[4] V←⍞
[5] N←⊃V
[6] M←⊃⌽V
[7] SUMX1←+/M[;1]
[8] SUMX2←+/M[;2]
[9] SUMX3←+/M[;3]
[10] SUMX4←+/M[;4]
[11] SUMX2SQ←+/M[;2]*2
[12] SUMX2X3←+/M[;2]×M[;3]
[13] SUMX1X2←+/M[;1]×M[;2]
[14] SUMX3SQ←+/M[;3]*2
[15] SUMX1X3←+/M[;1]×M[;3]
[16] SUMX1SQ←+/M[;1]*2
[17] SUMX2X4←+/M[;2]×M[;4]
[18] SUMX3X4←+/M[;3]×M[;4]
[19] SUMX1X4←+/M[;1]×M[;4]
[20] SUMX4SQ←+/M[;4]*2
[21] MEANX1←SUMX1÷N
[22] MEANX2←SUMX2÷N
[23] MEANX3←SUMX3÷N
[24] MEANX4←SUMX4÷N
[25] JITX2SQ←N×(MEANX2*2)
[26] JITX2X3←N×MEANX2×MEANX3
[27] JITX1X2←N×MEANX1×MEANX2
[28] JITX3SQ←N×(MEANX3*2)
[29] JITX1X3←N×MEANX1×MEANX3
[30] JITX1SQ←N×(MEANX1*2)
[31] JITX2X4←N×MEANX2×MEANX4
[32] JITX3X4←N×MEANX3×MEANX4
[33] JITX1X4←N×MEANX1×MEANX4
[34] JITX4SQ←N×(MEANX4*2)
[35] ' '
[36] ' '
[37] ⍞←'ADX2SQ          ';SUMX2SQ-JITX2SQ
[38] ⍞←'ADX2X3          ';SUMX2X3-JITX2X3
[39] ⍞←'ADX1X2          ';SUMX1X2-JITX1X2
[40] ⍞←'ADX3SQ          ';SUMX3SQ-JITX3SQ
[41] ⍞←'ADX1X3          ';SUMX1X3-JITX1X3
[42] ⍞←'ADX1SQ          ';SUMX1SQ-JITX1SQ
[43] ⍞←'ADX2X4          ';SUMX2X4-JITX2X4
[44] ⍞←'ADX3X4          ';SUMX3X4-JITX3X4
[45] ⍞←'ADX1X4          ';SUMX1X4-JITX1X4
[46] ⍞←'ADX4SQ          ';SUMX4SQ-JITX4SQ
[47] ' '
[48] ⍞←'MEANX1          ';MEANX1
[49] ⍞←'MEANX2          ';MEANX2
[50] ⍞←'MEANX3          ';MEANX3
[51] ⍞←'MEANX4          ';MEANX4
∇
```

```
PROGRAMME ***PARABOLA*** COMPUTES THE VALUES FOR SOLVING SIMULTANEOUS EQUATIONS FOR A LEAST-SQUARES PARABOLA
(WITH DIRECTRIX PARALLEL TO THE Y-AXIS) ACCORDING TO THE METHOD OF EZEKIEL AND FOX (1959).

∇ PARABOLA
 [1] 'VECTOR OF XY PAIRS'
 [2] V←⍞
 [3] 'MATRIX DIMENSIONS OF DATA TABLE (ROWS × COLUMNS)'
 [4] DIM←⍞
 [5] NO←(⍴V)↑2
 [6] M←DIM⍴V
 [7] SUMX←+/M[ ;1]
 [8] SUMY←+/M[ ;2]
 [9] SUMXSQ←+/M[ ;1]*2
 [10] SUMUSQ←+/M[ ;1]*4
 [11] SUMXY←+/(×/[2]M)
 [12] SUMXU←+/M[ ;1]*3
 [13] SUMUY←+/((M[ ;1]*2)×(M[ ;2]))
 [14] MEANX←SUMX÷NO
 [15] MEANY←SUMY÷NO
 [16] MEANU←SUMXSQ÷NO
 [17] DELTAXSQ←((SUMXSQ)-(NO×(MEANX*2)))
 [18] DELTAXU←(SUMXU-(NO×MEANX×MEANU))
 [19] DELTAUSQ←(SUMUSQ-(NO×(MEANU*2)))
 [20] DELTAXY←(SUMXY-(NO×MEANX×MEANY))
 [21] DELTAUY←(SUMUY-(NO×MEANU×MEANY))
 [22] ' '
 [23] ⍞←'A SIMPLE PARABOLA HAS THE EQUATION  Y = A + BX + CX*2.'
 [24] ⍞←'B AND C ARE FOUND BY SIMULTANEOUSLY SOLVING THESE EQUATIONS'
 [25] ⍞←'(DELTAXSQ)B + (DELTAXU)C = (DELTAXY, AND'
 [26] ⍞←'(DELTAXU)B + (DELTAUSQ)C = (DELTAUY);'
 [27] ⍞←'FOR THE FIRST EQUATION-'
 [28] ⍞←'COEFFICIENT OF B      ';DELTAXSQ
 [29] ⍞←'COEFFICIENT OF C      ';DELTAXU
 [30] ⍞←'CONSTANT              ';DELTAXY
 [31] ⍞←'FOR THE SECOND EQUATION-'
 [32] ⍞←'COEFFICIENT OF B      ';DELTAXU-
 [33] ⍞←'COEFFICIENT OF C      ';DELTAUSQ
 [34] ⍞←'CONSTANT              ';DELTAUY
 [35] ⍞←'AND THE CONSTANT A OF THE PARABOLA EQUATION IS EVALUATED BY'
 [36] ⍞←'THE EQUATION  A = (MEANY) - B(MEANX) - C(MEANU), WHERE'
 [37] ⍞←'MEANY                 ';MEANY
 [38] ⍞←'MEANX                 ';MEANX
 [39] ⍞←'MEANU                 ';MEANU
 [40] ' '
 [41] ⍞←'SAMPLE SIZE           ';NO
 [42] ⍞←'SUMX                  ';SUMX
 [43] ⍞←'SUMY                  ';SUMY
 [44] ⍞←'SUMXSQ                ';SUMXSQ
 [45] ⍞←'SUMUSQ                ';SUMUSQ
 [46] ⍞←'SUMXY                 ';SUMXY
 [47] ⍞←'SUMXU                 ';SUMXU
 [48] ⍞←'SUMUY                 ';SUMUY
 [49] ⍞←'N.B. U = X*2'
 [50] →0
 [51] →BEGIN
∇
```

PROGRAMME ***SCAT*** COMPUTES VALUES FOR ALL THE STATISTICAL PARAMETERS NECESSARY FOR THE CONSTRUCTION OF DICE-DIAGRAMS (DICE AND LERAAS, 1936).

```
∇ SCAT
[1] 'RUN NUMBER'
[2] NUM←⎕
[3] 'TYPE IN VECTOR'
[4] V←⎕
[5] N←⍴V
[6] MAX←⌈/V
[7] MIN←⌊/V
[8] RAN←(MAX-MIN)
[9] SUMV←+/V
[10] MEANV←(SUMV÷N)
[11] ST←(((+/((V-MEANV)*2))÷(N-1))*0.5)
[12] SEM←(ST÷(N*.5))
[13] ⍞←' '
[14] ⍞←'STATISTICS OF DISTRIBUTION:-'
[15] ⍞←'SAMPLE SIZE    ';N
[16] ⍞←'MAXIMUM VALUE  ';MAX
[17] ⍞←'MINIMUM VALUE  ';MIN
[18] ⍞←'RANGE          ';RAN
[19] ⍞←'MEAN           ';MEANV
[20] ⍞←'STANDARD DEV   ';ST
[21] ⍞←'STANDARD ERROR ';SEM
[22] ⍞←' '
[23] ⍞←'FOR DICE DIAGRAMS'
[24] ⍞←'+ONE STANDARD DEVIATION          ';MEANV+ST
[25] ⍞←'+TWO STANDARD ERROR OF MEAN      ';MEANV+(2×SEM)
[26] ⍞←'-TWO STANDARD ERROR OF MEAN      ';MEANV-(2×SEM)
[27] ⍞←'-ONE STANDARD DEVIATION          ';MEANV-ST
∇
```

```
PROGRAMME ***SEMICIRC*** COMPUTES THE VECTOR MEAN AND VECTOR MAGNITUDE FOR TWO-DIMENSIONAL
ORIENTATION DATA ACCORDING TO THE METHOD OF CURRAY (1956); THE TRIGONOMETRIC TABLE INCLUDED
IN THE PROGRAMME ENABLES EASY DETERMINATION OF THE QUADRANT CONTAINING THE VECTOR MEAN.


∇ SEMICIRC
 [1] 'ANGLES ARE ORIENTATIONS IN 180 DEGREE RANGE'
 [2] ' '
 [3] 'TYPE IN ANGLES IN DEGREES''
 [4] X←⍞
 [5] RAD←X÷57.296
 [6] Y←2×RAD
 [7] NS←+/2○Y
 [8] EW←+/1○Y
 [9] DUM←(EW÷NS)
 [10] THETA←¯3○DUM
 [11] ANGLE←THETA×57.296
 [12] R←(((EW*2)+(NS*2))*0.5)
 [13] N←⍴X
 [14] L←((R×100)÷N)
 [15] ' '
 [16] '                QUADRANT:      0-90        90-180        180-270        270-360'
 [17] '                SINE:          +VE         +VE           -VE            -VE'
 [18] '                COSINE:        +VE         -VE           -VE            +VE'
 [19] '                TAN(X):        0÷X         180-X         180+X          360-X'
 [20] ' '
 [21] ⍞←'SINE COMPONENT          ';EW
 [22] ⍞←'COSINE COMPONENT        ';NS
 [23] ' '
 [24] ⍞←'CURRAYS PARAMETERS:'
 [25] ⍞←'(2×)VECTOR MEAN         ';ANGLE
 [26] ⍞←'VECTOR MAGNITUDE        ';L
 [27] ⍞←'SAMPLE SIZE             ';N
 ∇
```

8.3 Triaxial dimensions of the clasts used in the experiments

Axial lengths are in centimetres. An asterisk denotes that the clast was used in the first set of experiments.

#	a	b	c
1	8.4	6.7	4.2
2	7.0	5.1	2.7
*3	11.0	5.4	2.5
4	8.8	7.9	2.4
5	8.3	7.2	2.5
6	7.6	5.6	2.7
7	7.7	7.0	2.5
8	8.3	5.4	2.8
*9	7.8	4.5	2.5
*10	6.5	3.3	2.1
*11	8.1	4.0	3.1
*12	8.4	6.5	2.5
13	8.5	7.2	2.8
14	10.2	7.1	3.4
15	6.8	6.8	3.0
16	9.5	5.3	3.7
17	9.2	5.8	3.9
*18	11.4	8.8	2.6
19	10.0	7.0	3.3
*20	9.0	4.6	2.4
21	11.3	7.6	2.7
22	10.0	6.8	4.0
23	8.7	6.4	2.7
25	8.5	6.5	3.0
26	12.9	10.0	3.1
27	8.1	6.9	1.3
*28	7.4	5.0	2.7
29	9.0	5.0	2.6
30	7.2	6.2	5.3
31	9.9	4.2	2.8
32	12.5	9.7	4.5
33	8.0	4.5	4.1
34	8.2	5.6	1.8
35	6.5	4.0	2.1
36	6.4	6.1	3.1
37	10.9	8.2	5.0
38	8.8	6.0	4.8
39	8.2	6.3	3.4
*40	9.3	4.7	3.7
41	10.1	10.0	2.8
42	11.0	7.9	2.7
43	11.2	7.7	3.6
44	11.5	5.2	3.6
*45	8.9	5.0	3.9
46	7.4	5.7	5.2
*47	6.7	4.2	2.6
*48	6.5	5.4	2.1
49	12.5	9.4	2.8
*50	6.4	4.6	3.0
51	15.5	10.1	3.3
52	10.4	9.6	5.8
53	16.1	10.7	4.5
54	9.7	8.0	2.7
*55	8.3	4.6	2.2
56	16.0	9.9	4.8
57	12.9	10.7	3.7
58	12.0	10.0	4.6
59	14.8	10.9	3.4
60	16.4	10.4	5.3
61	15.7	11.0	4.7
62	18.1	8.5	4.0
63	10.4	8.5	4.1
64	16.0	8.5	6.3
*65	12.8	11.2	3.5
66	13.7	9.5	5.9
67	11.1	7.8	5.3
68	13.4	8.5	5.2
69	9.4	8.5	4.4
70	12.8	10.6	3.5
*71	13.2	9.7	4.0
72	15.0	11.2	5.0
*73	18.5	13.4	5.2
74	13.3	11.0	2.9
75	13.4	11.4	5.6
76	10.9	10.9	2.7
77	12.4	8.0	2.9
78	9.8	7.4	3.4
79	20.2	8.8	4.9
80	13.2	11.1	2.3
81	11.5	9.5	3.7
82	11.8	8.6	3.8
83	11.3	9.4	6.7
84	10.9	5.8	4.2
85	14.0	8.6	4.2
86	17.7	8.5	3.9
87	10.8	5.8	1.9
*88	10.5	6.0	3.5
*89	16.2	5.9	4.0
90	16.5	7.8	5.7
91	13.6	9.7	4.3
92	8.0	5.7	2.3
*93	9.2	6.4	2.3
*94	6.5	5.2	2.5
95	11.0	5.2	2.5
96	10.7	10.2	3.6
97	8.4	7.6	3.1
98	9.7	6.0	2.7
*99	8.0	5.2	3.3
100	7.1	4.1	3.2
101	10.3	7.8	4.0
102	11.6	6.7	2.6
103	7.6	5.8	3.3
*104	6.9	5.0	2.8
105	11.4	6.3	4.2
106	10.7	7.6	2.8
*107	7.5	5.1	3.9
*108	10.4	3.6	2.6
109	6.5	3.8	3.6
110	10.4	7.8	3.8
111	10.0	8.8	3.8
*112	6.9	5.3	3.3
*113	10.4	7.2	6.7
114	8.4	8.0	3.0
116	10.6	9.7	4.8
118	9.3	8.1	3.7
*119	7.0	5.7	2.2
120	10.2	8.0	2.5
121	9.1	7.3	3.2
122	9.6	6.5	5.0
123	10.7	8.9	2.6
124	12.5	9.2	3.2
125	8.7	6.3	2.0
126	8.7	6.0	2.6
127	9.2	5.9	4.1
*128	6.4	6.0	1.8
129	8.5	7.6	1.1
130	8.8	4.7	1.9
131	9.3	7.5	3.0
132	8.9	7.0	3.1
133	9.9	5.6	2.7
*134	6.3	5.3	1.9
135	6.8	6.5	1.7
136	10.7	8.5	2.5
137	10.8	10.5	3.3
*138	6.3	5.7	3.5
139	10.2	6.5	2.4
140	9.3	7.0	2.7
141	8.9	7.2	5.3
142	7.8	6.7	3.5
143	8.9	6.3	3.6